Doctoral Dissertation
Doctoral Program in Material Science and Technology (31st Cycle)

Joining of oxide/oxide Ceramic Matrix Composites

By

Muhammad Yasir Akram
* * * * * *

Supervisors
Prof. Monica Ferraris,
Prof. Valentina Casalegno

Doctoral Examination Committee:
Prof. A.B. , Referee, University of….
Prof. C.D. , Referee, University of…
Prof. E.F. , Referee, University of….
Prof. G.H. , Referee, University of…
Prof. I.J. , Referee, University of….

Politecnico di Torino
2018

I hereby declare that, the contents and organisation of this dissertation constitute my own original work and does not compromise in any way the rights of third parties, including those relating to the security of personal data.

…….....

Muhammad Yasir Akram

Turin, 2018

Summary

Chapter 1 highlights the significance of joining of ceramic matric composites and on-going research programs for development of oxide/oxide ceramic matrix composites for different applications. This chapter also included objective of this research work

Chapter 2 includes the literature review of different joining materials and methods for oxide ceramics such as alumina (Al_2O_3), yttrium aluminium garnet (YAG) and zirconia (ZrO_2).

Chapter 3 is about joining of oxide/oxide ceramic matrix composite using existing brazing alloys and a newly developed brazing system. The chapter includes the experimental part, results and conclusion.

Chapter 4 describes the joining of two types of oxide/oxide ceramic composites with two different glass-ceramic systems. The results related to different thermal characterization, mechanical testing and long term testing are discussed.

Chapter 5 is conclusion of this research work.

Abstract

Ceramic matrix composites (CMC) are gaining attention due to their low density and high thermomechanical properties, which make them prominent material in aircraft turbine engines, rocket propulsion components and thermal protection systems. For these applications, high temperature oxidation resistance might be an issue for carbon and silicon carbide based CMC. Oxide fiber /oxide matrix composites (ox/ox CMC), composed of oxide based fibers and matrixes are inherently oxidation resistant, they have high thermomechanical properties, simple fabrication techniques and are generally less expensive than non-oxide CMC. Ox/ox CMC are nowadays potential candidates to replace nickel based super alloys .

However, CMC components have very often complex shapes and it is technologically more convenient and cheaper to fabricate simple shapes and then integrate them together into final components by using robust and reliable joining materials and methods. Of course, the joining materials must withstand the working conditions.

Brazing is a simple and cheap technique for joining ceramics and ceramic matrix composites. Silver based (AgCuSnTi) and zirconium based (ZrNiTiHf) brazing alloys were initially selected to join ox/ox CMC (Nextel^{TM} 610 fiber reinforced YAG-zirconia matrix) and a new brazing system based on Ti, Cu and Al was designed by using metallic interlayer approach.

Glasses and glass-ceramics are well known joining materials used for variety of technical applications. They have good thermo-mechanical properties, intrinsically high oxidation resistance and their properties can be tailored according to the final requirement. They are already used as joining materials, for high temperature components, such as, solid oxide fuel cells.

Nextel^{TM} 610/ YAG-zirconia and Nextel^{TM} 610/alumina-zirconia ox/ox CMC were joined and characterized using novel SiO_2-Al_2O_3-CaO-MgO and SiO_2-Al_2O_3-CaO-MgO-Y_2O_3-ZrO_2 based glass-ceramics. The joining was performed in air without applying any pressure. The coefficient of thermal expansion of each glass-ceramic was tailored and measured by using dilatometry. Their

crystallization behaviour was studied by differential thermal analysis and their sintering by hot stage microscopy. Matusita, Sakka and Ozawa equations were used to study the crystallization kinetic behavior of developed glasses.

The joints were analysed by using Field Emission Scanning Electron Microscopy and Energy Dispersive X-ray Spectroscopy. The phases formed in glass-ceramic joints were identified by X-Ray Diffraction.

To evaluate the mechanical strength of joined samples, Single Lap Off-set shear tests (SLO) and four-point bending tests were performed at room temperature and at 850 °C (850 °C tests at IKTS-Fraunhofer, Dresden, Germany). The bending strength of as-received and thermally treated composites (by the same thermal treatment as for joining) were also performed to evaluate the effect of joining conditions on composites strength.

The thermal stability of the joined samples was also studied by thermal ageing to 850 °C and 930 °C for 100 h and 50 h in air, respectively.

The mechanical and ageing test results showed that the novel glass-ceramics developed within this PhD thesis (SiO_2-Al_2O_3-CaO-MgO and SiO_2-Al_2O_3-CaO-MgO-Y_2O_3-ZrO_2) are promising materials for joining Nextel^{TM} 610/ YAG-zirconia and Nextel^{TM} 610/alumina-zirconia, respectively.

Acknowledgment

I am very thankful to my mother, father and wife. They are always supportive and sacrifice a lot for me.

I would like to thanks my supervisors, Professor Monica Ferraris and Professor Valentina Casalegno. All the time they are very cooperative, helping and kind in their attitude.

I want to convey my sincere and genuine gratitude to Professor Milena Salvo for helping me during my research work.

I am heartily thankful to Dr. Alexander Shapiro (Titanium Brazing Incorporation, USA) and people from TANKA, Japan, for sending us raw material for research work.

Finally, I would like thanks to all my colleagues who are always very cooperative and helping.

I would like to dedicate this thesis to my loving parents and wife whose prayers and efforts are countless in making me successful

Contents

List of Tables

List of Figures

Chapter 1

Aim of work

This chapter briefly describes the importance of joining of ceramic matrix composites. Different on-going programs for development and validation of oxide/oxide CMCs for high temperature application are highlighted. This research work was done with collaborations of Department of Ceramic Materials Engineering, University of Bayreuth, Germany.

1.1 Introduction

Ceramic matrix composites (CMCs) are potential candidates for high temperature structures such as land based turbines, space vehicles, military and commercial aircraft engines and advance rocket systems [1]–[3]. For these high performance applications, several CMC components require high temperature oxidation resistance. Non-Oxide CMCs have high strength and creep resistance at elevated temperatures, however, they have certain limitations in terms of oxidation resistance [4]–[6].To address this issue, several research groups have developed and tested a relatively new class of ceramic composites known as oxide fiber reinforced oxide ceramic matric composites (ox/ox CMCs). Ox/ox CMCs are composed of oxide based fibers (e.g. alumina based Nextel^{TM} 610, Nextel^{TM} 720) and oxide based matrixes (e.g. Yttrium Aluminium Garnet -YAG, Alumina, Zirconia). Due to their inherent oxidation resistance ($\leq$ 1200 $^{\circ}$C), higher thermo-mechanical properties and low density, these ox/ox CMCs have potential to substitute the existing alloys (e.g. Ni based super alloys),thus, reducing consumption of fuel and NOx/CO_2 emission. Ox/ox CMCs are produced by cheaper and simpler fabrication techniques as compared to non-oxide CMCs [3], [7]–[9].

Presently, General Electrics (GE 610/GEN-IV), German Aerospace Center (DLR) (WHIPOX ^{TM},OXIPOL), EADS Innovation Works, Germany (UMOX ^{TM}), University of California (UCSB 610/M,UCSB 720/M), Applied Thin Films USA (Cerablak^{TM}), and University of Bayreuth, Germany, are notable players working on development of ox/ox CMCs while ATK-COIC,USA (610/AS,720/AS) is a prominent commercial supplier (AS-N312, AS-N720, A-N720, AS-N650, AS-N610)[3] [10][11].

Ceramics and ceramic matrix composites are not easy to machine due to their inherent brittle nature. High performance structure often require parts that are complex in shape and in many cases it is cheaper and convenient to develop

simple geometrical shapes and then integrate them together into the final component using reliable joining materials and methods. However, it is important that joined components must perform efficiently in operational conditions with little or no degradation. Development of economical and efficient joining materials and methods could assist researchers to timely utilize CMC components in advance structures. Furthermore, it gives designers freedom of choice to develop hybrid structure which could reduce the fuel consumption and hazardous emissions[12][13][14].

1.2 Applications of oxide/oxide CMCs

An overview of the main projects related to these composites is provided in the following paragraphs. Each project results are briefly summarized:

1.2.1 High Performance Oxide Ceramic (HiPOC), Germany [15][10][16]

The main objectives of this program include:

i. Assessment of different approaches to manufacture ox/ox CMCs with specific application in combustion chamber and in gas turbines.
ii. Develop design concepts for the integration of heat resistance load bearing ox/ox CMCs components/modules into metallic load bearing components/ structures with low temperature resistance.
iii. Designing and characterization for cooling of combustion chamber wall parts/sections made of ox/ox CMCs having thermal barrier coating.
iv. Operation of a ceramic demonstrator combustion chamber (with cooling and fastening concepts) under engine specific conditions.
v. Development of quality assurance concept for ox/ox CMCs components for their non-destructive testing methods with specific application in combustion chamber and in gas turbines.

The HiPOC project involved three companies and four research institutes including ASTRIUM, EADS, Rolls-Royce and University of Bremen, Germany. Three composites, namely, WHIPOX^{TM}, UMOX^{TM} and OXIPOL were developed, improved and tested (figure 1 and figure 2). In all three composites the reinforcement was Nextel^{TM} 610 alumina fibers. WHIPOX^{TM} is slurry infiltrated alumina based composite while UMOX^{TM} and OXIPOL were developed by polymer infiltration and pyrolysis process and contain small amount of carbon in mullite/SiOC and SiOC matrices, respectively. Their mechanical characterization was performed by compression, tensile, four-point bending and in-plan shear tests from room temperature to working temperature. Furthermore, creep tests were also performed. In large civil engine the water vapor partial pressure can reach up to 5 bar, therefore the composites were coated with 0.6 mm Environment Barrier Coating (EBC) based on YSZ, magnesium spinel, mullite and rare earth mono-

silicate, using air plasma spray deposition method. Spallation behavior of EBC was also evaluated.

Design concepts for attaching these composite parts to metal components of engine with focused on combustion chamber was investigated. Other issues like mechanical attachments, EBC volatilization, and allowance for difference in thermal expansion were also addressed. Cooling schemes for these composites were developed and validated for target temperatures, density ratio and velocities. Lastly, the combustors were tested with representative conditions (temperature, pressure and air fuel ratio) of specific aero-engine. All the three these composites have promising performance in comparison to other ox/ox CMCs reported in literature. The results of this study paved the way for be combustion chambers of small gas turbines and stationary gas turbine and other application where oxidation resistance with non-brittle fracture is required. Due to degradation in Nextel^{TM} 610 mechanical properties a service temperature of less than 1200 $^{\circ}$C was recommended (depending upon the service time and load) for these composites.

Figure 1: Successful fit check of UMOX^{TM} combustion chamber (HiPOC) [15]

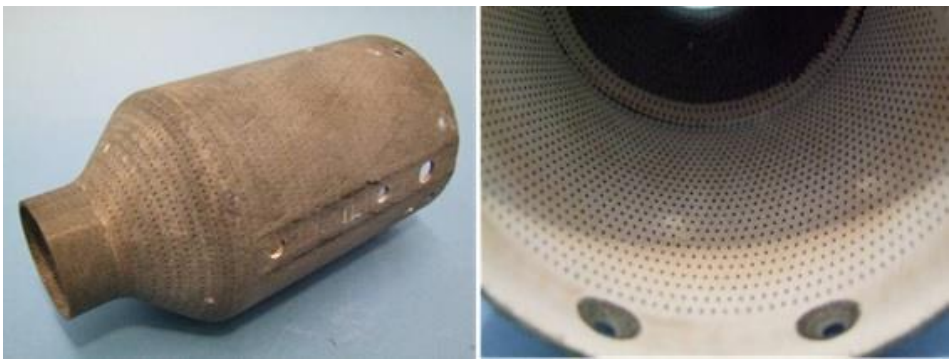

Figure 2: Condition of UMOX^{TM} combustion chamber and EBC after testing (HiPOC)-Overall in good condition [15].

1.2.2 Development of ox/ox CMC exhaust mixer nozzle technology

(NASA, Rolls-Royce liberty works and ATK COI Ceramic Inc.)[17][18]

NASA with ATK COI Ceramics, Inc and Rolls-Royce Liberty Works (RRLW) collaborated for development of ox/ox CMC exhaust mixer (figure 3 and figure 4) for turbofan engines in subsonic jet aircrafts .The ox/ox CMC mixer must be capable of working with increased performance and reduced noise. The work was pursued because improving in fuel efficiency is associated with engines operating at higher temperatures and existing titanium alloys are not able to bear this increase in temperature. Therefore, companies like Rolls-Royce, Snecma (Safran) and Boeing are reconsidering the use of Inconel, which has almost twice the density of titanium alloys and increases the fuel consumption and emissions.

The inert oxidation resistance at higher temperature and low density (2.5-3 g/cm^3) make ox/ox CMCs potential candidates for exhaust structures.

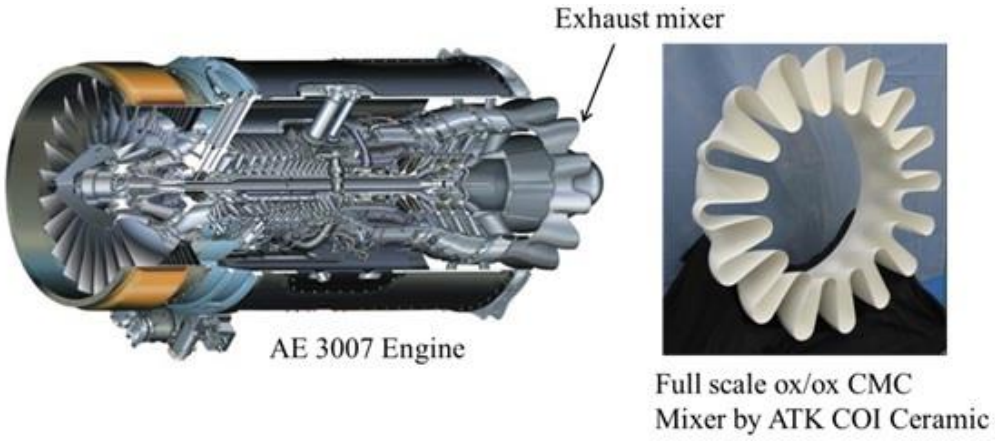

Figure 3: Full scale ox/ox CMC exhaust mixture developed by ATC COI Ceramic [18]

Figure 4: a) High temperature vibration testing and b) Vibration testing at Room Temperature [18]

A subscale ox/ox CMC mixer nozzle was developed by ATK COI Ceramic and its testing and characterization was performed at NASA Glenn Research Centre and ASE FluiDyne to achieve TRL5 (Technology Readiness Level). The collaboration is moving forward to develop a full scale ox/ox CMC exhaust mixer for engine test to reach TRL6.

1.2.3 Boeing continuous lower energy, emission and noise (CLEEN) program [19][3][20]

Recently (2014) Boeing has developed and tested inflight the largest built ox/ox CMC structure: - a CMC nozzle which is lighter, quieter and more efficient than the previous ones (Figure 5). The nozzle is made of Nextel^{TM} 610/AS (aluminosilicate matrix).Couple of hours of flight tests were performed with Rolls Royce Trent 1000 engine on ecoDemonstrator 787 flight test airplane.

Figure 5: Installation, testing and validation of nozzle cone for CLEEN project [21][20]

1.2.4 Other examples

Air Force Research laboratory, USA and Boeing collaborated to successfully design and preliminary test an ox/ox CMC structure to be used as Aft fairing heat shield (AFHS) for military and commercial aircraft as shown in figure 6 [19].Aft fairing heat shield are used to protect the aluminum struts from engine exhausts.

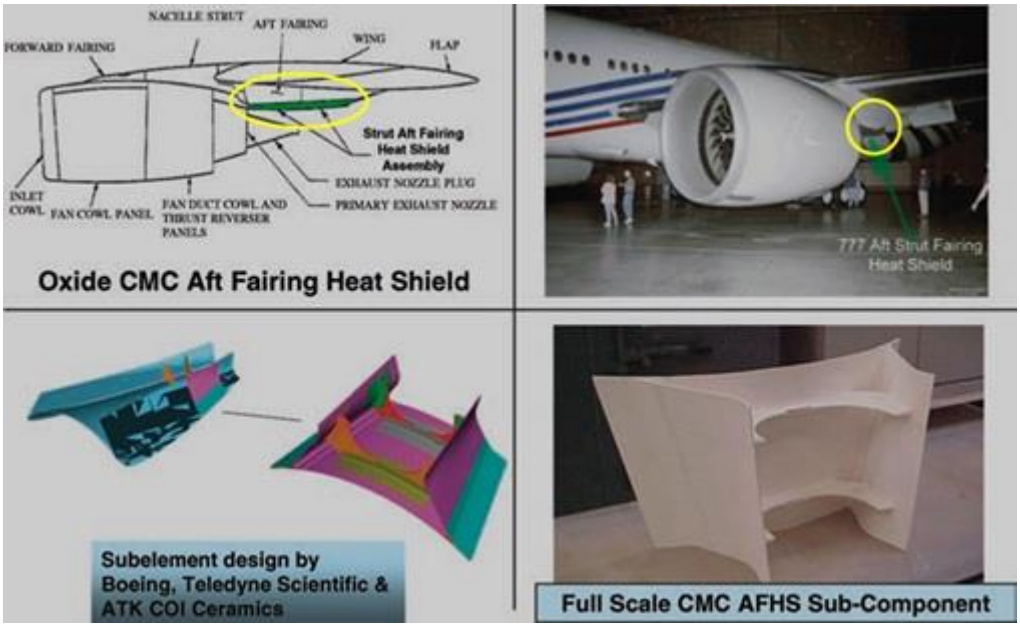

Figure 6: Full scale AFHS sub component developed by AKT-COI Ceramics [19]

WHIPOX^{TM} (Wound highly porous ceramic) was used in thermal protection system (TPS) and as a seal between carbon fiber based CMCs panels for SHEFEX II (Sharp Edge Flight Experiment) spacecraft as shown in figure 7 [22][23].

Figure 7: Integration of WHIPOXTM panels a) as TPS of SHEFEX II re-entry vehicle b) Successfully launched in 2012 [22].

In EU project Clean Sky, Fraunhofer, Walter E.C. Pritzkow Spezialkeramik (WPS) and MTU Aero Engines developed a liner segment (figure 8) for an aero engine for low pressure exhaust area. After validation, this ox/ox CMC component is used as impact tolerant housing and thermal insulation. This CMC is made of Nextel^{TM} 610/Al_2O_3-ZrO_2 (Keramikblech FW12).

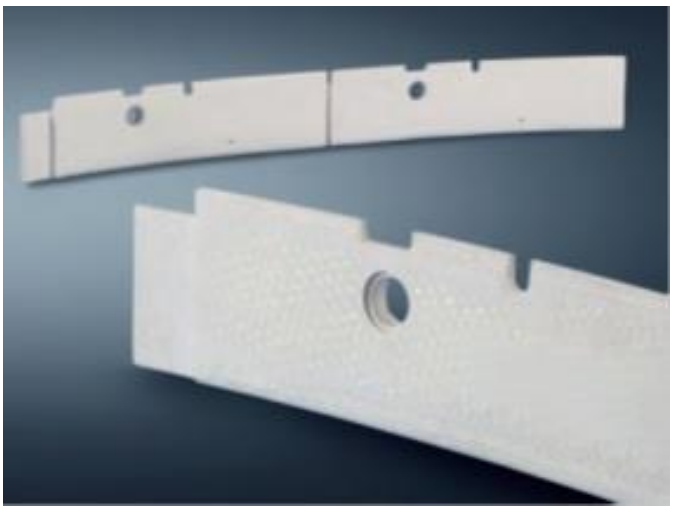

Figure 8: Keramikblech FW12 liner segment for aero engine [24]

Furthermore, these institutes developed a flame tube made of ox/ox CMC to replace metallic tubes used in different industrial applications.

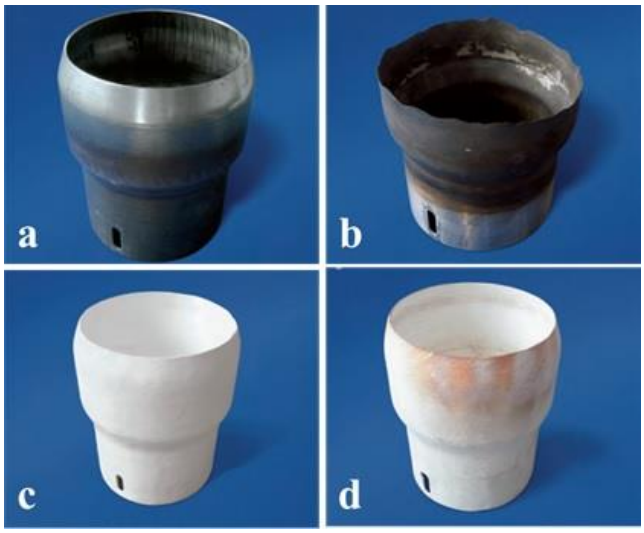

Figure 9: Metallic and ox/ox CMC flame tubes a) MFT before putting in operation b) MFT after 1000 h of operation c) Ox/ox CMC tube before putting in operation d) Ox/ox flame tube after > 20000 h in operation [24].

The metallic flame tube (MFT) has a small service life time of 1000 h while the tube made of ox/ox CMC could survive larger than 60000 h. A comparison of metallic and ox/ox flame tubes after service time of 1000 h and 20000 h, respectively, are shown in figure 9 [24]

1.3 Objective of thesis

The objective of this work is to join ox/ox ceramic matrix composites for high temperature applications, having the following requirements:

- Design and development of new joining material for ox/ox CMCs.
- Joined components with oxidation resistance up to 850°C for 100 h in air.
- Joined components with good mechanical strength at room (RT) temperature and at 850°C (measured by Single lap-off set test at RT and Four-point bending test at RT and at 850°C).
- Joining in air without any pressure and protective environment (argon or vacuum).

The joining materials and processes should be devised such that these cannot only meet the operational requirements of the components but these should also be commercially suitable for all shapes and sizes without any notable degradation in the substrate properties. Furthermore, cost effectiveness, maintenance and repairing flexibility have been also considered.

Due to high temperature stability and tailorable properties of glass-ceramics material, two types of silica based glass-ceramics, SiO_2-Al_2O_3-CaO-MgO and SiO_2-Al_2O_3-CaO-Y_2O_3-MgO-ZrO_2 were developed, characterized and optimized for joining of Nextel^{TM}610/YAG-zirconia and Nextel^{TM} 610/alumina-zirconia ox/ox CMCs. The results of this research work showed that the glass-ceramics are promising materials for integration of ox/ox CMCs and the proposed joining process is simple and commercially suitable for different shapes and sizes.

Chapter 2

Literature review

This chapter provides details of different joining techniques and materials used for joining of oxide ceramics and oxide ceramic matrix composites. Advantages and disadvantages of each joining technique is highlighted and discussed.

2.1 Joining methods

Scant literature is available on the joining of ox/ox CMCs; however since the ox/ox CMCs are made of oxides, it is important to start with the joining methods used for joining of oxide ceramics such as alumina (Al_2O_3), yttrium aluminium garnet (YAG) and zirconia (ZrO_2).

The following methods are often used in joining of oxide ceramics:

- Adhesive bonding
- Pre-ceramic polymers joining
- Brazing
- Transient liquid phase bonding
- Microwave assisted joining
- Laser assisted joining
- Diffusion bonding
- Glasses and glass-ceramics as joining materials

2.1.1 Adhesive bonding

Adhesive joining is a simple and easy technique for integration of similar and dissimilar components with complex shapes. However, mostly ceramics are intended for higher temperature applications and most adhesives are not stable for

high temperatures, therefore, these joined components are limited for low temperature applications, for instance, Harris et al. joined alumina, using epoxy resin, for armor systems [25].

2.1.2 Pre-ceramic polymers joining

Pre-ceramic polymers are the organic compounds which transform from polymer to ceramic when heated to a suitable temperature (> 800 °C) [26]. In recent years, joining of ceramics and CMCs, using pre-ceramic polymers, have been reported by several authors as a promising technique for high temperature applications. However, problem such as presence of cracks, amount of residual porosity, shrinkage stresses, heat treatment (temperature, heating rate, dwell), joint thickness, low ceramic yield etc. are the issues needed to be address properly [27][28] [29].

Wang et al. [30] joined alumina with a pre-ceramic polymer, prepared by using modified polymethylsilane as matrix and B_4C and glass powder as fillers. The samples were cured at 200 °C for 2 h in air and later heat treated from 400-1200 °C for 2 h at each temperature in air. The obtained shear lap strength values ranged between 18-67 MPa (after heating between 200-1200 °C). Higher lap shear strengths at 800 °C could be attributed to transformation of B_4C to B_2O_3 which formed strong chemical bonding with alumina. Laun et al. [29] used polyborosilazanes based pre-ceramic polymer to join alumina and study the effect of temperature (1300 °C, 1400 °C, 1500 °C), dwell (0.5h, 1h, 1.5h, 2 h), heating rate (2, 5, 8 °C min^{-1}) and pressure (1.5, 6, 9 KPa) on compressive lap shear strength. It was concluded that 1500 °C with dwell of 2 h, pressure 1.5 KPa and heating rate of 2 °C min^{-1} gave the maximum lap shear strength of 16 MPa tested at room temperature. The maximum lap shear strength was reduced to 13 MPa, when the test was performed at 800 °C.

Qin et al. [31] joined alumina by using commercially available SAR-9 polysiloxane based pre-ceramic polymer as matrix and TiB_2 and silica based glass powder as additives and study the effect of these additives on lap shear strength. Curing was performed at 200 °C for 4 h and then heat treated from 400-1200 °C for 2 h at each temperature. The maximum lap shear strength at room temperature for SAR-9 + TiB_2 was 12 MPa when heat treated at 1000 °C for 2 h, while the lap shear strength for SAR-9 + TiB_2 + glass powder was 21 MPa when heat treated 1200 °C for 2 h.

It must be underlined that none of these lap shear tests were done on samples of the same size: it means that a comparison among them is not possible.

Kita et al. [32] studied the effect of pyrolysis temperature on four-point bending strength at room temperature for alumina joined samples using polycarbosilane pre-ceramic polymer. The samples were pyrolysis at 1400 °C and 1600 °C for 1 h in air. The maximum strength of 109 MPa was obtained when pyrolysis was performed at 1600 °C while strength of 82 MPa was obtained when

pyrolysis was performed at 1400 °C. The higher bending strength was attributed to the complete diffusion and reaction of joining materials with alumina.

2.1.3 Transient liquid phase bonding (TLP bonding)

TLP bonding is a joining process that produces joint components without any remnant of the joining material (e.g. metal or glass) [33]. The resultant bond formed at the joint zone has a higher melting point than the joining temperature. Therefore, this technique can be utilized for high temperature applications. Partial transient liquid phase bonding (PTLP) is a modified form of TLP bonding which utilizes an X/Y/X multilayer configuration, which is selected such that the outer thin lower melting point element (X) form a TLP upon heating and diffuse completely in the, thick high melting point, core element (Y), for example, a refractory metal [34][35]. The formed phases at the interface has significantly higher melting point than the joining temperature. Schematic of PTLP is shown in figure 10.

Chang et al. [36] joined alumina with 3 µm boron oxide at different temperature (500 °C, 600 °C, 700 °C, 800 °C, 900 °C and 1000 °C) and time (2 h, 6 h, 10 h,15 h, 24 h and 48 h) using TLPB process. The maximum four-point bending strength of 71 MPa (at RT) was obtained with joining condition of 800 °C for 15 h. At these conditions, three compounds namely, $2Al_2O_3$-B_2O_3, $3Al_2O_3$-B_2O_3, $9Al_2O_3$-B_2O_3 coexist at the interface. Above 800 °C, the formation of pores reduced the joint strength.

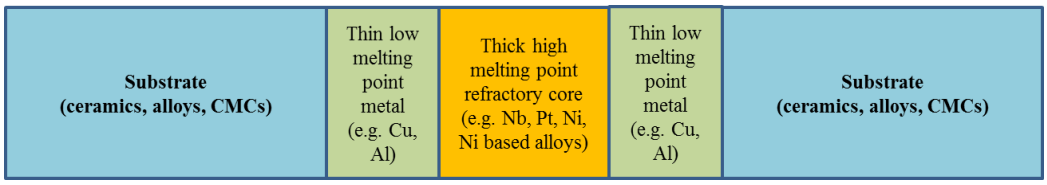

Figure 10: Schematic of PTLP

Dehkordi et al. [37] used bismuth oxide interlay to join alumina using TLPB process and performed joining at various temperatures (900 °C, 1000 °C and1100 °C) and dwell (4 h , 6 h, 10 h, 20 h and 28 h). The maximum single lap shear strength of 80 MPa (at RT) was obtained when joining was performed at 900 °C for 10 h and compound formed at the interface was $AlBiO_3$.

Kato et al. [38] found that high temperature strength of TLPB process joined alumina using Al/SiO_2 interlayer was decreased near and above the melting point of Al. The RT strength was 50 MPa (approx.) which decreased to just 20 MPa (approx.) at 850 °C and near the melting point of Al. Furthermore Lo et al. [39] suggested that the flexural strength of alumina joints vary drastically with interlayer thickness. Therefore, time, temperature, interlayer thickness and interlayer material selection are the key factors in obtaining the optimum results when using TLP bonding process.

Shalz et al. [40] [41][42] used PTLP bonding process to join alumina using Cu/Pt/Cu (3/127/3 microns, respectively), Cu/Ni/Cu (3/100/3 microns, respectively) and Cu/Nb/Cu (3/127/3 microns, respectively) interlayers at 1150 °C for 6 h in vacuum. Cu was selected in each case because Cu forms a complete solid solution at higher temperature with Pt, Ni and Nb and has wettability with alumina. The annealing was performed at 1000 °C for 10 h in air and after the annealing process the four-point bending strength was determined. The average four-point bending strength was 217 MPa, 138 MPa and 215 MPa for Cu/Pt/Cu (3/127/3 microns, respectively), Cu/Ni/Cu (3/100/3 microns, respectively) and Cu/Nb/Cu (3/127/3 microns, respectively), respectively. A considerable decrease in joint strength after annealing was also reported for Cu/Ni/Cu (3/100/3 microns, respectively) Additionally, the large difference in CTE of Ni and Al_2O_3 may have caused cracks during thermal cycling.

Akashi et al. [43] utilized PTLP process to join yttria stabilized zirconia (YSZ) using Al/Inconel 600/Al (0.8/600/0.8 microns, respectively) for different joining temperatures (1000 °C , 1100 °C and time 1200 °C) and time (1 h, 4 h, 8 h) with applied load of 80 MPa in vacuum: a joint strength of 170 MPa was obtained when joined at 1200 °C for 4 h. But, a lower strength (< 1 MPa) was reported, when joining temperature and dwell was 1000 °C and 1 h. The lower strength values were attributed due to presence of NiAl based intermetallics.

Therefore, it can be concluded that, wetting , matching CTE, decrease in strength after ageing and formation of intermetallic at the interface is challenging in PTLP joining process [34] and need careful considerations when design joints for high temperature applications.

2.1.4 Brazing

Brazing is the oldest and most widely used technology for joining similar and dissimilar substrates by utilizing a filler material (e.g. pure metals, alloys) which has melting temperature above 450 °C. Brazing has been successfully utilized for joining metals, alloys, ceramics and CMCs. A number of brazing alloys are available and continuously modified by suppliers to meet the specific applications.

For joining, the brazing filler (foil or paste) is sandwiched between the substrates and the temperature is raised above the liquidus temperature of the brazing filler. In most cases, a vacuum or protected environment (e.g. Argon) is necessary to avoid the oxidation of the brazing filler or substrate.

One of the main issues of brazing is the wetting of substrates by brazing alloys. The wetting is measured in terms of the contact angle between the molten brazing alloy and the substrate. Eq 2.1 represents this relation (figure 11)

$$\cos \Theta = (\Upsilon_{SV} - \Upsilon_{SL}) / \Upsilon_{LV} \qquad \text{Eq.2.1}$$

where Θ is the angle of contact between the molten alloy and solid surface, Υ_{SV} is the surface tension between vapor and solid, Υ_{SL} is the surface tension between liquid and solid and Υ_{LV} is the surface tension between vapor and liquid. If 90° < Θ < 180° the condition is not favorable for brazing and liquid will not spread on surface. For Θ < 90° the condition will favor brazing and spreading as well as wetting will take place. With decreasing the contact angle, the spreading area will be increased. Furthermore, the Cos Θ in Eq. 2.1 can be increased by increasing the value of Υ_{SV} and decreasing the value of Υ_{SL} and Υ_{LV}. Υ_{SV} can be increase, e.g., by cleaning the surface. Υ_{SL} is temperature dependent and decrease in range from 0.1 to 1% per Kelvin and Υ_{LV} can be decreased by reducing the atmospheric pressure [44].

For brazing of oxide ceramics, wetting can be improved by either using a multi-step indirect brazing process or a one-step direct brazing process. In indirect brazing process, the metallization of ceramic surface is mandatory before the brazing process, while in case of direct brazing, the brazing alloy with an active element (e.g. Ti, Zr) is used to increase the wetting and reactivity [45]. Figure 12 represents the schematic of direct and in-direct brazing. The discussion below is only related to the direct brazing technique for joining oxide ceramics by active fillers.

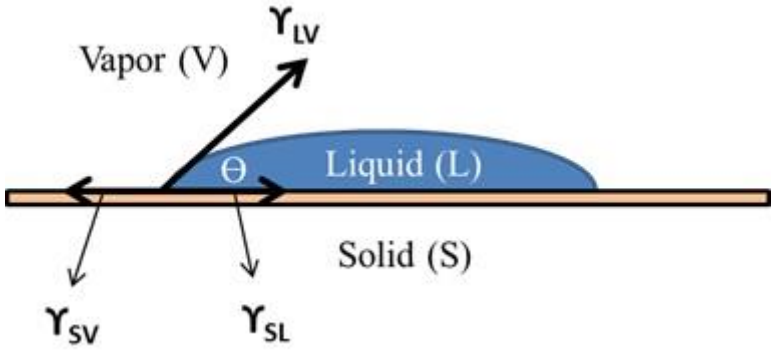

Figure 11: Wetting of solids by liquid melts [45]

Several researchers reported that the contact angle of Ag-Cu alloys on alumina is significantly reduced by adding small amount of titanium in Ag-Cu alloy [46][47]. Ti react with the oxygen ions of oxide ceramics (e.g. alumina, zirconia) and form a number of oxides including TiO,TiO_2, Ti_2O_3 etc. [46][48][49]. Furthermore, Gambaro et al. [50] investigated the wetting of YAG ($Y_3Al_5O_{12}$) by AgCuTi, AgCu, AgTi, Ag and Cu above their respective melting points. For AgCu, Ag and Cu the wetting angles were greater than 90°. For AgTi the wetting angle was 64° at 1050 °C. For AgCuTi the wetting angles were 71°, 73° and 10° at 820 °C, 850 °C and 950 °C, respectively.

Asthana et al. [51] joined partially sintered alumina using 63Ag-35.25Cu-1.75 Ti (CusilABA) and 68.8Ag-26.7Cu-4.5Ti (Ticusil) and identify TiO and Ti_3CuO_3 compounds at the alumina/Ag-Cu-Ti interface. Though, the CTE of of Cusil-ABA and Ticusil is in the range of ~ 18.5 $x10^{-6}$ $°C^{-1}$ and for alumina (partially sintered) the CTE was ~ 7-7.4 $x10^{-6}$ $°C^{-1}$, crack free joint were reported. This showed the ability of AgCuTi alloy to accommodate thermal stresses originate due to

difference in CTE of AgCuTi alloys and alumina. However, this is not valid when this partially sintered alumina was joined with unpolished C-SiC composite (CTE ~ 3.6 - 4.3 x 10^{-6} $°C^{-1}$) because interfacial decohesion was observed at AgCuTi/Composite interface.

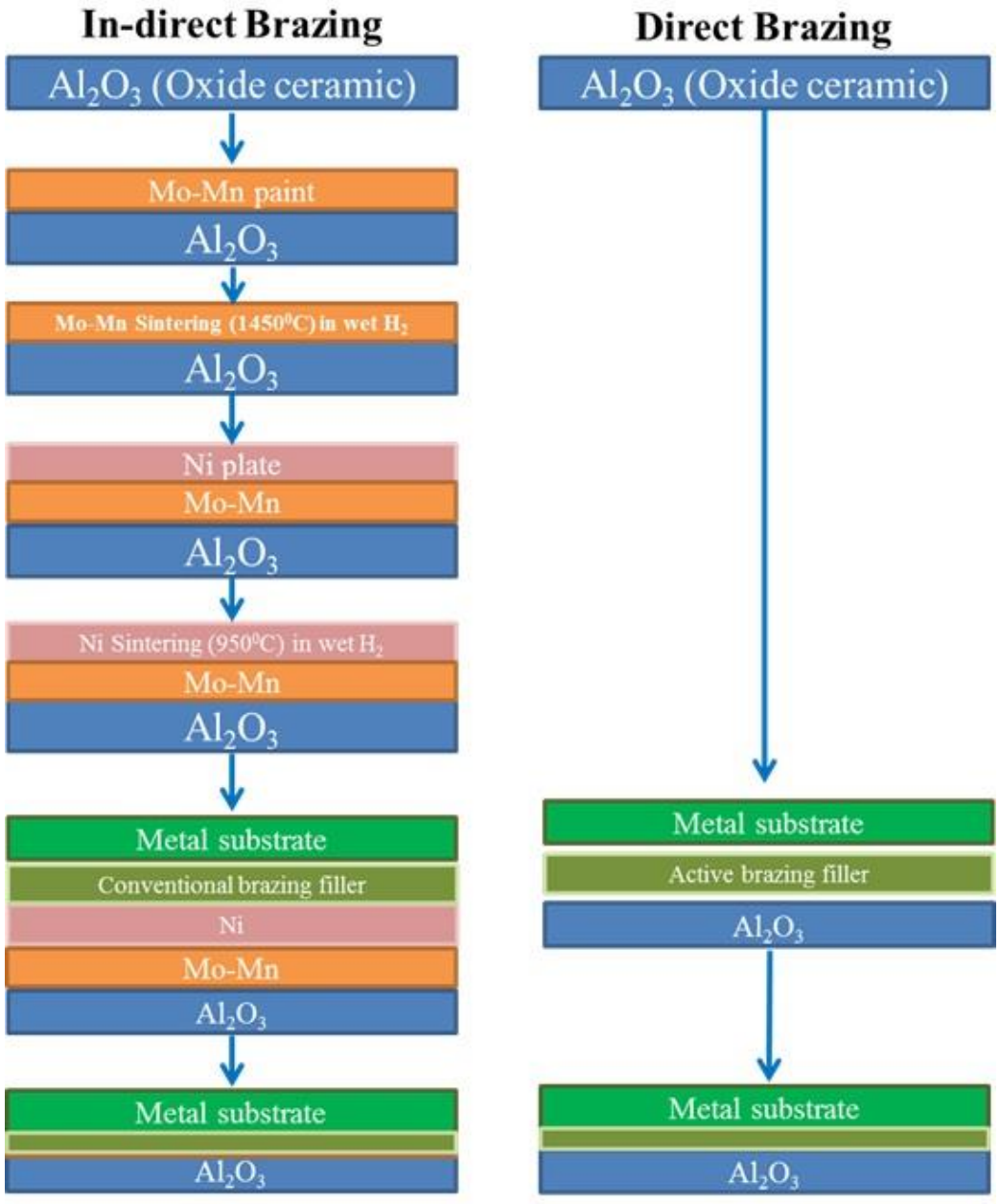

Figure 12: Comparison of direct and indirect brazing method for joining alumina

Hao et al. [48][52] investigated the alumina to alumina and zirconia to zirconia joining under varying condition of temperature, time, pressure using Ag38Cu5Ti filler. The maximum shear strength was obtained when brazing was performed at 850 °C for 30 minutes with a pressure of < 0.01 MPa. Higher temperature and more time results in formation of more brittle phases, i.e., TiO_2

and TiO which decreased the joint strength. However, the more interesting result was the dependency of shear strength on the joint thickness. Though, a similar composition and thickness of brazing alloy was used in both cases, the maximum strength for alumina to alumina joint was observed when joint thickness was 2 μm, conversely for zirconia the maximum shear was obtained when the joint thickness was 4.4 μm.

Chuang et al. [53] used Ag27Cu3Ti and Sn10Ag4Ti brazing alloys for joining partially stabilized zirconia to itself and reported four-point bending strength (RT) of 227 MPa and 137 MPa for Ag27Cu3Ti and Sn10Ag4Ti joints, respectively, when brazing was performed at 900 °C for 10 minutes. TiO was the predominating reaction layer at the interfaces in both cases.

Hanson et al. [54] reported the brazing of partially stabilized zirconia to itself with Cusil ABA (Ag 35.25Cu1.75Ti), Incusil ABA (Ag 27.25Cu12.5ln1.25Ti) and Ticusil (Ag26.7Cu4.5Ti) and found that the higher percentage of titanium leads to higher four-point bending strength. The possible phases at the interface were found to be TiO, Ti_2O_3, Ti_3O_5, Ti_4O_7 and TiO_2.

Recently, Kassam et al. [55] studied the effect of alumina purity (96 % alumina and 99.7 wt. % alumina) on joint strength when brazing with Ticusil (Ag26.7Cu4.7Ti). A 27 % increase in four-point strength was reported for 96 % alumina/Ticusil joined samples due to presence of SiO_2 as main secondary phase in 96 % alumina. This secondary phase interaction with Ticusil results in formation of Ti_5Si_3 compound at sites where triple pocket grain boundaries of alumina (96 wt%) surface intersected the titanium rich reaction layers. This interaction leads to a nanostructured interlocking mechanism which improved the joint strength.

2.1.5 Microwave assisted joining

Microwaves are type of electromagnetic radiations having wavelength between 1 m to 1 mm, having frequencies between 300 GHz to 300 MHz. Microwave heating is fundamentally different from conventional heating. In conventional process, the heat is delivered by convection, radiation or conduction and transferred to the interior of substrate through conduction. However, in microwave heating the heat is developed within the material by interaction of molecules in the presence of an electrical field.

Microwave assisted joining is comparatively a new method for joining of ceramics [56]. Though, it is difficult to heat ceramics by using microwave because of small dielectric loss factor, however with increasing temperature, the loss factor of alumina start to increase. At 1800 °C the loss factor increase to two orders of magnitude higher than at room temperature and hence it is possible to join ceramics through microwave heating method [57]. Microwave heating gives the flexibility of rapid and local heating near the joining zone [58]. Several researchers describe the designing of microwave apparatus for ceramic joining [59][60][61].

Fukushima et al. [58] joined different purity alumina (92-99%) in temperature range from 1400-1850 °C using direct (without any intermediate joining material) and indirect joining (with ceramic discs as joining material). The direct joining work well for 92-96 % pure alumina samples however, for 99% pure alumina indirect joining was adopted due to poor performance of alumina joint produced by direct joining. The maximum four-point bending strength (RT) was obtained for alumina with 92-96 % purity (equal to parent material strength) while for 99% purity the joints show comparatively less strength (70-90% of parent material strength). Furthermore, for 99% pure alumina samples, high strength was obtained with intermediates having similar composition to parent material. In terms of joining temperature and time the maximum strength was obtained at 1850 °C for 92-96 % purity, while for 99% purity the maximum strength was obtained between 1600-1800 °C. In both cases 3 min dwell yield the maximum strength. A similar effect of alumina impurity on joining was also reported in [62][62] .

Sato et al. [63] investigated the effect of joining temperature (1577 to 1877 °C), pressure (0.03 to 0.5 MPa) and dwell (2-10 min) for joining alumina to magnesia. The maximum three-point bending strength of 90 MPa was obtained at 1877°C with a dwell of 4 min with 0.5 MPa pressure.

Kondo et al. [64] studies the effect of temperature (1650 °C, 1700 °C and 1750 °C) on joining alumina using alumina/zirconia insert as joining material. The maximum strength was obtained at 1750 °C, however, at this temperature grain coarsening was observed at joining seam. At 1650 °C and 1700 °C pores and discontinuities at the joining interfaces were observed.

Binner et al. [65] joined yttria partially stabilized zirconia (able to readily absorb microwaves) without any interlayer at 1565 °C with a pressure of 2.7 MPa and 10 min dwell time. Grain boundary sliding and/or solid state diffusion were believed to be responsible for bonding mechanism.

Parsad et al. [66] studied the process parameters of microwave joining for different ceramics including alumina. It was found that at high powers (> 600 W), the heating was more focused at a specific area of joint. This increase in temperature at a particular spot causes a blow hole which significantly reduces the flexural strength.

Zhao et al. [67] used a low eutectoid (≤ 577 °C) microwave absorbing Al-Si alloy for joining alumina. The joining was performed at 850 °C by using a very high power of 1000 W. However, partial oxidation of Al was reported in XRD analysis.

2.1.6 Laser assisted joining

Laser joining is the technique in which joining material is heated locally through a laser beam. Due to advancement in laser technology and commercial availability of continuous wave beam power of different kW, the laser assisted joining can be successfully employed for joining of ceramics. Oxide ceramics have the peculiar property of being partially transparent to wavelengths of 808 nm and 940 nm: as a result, these ceramics can be heated inside their volume instead

their surface. Thus, joining can be done locally without high thermal stress of the whole component[68]. Furthermore, this joining technique can be performed in air without any protective atmosphere or vacuum needed. However, there are some limitations on the dimensions of joining zone due the existing laser power systems [68].

Borner et al. [69] joined zirconia using SiO_2-BaO-B_2O_3 and SiO_2-BaO-SrO based glasses and glass-ceramics and able to produce good mechanical properties. However, it was observed that viscosity of glasses is a very crucial parameter and even small changes in viscosity led to change in process control and application area. Furthermore, the joining temperature must be below the couple-in temperature of zirconia. Couple-in temperature is considered to be a point at which there is an exponential increase in temperature at a constant laser power. Reliability and reproducibility of joints could be badly affected for the temperatures near this point.

In another study, Borner et al. [70] joined alumina to alumina and zirconia to zirconia using SiO_2-B_2O_3-Al_2O_3-MeO glass fillers (Me^{2+} = Sr, Ba ; Me^{3+}= La, B, Al) and were able to obtained four-point bending strength (RT) of 158 MPa and 190 MPa for joined alumina and zirconia, respectively. Furthermore, it was concluded by Borner et al. that optimization of laser joining processes depend on process related properties of both ceramics and fillers (joining material). For ceramics, properties such as couple-in temperature, emissivity, heating behavior and optical properties; for fillers, softening, CTE and absorption of laser radiation, are crucial parameters for optimization.

2.1.7 Diffusion Bonding

The diffusion bonding is a joining technique in which bonding is achieved through solid state diffusion process [71]. The diffusion bonding can be performed with and without interlayers by applying an interfacial pressure which may vary from minutes to hours [72]. Diffusion process between ceramics are quite complicated as compared to diffusion between metals due to low diffusivity of anions. To enhance the diffusion rate in ceramics, an intermediate is used which improve the mass transportation process [73]. From industrial point of view, the diffusion bonding cost is high, due to design of equipment which combines high temperature and high pressure in vacuum. This put limitation on component size and shape [71].Furthermore, presence of pores and voids was also reported in [74], even though high temperature, pressure and longer dwell time were used.

Hosseinabadi et al. [75] joined alumina to alumina using AlH_3 and $Mg(AlH_4)_2$ nano powders as interlayer using a pressure of 20MPa in temperature range from 200-400 °C for 30 min. in vacuum. During heating, the decomposition of nano powders resulted in formation of metals and alloys nano particles. These particles react with alumina to form spinel oxides ($MgAl_2O_4$) which improve the shear strength of the joints to 202 MPa, when joining was performed at 400 °C.

Scott et al. [76] investigated the joining of alumina to alumina without any interlayer and was able to achieve a joint strength which was 60% of parent alumina. The parts were first forged in vacuum at 1500 °C by applying a pressure of 69 MPa and then samples were heated to 1875 °C for 3 h in vacuum. Grain growth across the interface led to joining of components. The maximum three-point bending strength was obtained at forged deformation of 18%.

Nagano et al.[77] studied the joining of coarse grain alumina, fine grain alumina, zirconia and alumina/zirconia composites (alumina content from 0-100%) without interlayer approach. The joining was performed at 1450 °C, 1475 °C and 1500 °C in air for 30 min and by applying pressure of 12.5 MPa. The maximum four-point bending strength (RT) was obtained at 1475 °C. Coarse grain alumina was difficult to self-bond, however, it can be joined to fine grain alumina and alumina/zirconia composites. The bonding mechanism was superplastic deformation of ceramics. However, the selected joining conditions considerably decrease the strength of parent material.

Ozturk et al. [78] used electrophoretic technique to deposit yttria stabilized zirconia as interlayer on MgO-stabilized zirconia substrate. The bonding was performed with and without interlayer at a very low pressure of 0.2 MPa. Little or no bonding occurred without interlayer at 1500 °C, however, with interlayer a continuous joining seam was obtained at 1450 °C in air using 2 h of dwell. Joining of alumina at a very low pressure (0.03 MPa) was also reported in [79].

2.1.8 Glasses and Glass-ceramics

According to ASTM C162-04, glass material is "*inorganic product of fusion that is cooled to a rigid condition without crystallization"*. However, melting is not the essential requirement for formation of glasses. Glasses can be formed through vapor deposition, sol gel route and by neutron irradiation of crystalline materials. Traditional glasses are non-metallic and in-organic in nature, however, metallic glasses and organic glasses are also in use. Therefore, more precisely, "*a glass is an amorphous material which has no long-range atomic order and exhibit a region of glass transformation behavior"*. The glass forming substances include, for example

- Oxides and their mixtures: silicates, phosphates, borates, germanates etc.
- Organic compounds and organic polymers: methanol, ethanol glucose, glycerol, toluene, polyvinyl chloride, polyethylene, polystyrene, etc.
- Halides and fluorides: $ZnCl_2$, BeF_2 , ZrF_4, etc.
- Molten salts: KNO_3-$Ca(NO_3)_2$, K_2CO_3-$MgCO_3$, certain binary and ternary structures of acetates, phosphates etc.
- Aqueous solutions of acids, bases and salts: KOH, H_2SO_4, LiCl etc.
- Metals: metallic glasses include metal-metal alloys and metal-metalloid alloys for example Cu-Zn, Ni-Nb, Fe-B, Pd-Si, Fe-Ni-P-B, etc.

- Chalcogenides: binary systems such as As-Se, As-S, Ge-Se, P-Se etc. Furthermore, complex systems of glasses could be formed by using suitable combination with selenides and sulphides etc.
- Elements: Selenium, sulfur and phosphorous alone are able to form glass.

In order to understand, why certain melts form glasses and what are the criteria to make any material virtually a glass, two sets of theories are available, and will be briefly summarized in the next paragraphs.

2.1.8.1 Structure theories of glass formation

Goldschmidt (1926) [80] proposed that all oxides (of formula X_mO_n) that form glasses have R_c/R_a= 0.2-0.4, where R_a and R_c are the ionic radii of anion and cation, respectively. Furthermore, he believed that only melts with tetrahedral coordination, that is, metal ion is surrounded by four oxygen atoms in tetrahedral shape, form glasses upon cooling. Ionic radius ratio of glass formers is given table 1.

Zachariasen (1932) [80] proposed certain rules for glass forming: 1. The substance contains high amount of cations, which are surrounded by oxygen in trigonal or tetrahedral arrangement. 2. These polyhedral share corners/vertices but neither faces nor edges. 3. Oxygen is linked to no more than two cations. 4. Polyhedral units form a 3-D continuous random network and in this network every polyhedron shares at a minimum of three corners with its neighbors. Furthermore, Zachariasen categorize the cations in three groups: 1- Network formers, for example, Si, P, B, Sb, As, Ge, V etc. having coordination numbers generally 3 or 4. 2- Network modifiers, for example, K, Na, Li, Ba, Ca, Sr etc. having coordination number generally ≥ 6. 3- Intermediates, for example, Al, Ti etc. they either loosen the network (with coordination number 6-8) or reinforce the network (with coordination number 4).

Table 1: Ionic radius ratio of glass formers (Goldschmidt)

Compound	Ionic Radius ratio (R_c:R_a)
SiO_2	R_{Si} : $R_O \approx 0.28$ (where, R_{Si} = 0.39 Å and R_O = 1.4 Å)
B_2O_3	R_B : $R_O \approx 0.15$ (where, R_B = 0.20 Å and R_O = 1.4 Å)
P_2O_5	R_P : $R_O \approx 0.25$ (where, R_P = 0.34 Å and R_O = 1.4 Å)
GeO_2	R_{Ge} : $R_O \approx 0.31$ (where, R_{Ge} = 0.44 Å and R_O = 1.4 Å)
BeF_2	R_{Be} : $R_F \approx 0.25$ (where, R_{Be} = 0.34 Å and R_F = 1.36 Å)

Dietzel (1941) [82] made a classification of cations by introducing a new term called field strength, given as $F_S = Z_c/a^2$

Where Z_c is the charge of cation and a = cation-oxygen distance. Based on field strength it is possible to classify ions as network former, network modifier and intermediates as shown in table 2.

Table 2: Grouping of cations according to field strength [82]

Element	**Valence Z**	**Ionic radius** (Å)	**Coordination number**	**Ionic distance a** (Å)	**Field strength Z/a^2**	**Functionality in glass structure**
Si	4	0.39	4	1.60	1.57	Network formers $Z/a^2 \approx 1.3\text{-}2.0$
B	3	0.20	4	1.50	1.34	
			3	1.36	1.63	
Ge	4	0.44	4	1.66	1.45	
P	5	0.34	4	1.55	2.1	
Mg	2	0.78	6	2.10	0.45	Intermediates $Z/a^2 \approx 0.5\text{-}1.0$
			4	1.96	0.53	
Zr	4	0.87	8	2.28	0.77	
Be	2	0.34	4	1.53	0.86	
Fe	3	0.67	6	1.99	0.76	
			4	1.88	0.85	
Al	3	0.57	6	1.89	0.96	
			4	1.77	1.04	
Ti	4	0.64	6	1.96	1.04	
Mn	2	0.83	4	2.03	0.49	
K	1	1.33	8	2.77	0.13	Network modifiers $Z/a^2 \approx 0.1\text{-}0.4$
Na	1	0.98	6	2.30	0.19	
Li	1	0.78	6	2.10	0.23	
Ba	2	1.43	8	2.86	0.24	
Pb	2	1.32	8	2.74	0.27	
Sr	2	1.27	8	2.69	0.28	
Ca	2	1.06	8	2.48	0.33	
Mn	2	0.91	6	2.23	0.40	
Fe	2	0.83	6	2.15	0.49	

Sun (1947) [80] correlate the bond strength to glass forming ability. He proposed that glass forming oxides have high single bond strength (SBS). That is, during quenching the stronger the bonds (cation-anion), the more challenging is the structural rearrangements, which lead to ease of glass formation. The single bond strength can be obtained by dividing the dissociation energy with number of cation-anion bonds in the coordination unit. The classification of oxides according to their bond strength is:

1. Oxides having SBS values greater than 80 kcal/mol are consider as glass formers (e.g. SiO_2, GeO_2,B_2O_3, P_2O_5)
2. When the SBS values are less than 60 kcal/mol, the oxides are glass modifiers (e.g. Na_2O, K_2O, CaO, MgO)

3. For intermediate oxides, the value of SBS are between 60-80 kcal/mol (e.g. ZnO,TiO_2)

Stanworth (1946-52) [81] presented criteria for glass formability in metal oxide based glasses as:

1. The electronegativity of the cation lies between 1.5 - 2.1.
2. With decreasing cation size the glass forming tendency increase.
3. The valence value of cation is ≥ 3.

SiO_2, GeO_2 and B_2O_3 are well known glass forming oxides and Stanworth's work justifies their ability, for example Si, Ge and B have electronegativity values of 1.9, 2.01, and 2.04, respectively. They have valence values greater ≥ 3 (Si^{4+}, Ge^{4+}, B^{3+}) and finally the cation size is small (Si^{4+}= 0.39 Å, Ge^{4+}=0.44 Å and B^{3+}= 0.2 Å).

2.1.8.2 Kinetic theory of glass formation

All the above empirical approaches provide details about the oxides/compounds which are likely to form glasses, however, in order to understand exactly under what conditions a glass can be formed, it is vital to look into kinetics of the glass forming process. Kinetic theories of glass formation explained the crystal and nucleation growth process and help to understand the conditions which lead to glass formation. It is well documented that all liquids including molten metals can form glasses, but only if the cooling rate is fast enough to avoid the crystallization below the freezing point [83][80]. Likewise, the viscosity plays a dominant role in the glass forming process. Glass formation is promoted if the viscosity of the glass forming material is very high at the melting point or if there is rapid increase in viscosity with decreasing the temperature [80]. Furthermore, the glass formability of different materials can be studied using TTT (Time-Temperature-Transformation) diagrams and the critical cooling rate, i.e. the minimum cooling rate to avoid crystallization which results to formation of a glass.

2.1.8.3 Glasses and Glass-ceramics as joining materials

Glass-ceramics are the materials which are formed by controlled nucleation and crystallization of glass. Glass-ceramics have one or more crystalline and glassy phases. The crystalline phases evolved from the glassy phase and resultant glass-ceramic may have unique properties. They are well established engineering materials and are used for different technical application.

They are potential materials for joining/bonding of different substrates due to:

a) Able to wet a wide variety of substrates including metals, alloys, ceramics and ceramic matrix composites.
b) High thermo-mechanical properties and good hermeticity.
c) High oxidation resistance and low chemical reactivity.

d) Coefficient of thermal expansion (CTE) can be tailored by changing the composition of constituents and by controlling the crystalline phase content.
e) Possibility of joining oxidation resistant substrates (e.g. alumina, zirconia) without the use of vacuum or protective environment (e.g. argon) during joining process.
f) Wide joining temperature window (softening point to melting point) and possibility of pressure less joining.
g) The mechanical properties of joint can be retained up to the softening point of residual glassy phase in glass-ceramic. However, maximizing crystallinity by proper heat treatment and/or introducing small amount of crystallization agents during glass forming (e.g. Zr ions) could further increase their working temperature. Furthermore, at high temperature, near or above the glass transition point, the failure of glass-ceramic joint is not brittle, thus preventing the catastrophic failure of joined assembly.

For joining substrates, the key criteria for selection of particular glass composition are the CTE of the resultant glass-ceramic and softening temperature of the glass. The CTE of the resultant glass-ceramic should match with CTE of the substrate. High differences CTEs could lead to higher residual thermal stresses which could eventually cause failure of joints. Likewise, the softening temperature (T_s) is crucial because at and above the softening temperature the glass have low viscosity properties which could assist in pressure-less spreading and joining of substrates.

Silicate based glass-ceramics have been extensively reported for high temperature applications as sealant for solid oxide fuel cells which operated in a temperature range of 750-800 °C in oxidizing and reducing atmospheres for hundreds of hours without considerable degradation [84]–[91]. Furthermore, silica based glass-ceramics have high mechanical strengths, which is prerequisite for joined components [92][93]. Howard et al. [94] studied the corrosion of silica based glass-ceramics in 85 % steam/15% hydrogen atmosphere with flow speed of ≈ 6 mms^{-1} at 800 °C up to 1000 h. It was concluded that corrosion rate was high for compositions containing alkali metal oxides, zinc oxide and boric oxide, therefore, their quantities should be kept minimum. Hence, corrosion resistance of silica based glass-ceramics can be reduced/controlled by suitable selection of constituents. Glass constituents (network former, intermediates and modifiers) play a major role in modifying properties of glasses and glass-ceramic as summarized in table 3 [95]–[99].

Several researchers used silicate based glasses/glass-ceramic to join oxide ceramics, for example, Tomsia et al. [100] performed wetting experiments on alumina using silicate based glasses in temperature range from 1600-1650 °C and found most of the glasses wet alumina substrate. Zhu et al. [101] joined alumina using silicate based glass in temperature range from 1150-1250 °C. The maximum four-point strength (285 MPa) at RT was obtained at 1200 °C. Lower values were

obtained at 1100 °C and 1250 °C due to presence of pores and cracks at 1100 °C and 1250 °C, respectively.

Table 3: Glass constituents and their general functionality

Glass constituents (Oxides)	General functionality
Al_2O_3	Control the viscosity through rate of crystallization
CaO	Increase CTE, decrease T_g and T_s
MgO	Increase CTE, decrease T_g and T_s
Y_2O_3	Long term CTE stabilizer and viscosity modifier, increase CTE, T_g and T_m
ZrO_2	Nucleating agent, could leds to increase in mechanical strength of glass-ceramic
B_2O_3	Reduce viscosity, T_g and T_s
SiO_2	Decrease the CTE, increase T_s

Esposito et al. [102] joined alumina, zirconia and alumina-zirconia composite to itself using silicate based glasses in temperature range from 1250-1500 °C with two heating cycles and dwell vary from 10 min to 60 min. The presence of pores and cracks in some sample leads to lower strength and wide scattering of flexural strength. The maximum flexural strength (RT) were obtained at 1250 °C,1500 °C and 1450 °C for alumina (228 MPa), zirconia (173 MPa) and alumina-zirconia (250 MPa) composite, respectively.

Borner et al. [70] reported the joining of alumina to alumina and zirconia to zirconia using different silicate glasses using laser joining process and able to yield four-point bending strength (RT) of 158 and 198 MPa for alumina and zirconia, respectively.

Lin et al. [103] reported joining of mullite to mullite and mullite to 3 mol % yttria-zirconia using silicate glass in temperature range 1390 to 1420 °C with a dwell of 1- 5 h. The presence of cracks due to CTE mismatch was observed near the joining interface. The three-point bending strengths (RT) were 139 MPa and 76 MPa for mullite and mullite to 3 mol % yttria-zirconia joints, respectively.

Chiou et al.[104] investigated the effect of glass powder vs organic binder ratio (in glass slurry) on joint strength for zirconia to zirconia joining. The glass slurry was made by blending the 325 mesh sieved glass powder with 70 wt% N-200 ethyl cellulose in butyle carbitol. The joining was performed in temperature range from 1340-1600 °C and glass powder vs organic binder ratio (gp/ob) was less than 1 to 3.17. For gp/ob = 1.82, the strength increase with increasing the joining temperature and maximum three-point bending strength of 300 MPa (approx.) was observed at 1424 °C, above this temperature the joint strength starts to decrease. The decrease in strength was due to diffusion of glass to zirconia and phase transformation of zirconia (from tetragonal to monoclicnic). For gp/ob = 3.17, no simple relation between temperature and flexural strength exist. For gp/ob < 1 the unwetted regions in joining zones and wide scattering of joint

strength was observed. Zirconia to zirconia joining using glass/glass-ceramics has been also reported in [105][106].

Limited literature is available on joining of ox/ox CMC by glasses/glass-ceramics. According to author's best of knowledge, in literature, there are only two studies conducted by Gadelmeier et al.[107][108].In the first study [107], the CerOx ox/ox CMC (Nextel 610^{TM} reinforced zirconia matrix) was joined with commercially available SiO_2-BaO-CaO-Al_2O_3 glass-ceramic using furnace joining technique: however the four-point bending strength (RT) was 32.5 MPa which is only 13 % (approx.) of as received four-point bending strength (263MPa) which could be related to the behavior of zirconia present in matrix. In the second study [108], the CerOx ox/ox CMC was joined by using SiO_2-CaO-Y_2O_3 based commercially available glass-ceramic using CO_2 laser and furnace joining methods, but the reported four-point bending strength was 39 MPa (furnace joined) and 15 MPa (CO_2 laser joined) which was only 11 % (approx.) and 4 % (approx.) of as-received (368MPa) values, respectively.

Chapter 3

Joining of oxide/oxide CMC using metallic brazing fillers

This chapter discusses ox/ox composite (Nextel^{TM} 610/YAG-ZrO_2) joining using commercial nickel-chromium based, silver-copper based and zirconium based metallic brazing system. A new brazing system based on copper-aluminum-titanium metallic interlayers was also developed and used in joining of Nextel^{TM} 610/YAG-ZrO_2. Field emission scanning electron microscope, oxidation tests and mechanical testing was performed to evaluate the suitability and performance of metallic brazing systems.

Part of the work described in this chapter is already published by author (M. Y. Akram *et al.*, "Journal of the European Ceramic Society Joining and testing of alumina fibre reinforced YAG-ZrO_2 matrix composites," vol. 38, no. November 2017, pp. 1802–1811, 2018).

3.1 Oxide/oxide ceramic matrix composite

Two types of oxide/oxide ceramic composites were used in this study. Both these composite were designed and manufactured by Department of Ceramic Material Engineering; University of Bayreuth, Germany, using different manufacturing techniques and compositions. The detail are available in [11] and are summarize below.

3.1.1 Nextel^{TM} 610/YAG-ZrO_2 ceramic composite

This composite was prepared using aqueous freeze casting technique. The reinforcement used in the composite was alumina based (> 99 % alpha-alumina) Nextel^{TM} 610, DF11, 8 harness, 8 layer, 2D Satin fabric woven from continuous filament roving of 1500 denier (3M Corporation, US). The specifications of Nextel^{TM} 610 reinforcement are summarized in table 4 [109] .

Table 4: Physical properties of Nextel^{TM} 610

Physical property	Value
Density	3.9 g/cm^3
Thickness	0.25 mm
Coefficient of thermal expansion (100-1100 ^oC), Linear	8 x10^{-6} K^{-1}
Melting point	2000 °C
Tensile strength at break (25.4 mm gauge)	2800 MPa
Filament tensile modulus	370 GPa
Crystal Phase	α- Al_2O_3
Crystal size	< 500 nm
Weight (Heat treated) DF11 (1500 denier)	370 g/cm^2
Weight (Heat treated) DF19 (3000 denier)	610 g/cm^2
Thread count DF11 Warp and Fill	11 warp and 11 fill (per cm)
Thread count DF19 Warp and Fill	9 warp and 9 fill (per cm)
Creep limit temperature °C (Single filament ≤ 1% strain under 69 MPa after 1000 h) (Continuous use temperature)	1000 °C

The matrix was composed of Yttrium aluminum garnet (YAG,$Y_3Al_5O_{12}$) stabilized with zirconia. The Nextel 610^{TM} (Alumina), YAG and Zirconia system is thermally stable. YAG powder with average particle size 1µm is consolidated with nano powder zirconia having average particle size of 0.1 µm. In order to develop composite the suspension was prepared with ceramic powder and 1 wt % polyacrylic acid (Sokalan PA15, BASF, Germany) as netting and dispersant agent. The particle loading was adjusted to 75 wt % and slurry was homogenized for approx. 12 h using rolling machine assisted with 3 mm diameter zirconia ball. The glycerol was selected as cryoprotectant which modifies the crystallization and avoids the expansion of water during freezing. To adjust the pore size/ dimension of crystal growth 0.25 wt % Gelatin (Gelita Novotec 100, 85 g Bloom, Gelita Deutschland GmbH, Germany) was added with respect to slurry quantity and then slurry was heated to 60 °C to dissolve the added gelatin. The addition of gelatin also enhanced the strength of green body. The slurry is subsequently cooled to 40 °C to avoid water evaporation and then transferred to ultrasonic bath where infiltration of Nextel^{TM} 610 was performed. The laminated fabric was press to defined size to obtained the fiber volume of 40%. The temperature was lowered to -70 °C and green composite was removed from mold and freeze-dried (Laboratory freeze drier ALPHA 1-4 LSC, Martin Christ, Germany) and then subsequent sintering was performed at 1225 °C. Densification of composite matrix was obtained by performing up to three vacuum infiltration cycles with zirconia precursor (zirconium IV butoxide solution, 80 wt % in 1-butanol, Alfa Aesar Gmbh & Co KG, Germany) in an exsiccator with 50 mbar. To hydrolyze the precursor, after infiltration and before sintering, the composite was stored for 12 h

in air. The sintered composite has density of 2.94 g/cm^3, apparent porosity of 30.9 vol% and fiber volume fraction of 37%. After the three infiltration cycles, the resulting composite have bending strength (using EN 658) of approx. 304 MPa (± 23 MPa), interlaminar shear strength of 11.7 MPa (± 1 MPa) and undergo a non-brittle fracture during flexural testing with tensile fracture mode. The CTE of composite was 8.7 x10^{-6} K^{-1} (125 °C -500 °C) and 8.9 x10^{-6} K^{-1} (125 °C - 900 °C). Further details of this composite can be find in [11].

3.1.2 Nextel ™ 610/alumina-zirconia ceramic composite

In this composite the Nextel™ 610 2D, DF19, 8 harness, 6 layer, 2D Satin fabric woven from continuous filament roving of 3000 denier were used. The matrix was composed of 75 wt % alumina and 25 wt% zirconia contents. The slurry was prepared with 66.3 wt% of solid contents. The 25 wt% of solid content was consisted of 3 mol % yttria stabilized zirconia (3YSZ) (TZ-3Y-E, Tosoh, Japan, purity level > 99.99 %).The mean particle size of 3YSZ was 0.5 µm. In remaining 75 wt% of solid contents, 70 wt% was consisted of alumina with mean particle size of 0.7 µm (CT 3000 SG, Almatis, Turkey, purity level >99.7 %) while remaining 5 wt% was consisted of fine grained alumina with mean particle size of 0.1 µm (TM-DAR, Taimicron, Japan, purity level > 99.99 %).The remaining 33.7 wt % slurry was consisted of 1 wt % dispersant agent (Sokalan PA 15, BASF, Germany) while 26 wt% was glycerin (AnalaR NORMAPUR®, VWR, Germany, purity level ≥99.5%) and remaining was distilled water. To obtain complete infiltration the slurries were ball milled until the mean particle size was lower than 1 µm and maximum particles size was less than 5 µm. The Nextel 610™ reinforcements was then impregnated in the slurry with the aid of brush and slurry contents were defined using a doctor blade with gap of 800 µm over the prepegs. To obtain a final oxide/oxide CMC thickness of approximately 2 mm six prepegs were laminated. Each lamination stage comprise of several steps, using different roller gap in each step. After lamination, the green bodies were dried in drying cabinet (FDL 115, Binder, Germany) for 12 h at 100 °C. Finally the sintering was performed in air at 1225 °C for 2 h.

3.2 Metallic brazing systems

All the metallic brazing alloys were used with Nextel™ 610/YAG-ZrO_2 based oxide/oxide CMC only. The details of brazing alloys and their characteristic properties are reported in Table 5 and Table 6

3.2.1 Nickel-Chromium based systems

Two commercial metallic glasses, nickel-chromium based brazing materials, namely MBF 51 and MBF 80, were initially shortlisted due to well established oxidation and corrosion resistance behavior of Ni-Cr systems [110]. The NiCr

based metallic glass based system were utilized in joining of C/C, C/SiC and SiC/SiC CMCs [111], but never reported to use for joining of ox/ox CMCs. Furthermore, the recommended brazing temperatures of these two systems were below the sintering temperature (1225 °C) of Nextel^{TM} 610/YAG-zirconia CMC. Above sintering temperature, the grain coarsening started to occur which modified the microstructure and may affect the mechanical properties of the substrate. According to manufacturer (Metglas Inc.,USA) these brazing systems were produced by rapid quenching of molten metal at a very high rate i.e. greater than 1000000 °C sec^{-1} which produced uniform and ductile brazing foil [112]. The details of MBF 51 and MBF 80 (supplied by Hitachi metals Europe GmbH, Germany) are given in table 5.

3.2.2 Silver-Copper based system

Active brazing systems based on Ag-Cu-Sn-Ti (TKC 651, Tanaka, Japan) was selected. The advantage of using Ag-Cu system is that it has low eutectic temperature (780 °C) and has ductile properties which can limit the thermal stresses due to difference in CTE of the substrate and brazing alloy. However, this system requires addition of active element (e.g. Ti) for wetting of oxide ceramics such as YAG[50], zirconia[113] and alumina[114].Since the ox/ox CMC is a α-alumina/YAG-zirconia system, it was expected that AgCuSnTi wet the Nextel^{TM} 610/YAG-ZrO_2 CMC which is prerequisite for the formation of mechanically sound joints.

Table 5: Composition and properties of selected commercial brazing systems [112]

Designation	MBF 80	MBF 51	TKC 651	Ti braze590
Composition (wt%)	Ni-15Cr-0.06C-4B	Ni-15Cr-7.3Si-0.06C-1.4 B	Ag-28Cu-5Sn-2Ti	Zr-17.3Ti-20 Ni-1Hf
Solidus (°C)	1048	1030	---	796
Liquidus (°C)	1091	1126	780	813
Recommended brazing temp. (°C)	1120	1195	790-850	> 900
CTE 10^{-6} K^{-1} (RT-500 °C)	Not known	Not known	19.5	8.8
Density (g/cm^3)	7.94	7.73	9.6	6.72
Thickness (µm)	38	40	100	50

(www.pro.tanka.co.jp), (www.princeizant.com)

3.2.3 Zirconium-Nickel-Titanium based system

A commercial brazing system based on zirconium-nickel-titanium (Ti braze 590, Titanium Brazing, Inc., USA) was selected due to matching CTE with Nextel^{TM} 610/YAG-ZrO_2 composite and heat resistance up till 550 °C for long term and 650 °C for short term. Further, due to presence of active elements such as titanium and zirconium it was expected that this brazing alloy wet the Nextel^{TM} 610/YAG-ZrO_2 composite [115]. Moreover, with this brazing alloy, the shear strength of brazed joints for titanium to titanium and Ti6Al4V to Ti6Al4V can reach up to 200 MPa [116].

3.2.4 Copper-Titanium-Aluminum based system

The new system based on TiCuAl (metallic foils suppliers; Sigma Aldrich and Alpha Aesar) was developed for brazing of Nextel^{TM} 610/YAG-ZrO_2. The rationale behind selection of this system was based on the fact that the Cu-Ti system is capable to wet the oxide ceramics and addition of Al can increase the oxidation resistance of this system. It is well established in literature that Al containing alloys have the capabilities to develop thermodynamically stable protective scale of α-Al_2O_3 even at low partial pressures of oxygen [117][118]. This oxide scale has strong adherence, low defect densities and low growth rate and remain protective at high temperature (approx.1400 °C) for longer operational hours in air [118]. Ding et al. [119] reported the improvement in the oxidation resistance of pure Cu by just adding 1 at% of Al. Tannyan et al. [120] investigated the oxidation of Cu and Cu-Al alloys in temperature range from 700-1000 °C in air and found that addition of 3 wt % Al in Cu-Al alloy oxidized 100 times lower than the pure Cu [121]. Furthermore, Akimov et al. [122] examined the addition of 2-12 at% Al in Cu-Al and observed oxidation in temperature range of 267 °C to 697 °C at low oxygen partial pressures (5 x 10^{-7} to 5 x 10^{-4} mbar). It is found that a very uniform layer of Al_2O_3 was developed on the alloy surface with addition of 12 at % Al in Cu-Al alloys. Based on these studies, it was decided to add approximately 8 wt % Al in TiCuAl brazing alloy.

Jasim et al.[123] inspected the joining of alumina with several CuTi based alloys (Cu 2wt% Ti, Cu 4wt% Ti, Cu 6wt% Ti, Cu 8wt% Ti and Cu 10 wt% Ti) and found that highest RT shear strength was obtained with Cu 10 wt% Ti. Keeping this in view, 10 wt % titanium was selected as optimum amount for TiCuAl system. The thickness of metallic alloys was selected to obtain an alloy with Cu-11.7 T i-8.2 Al wt % composition. An interlayer metallic foils approach, as shown, in figure 14 was adopted. Due to limitation in commercial availability of thicknesses of foils, the wt % of Al and Ti was not exactly 8 wt % and 10 wt %, but 8.2 wt% and 11.7% respectively for TiCuAl brazing alloy. As copper is the main constituent (approx. 80 wt%) in TiCuAl system so the brazing temperature was selected on the basis of melting point of the copper. The details are given in table 6.

Table 6: Specification and brazing conditions of TiCuAl system

Designation	TiCuAl
Composition	Cu-11.7 Ti-8.2 Al (Wt% approx.)
Brazing temperature (°C)	1100 (based on melting point of Cu)
Thickness of foils	Cu = 100 µm,Ti = 30 µm and Al = 60 µm

3.3 Experimental

The brazing alloys/metallic foils were cut in 10 mm x 10 mm size while Nextel^{TM} 610/YAG-ZrO_2 composite samples have dimension of 10 mm x 10 mm x 2 mm. The brazing alloy or metallic foils and composite were cleaned ultrasonically with acetone for 15 minutes. The brazing alloys or metallic foils were then sandwich between the composite as shown in figure 13 and figure 14. A tungsten weight of 50 g was placed on the top of assembly to ensure alignment.

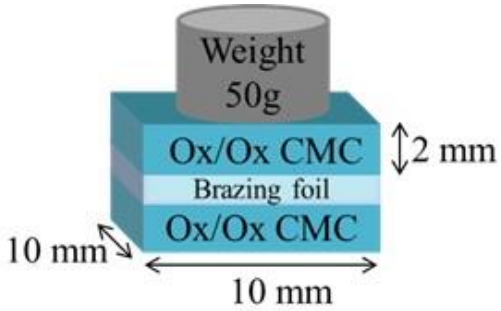

Figure 13: Joining configuration of Nextel^{TM} 610/YAG-ZrO_2 using different commercial brazing foils.

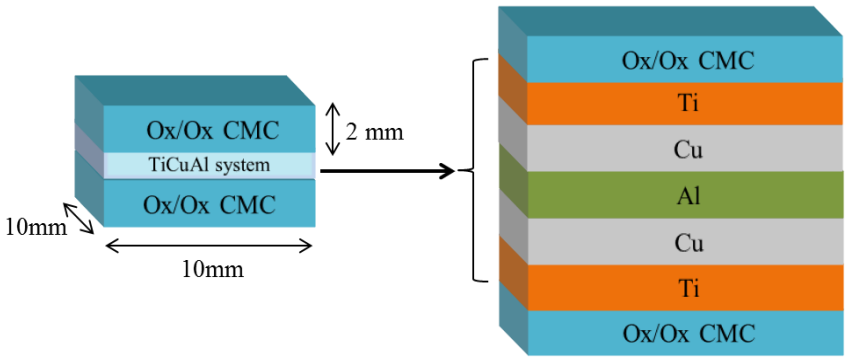

Figure 14: Joining configuration of Nextel^{TM} 610/YAG- ZrO_2 using TiCuAl brazing system.

Table 7: Heating treatment parameters for different brazing materials [124]

Braze materials	Heat treatment (in Argon)		
	Joining Temp. (°C)	Dwell (min)	Heating rate and cooling rate (°C min^{-1})
MBF 51	1195	15-60	16.67
MBF 80	1120	15-60	16.67
AgCuTi	850	15	16.67
AgCuSnTi	900	10	16.67
ZrNiTiHf	920	30	16.67
TiCuAl	1100	10	16.67

For the preliminary oxidation test, the joined samples were placed in static air furnace (Carbolite 1300, UK) and the temperature was raised to 550 °C with heating rates of 16.67 °C min^{-1} and hold for 1 h while the cooling rate was 16.67 °C min^{-1}.The samples were removed from the furnace, polished and observed under FESEM.

To observe the mechanical properties of joined samples, a single lap off-set (SLO) shear test were performed in triplicate on joined samples in each case. The tests were conducted with Universal Testing Machine (SINTEC D/10) with cross head speed of 0.5 mm/min. The samples dimensions were 13-14 mm x 4 mm x 2 mm and joined area varied from 36 m^2 to 40 m^2 approximately as shown in the figure 15.

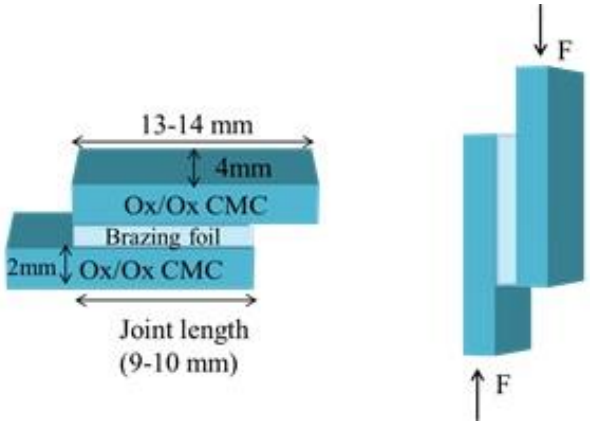

Figure 15: Joined samples configuration for single lap off-set shear test

3.4 Results and discussion

3.4.1 Joining with MBF 51 and MBF 80 brazing alloys

The joining experiments with Ni-Cr based brazing material (MBF 51 and MBF 80) were initially performed with 10 min dwell time, however, the MBF 51 and MBF 80 failed to wet the Nextel^{TM} 610/YAG-ZrO_2 composite. In one study,it

is reported that the wetting angle of Ni-Cr-Co-Mo-Ti based brazing alloys on oxide ceramic such as alumina, decreases with increasing of dwell time and temperature [125]. Keeping in view this result, the brazing dwell time was increased to 30 min and then to 60 min for both MBF 51 and MBF 80. Furthermore, the brazing temperature of MBF 80 was also increased from 1120 °C to 1150 °C and 1175 °C with dwell of 30 min and 60 min; the brazing temperature of MBF 51 was not increased because its brazing temperature, 1195 °C, was already approaching the sintering temperature (1225 °C) of Nextel^{TM} 610/YAG-ZrO_2 composite. However, under all these conditions both brazing alloys failed to wet the Nextel^{TM} 610/YAG-ZrO_2 composite. This may be due to the presence of strong ionic and covalent bonds as well as absence of free electrons in ceramics, which provide chemical inertness and low wettability towards molten metals. Furthermore, non-wetting may also be associated with absence of reactive species (Ti, Zr etc) in these brazing fillers. These reactive species can wet the oxide ceramics by thermodynamically favorable reduction of oxides surfaces [126]. A similar result has been reported in which molten NiCr alloy yield non-wetting equilibrium angles of 148°, 154°, 157° for Y_2O_3, Al_2O_3 and ZrO_2 respectively, even at much high temperature of 1500 °C in vacuum with dwell time of 17 min, approximately [125].

3.4.2 Joining with TKC 651 brazing alloy

The joining of Nextel^{TM} 610/YAG-ZrO_2 composite with and TKC 651(AgCuSnTi) is shown in the figure 16. The joining interface is continuous and free from voids, confirming that AgCuSnTi brazing alloy readily wet the composite.

From the EDS analysis shown in the figure 17, two distinct regions are visible, i.e. Cu rich Ag-Ti zone at the joining interface and Ag-rich Cu zone away from the interface towards the center [127]. EDS at point 1, shows that there is no clear evidence of diffusion of brazing alloy in the composite. In order to further investigate diffusion, a line scan was performed at the AgCuSnTi/composite interface as shown in the figure 18. From the line scan and EDS analysis, it was concluded that Cu rich AgTi compound could be responsible for the wetting of this composite.

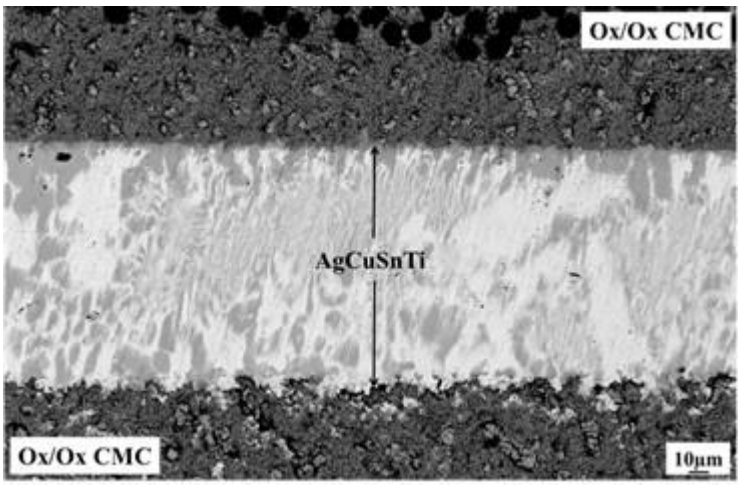

Figure 16: Joining of Nextel^{TM} 610/YAG-zirconia with TKC 651

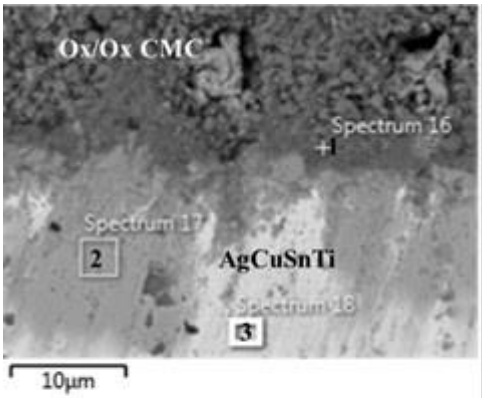

Element	Weight %			Atomic %		
	1	2	3	1	2	3
Cu	0	85.25	9.96	0	80.24	12.11
Ag	0	5.67	81.49	0	3.15	58.33
Ti	0	1.16	0	0	1.45	0
Sn	0	4.46	2.80	0	2.25	1.82
Al	18.01	0	0	19.07	0	0
Y	36.05	0	0	11.58	0	0
Zr	8.61	0	0	2.70	0	0
O	37.33	3.46	5.75	66.65	12.92	27.75

Figure 17: EDS analysis of different zones at Nextel 610^{TM}/YAG-zirconia /AgCuSnTi interface

Furthermore from the EDS, it is clear that Ti is found only in copper rich zone at the interface. Several authors reported the formation the Ti_XO_Y, based compounds at the interface when joining YAG, ZrO_2 and Al_2O_3 with AgCuTi based brazing filler, identified through Transmission Electron Microscopy (TEM) [127][128][49].

As shown in the figure 18, the presence of high concentration of titanium at the interface as well as 2 µm towards the composite and simultaneous presence of oxygen in this zone may support the possible formation of Ti_XO_Y compounds which could not detectable through SEM-EDS analysis.

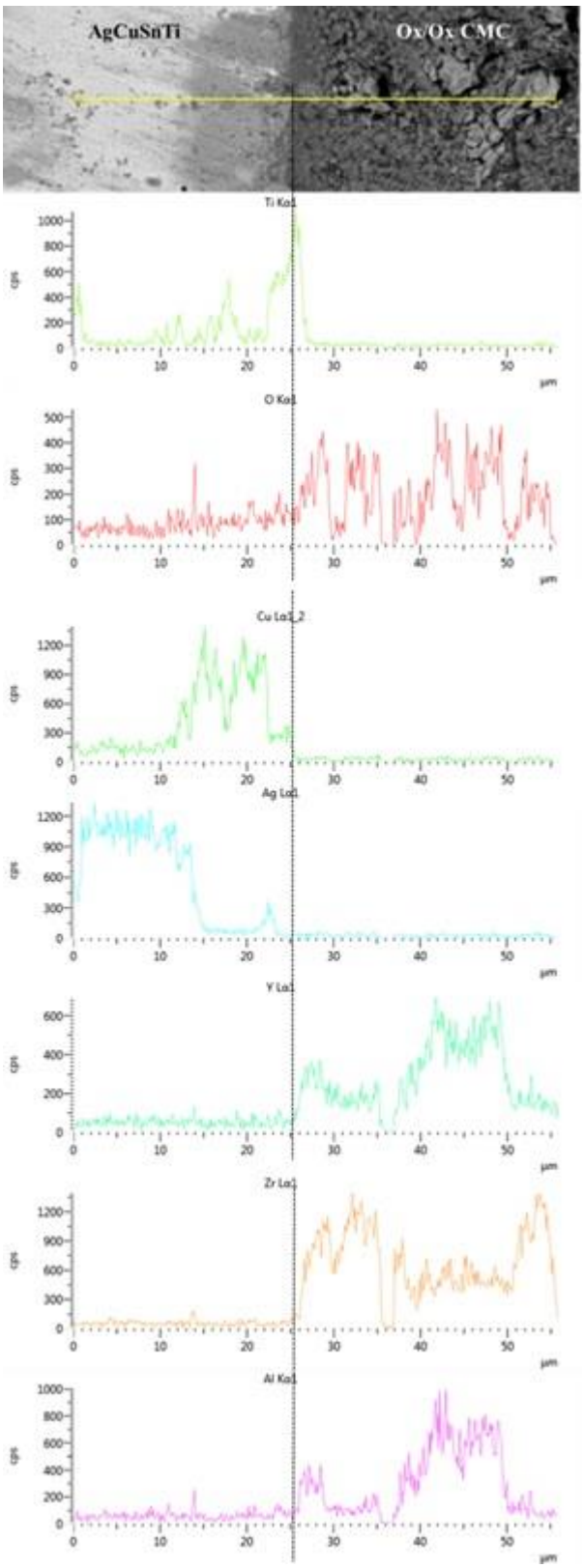

Figure 18: EDS line scan of Nextel^{TM} 610/YAG-ZrO_2 /AgCuSnTi interface

The titanium acts as oxygen getter and it is possible that stable oxides of titanium can be formed even at low partial pressure of oxygen $pO_2 \approx 10^{-28}$ atm [129]. These oxides might not be formed by reduction of ZrO_2 or YAG by Ti because it is not thermodynamically favorable at this brazing temperature due to

positive Gibbs free energy (ΔG°) values (Approx. 16 kJ/mol to 145 kJ/mol) at 900 °C, as given in table 9, from [54] and figure 19.

However, due to the possible presence of residual oxygen in the furnace atmosphere, and air entrapped in the porous Nextel 610^{TM}/YAG-ZrO_2, the likelihood of forming these oxides cannot be ignored. From the work of Chang et al. [130], it is possible to find the standard Gibbs free energy change (ΔG°) of different titanium oxides at 900 °C which are reported in table 8 and are consistent with the work of Xin et al.[131]. These negative values (table 8) show that formation of titanium oxides is thermodynamically favorable at brazing temperature.

Table 8: Formation of different titanium oxides at 900 °C [130]

Possible Reaction	**ΔG° (kJ/mol) at 900 °C**
$2Ti + O_2 = 2TiO$	-830 approx.
$Ti + O_2 = TiO_2$	-708 approx.
$2Ti + 1/2O_2 = Ti_2O$	-955 approx.
$4/3Ti + O_2 = 2/3Ti_2O_3$	-798 approx.
$6/5Ti + O_2 = 2/5Ti_3O_5$	-774 approx.

Table 9: Formation of different titanium oxides at 900 °C by zirconia reduction [54]

Possible Reaction	**ΔG° (kJ/mol) at 900 °C**
$ZrO_2 + 2Ti = Zr + 2TiO$	+16 approx.
$ZrO_2 + Ti = Zr + TiO_2$	+145 approx.
$ZrO_2 + 4/3Ti = Zr + 2/3Ti_2O_3$	+80 approx.
$ZrO_2 + 6/5Ti = Zr + 2/5Ti_3O_5$	+104 approx.
$ZrO_2 + 8/7Ti = Zr + 2/7Ti_4O_7$	+115 approx.

Furthermore, some studies also suggested the formation of sub-stoichiometric O-deficient ZrO_{2-X} compound due to reaction of active titanium with oxygen ions (from zirconia) according to reaction given in [128][132].

$$ZrO_2 + XTi = ZrO_{2-X} + XtiO$$

Pereira et al. [133] reported that this reaction is thermodynamically favored at 880 °C and have ΔG° value of -12.2 KJ/mol. This temperature is very close to brazing temperature (900 °C) of the system and it could be assumed that ΔG° could also be negative at 900 °C. Hence this reaction may proceed at the interface during brazing of Nextel 610^{TM}/YAG-ZrO_2 with AgCuSnTi. According to Ti-O phase diagram the titanium dissolve almost 34 atomic% of oxygen, so it is possible that as the concentration of dissolved oxygen in titanium increase, the formation of other oxides of titanium could also be possible [128].The formation of copper-titanium phases such as Ti_3Cu_3O or Ti_4Cu_2O, though have high ΔG°

near the brazing temperature [133], could not be possible due to very small percentage of titanium detected during EDS analysis.

Furthermore, other than titanium, no elements of the brazing alloy and composite (Al, Zr, Y) diffused towards or away from the composite, respectively. This may represents the suitability of the brazing alloy and Nextel 610^{TM}/YAG-ZrO_2 as far as joining is concerned.

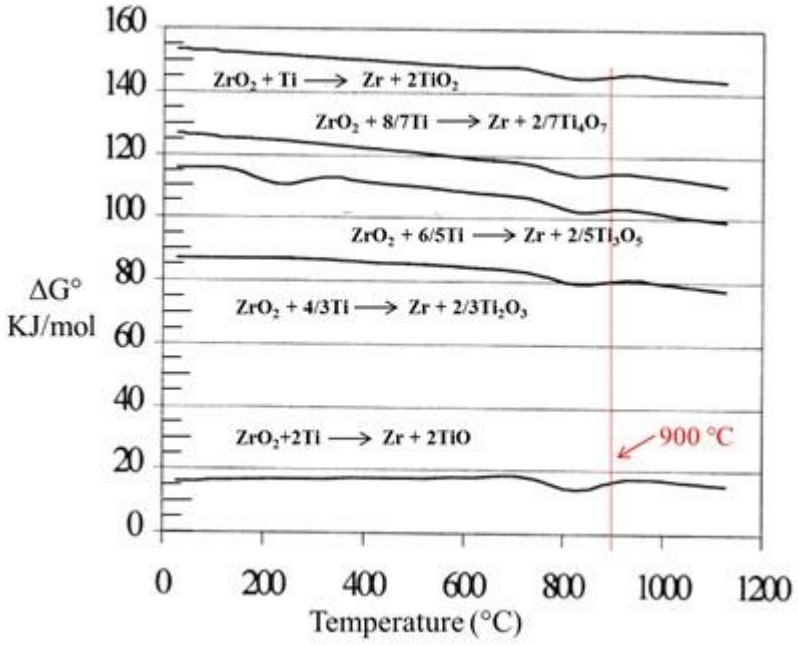

Figure 19: ΔG° values for possible reaction between zirconia and titanium at different temperatures

3.4.3 Joining with TiB 590 brazing alloy

Figure 20 shows the SEM micrograph of Nextel^{TM}610/YAG-ZrO_2 composite joined with ZrNiTiHf brazing filler. A defect free continuous joining is observed without any evident reaction zone at the interface as shown in figure 20.

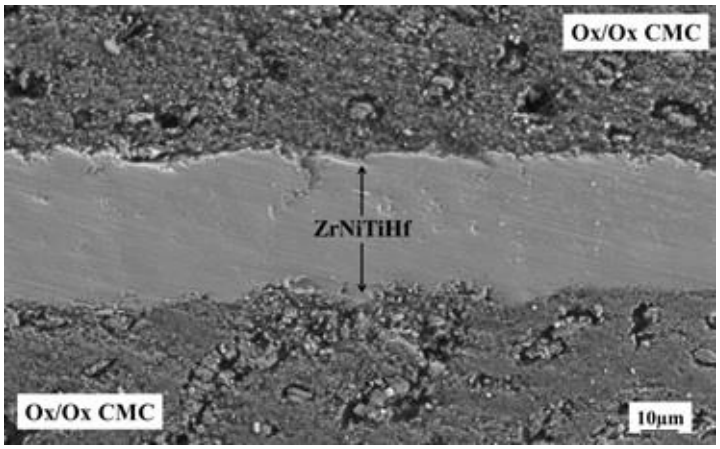

Figure 20: SEM micrograph of Nextel 610TM/YAG- ZrO_2 joined with ZrNiTiHf

As shown in EDS in figure 21, at point 1 and point 2 the composition is similar to as-received brazing alloy however at interface (at point1) there are some evidence of very small amount of diffusion of composite element with ZrNiTiHf brazing alloy especially Yttrium (Y) which is also evident in line scan (figure 22).

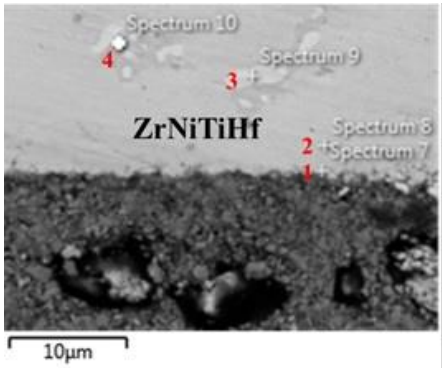

Element	Weight %				Atomic %			
	1	2	3	4	1	2	3	4
Zr	56.34	58.51	66.40	49.76	31.28	34.15	41.47	29.89
Ni	16.59	17.80	8.99	21.45	14.31	16.14	8.73	20.02
Ti	12.11	13.15	15.18	20.23	12.80	14.62	18.07	23.14
Hf	0.33	0	0.56	0.76	0.09	0	0.18	0.23
Al	0.67	0	0	0	1.25	0	0	0
Y	1.52	0	0	0	0.87	0	0	0
O	12.44	10.55	0	7.80	39.39	35.10	0	26.72

Figure 21: EDS analysis of different zones near Nextel^{TM}610/YAG-ZrO_2 /ZrNiTiHf interface.

As shown in figure 22 (line scan) it seems that very small amount of titanium also diffused few microns inside Nextel^{TM} 610/YAG-ZrO_2 composite. Gambaro at al. [50] proposed the formation of $Ti_2Y_2O_5$ compound at 1050 °C by reaction of YAG with titanium from brazing alloy according to reaction:

$$Ti + 2Y_3Al_5O_{12} = 3TiY_2O_5 + 3Al_2O_3 + 4Al$$

However, due to very small amount of yttrium detected at the interface in EDS, this reaction seems to not occur in this case. In another study, Gambaro at el.[134] reported some difficulty in precisely predicting the reaction layer at interface through SEM-EDS analysis during brazing of YAG with titanium containing brazing alloy at 850 °C. Therefore, for brazing of Nextel 610^{TM}/YAG-ZrO_2 composite with ZrNiTiHf brazing filler it can be concluded that even with a very high amount of active elements (Ti and Zr) in the brazing filler the diffusion could not be enough to initiate phase formation at brazing alloy/YAG-ZrO_2 interface for the selected brazing conditions. Nevertheless, due to high affinity of titanium for oxygen it might be possible that different oxide of titanium Ti_YO_X may be formed at the interface as discussed in section 3.4.2. Furthermore, Zr may also react with ZrO_2 present in the composite matrix to produce sub-stoichiometric O-deficient cubic ZrO_{2-X} compound ($O \leq X \leq 0.44$) and ZrO by the following reaction [133] [135][132]:-

$$ZrO_2 + XZr = ZrO_{2-X} + XZrO \quad (\Delta G° = -12.2 \text{ kJ/mol at } 880 °C)$$

The heat of formation of zirconium oxide by reaction of metallic zirconium with oxygen is second highest in 4d transition metals [136].

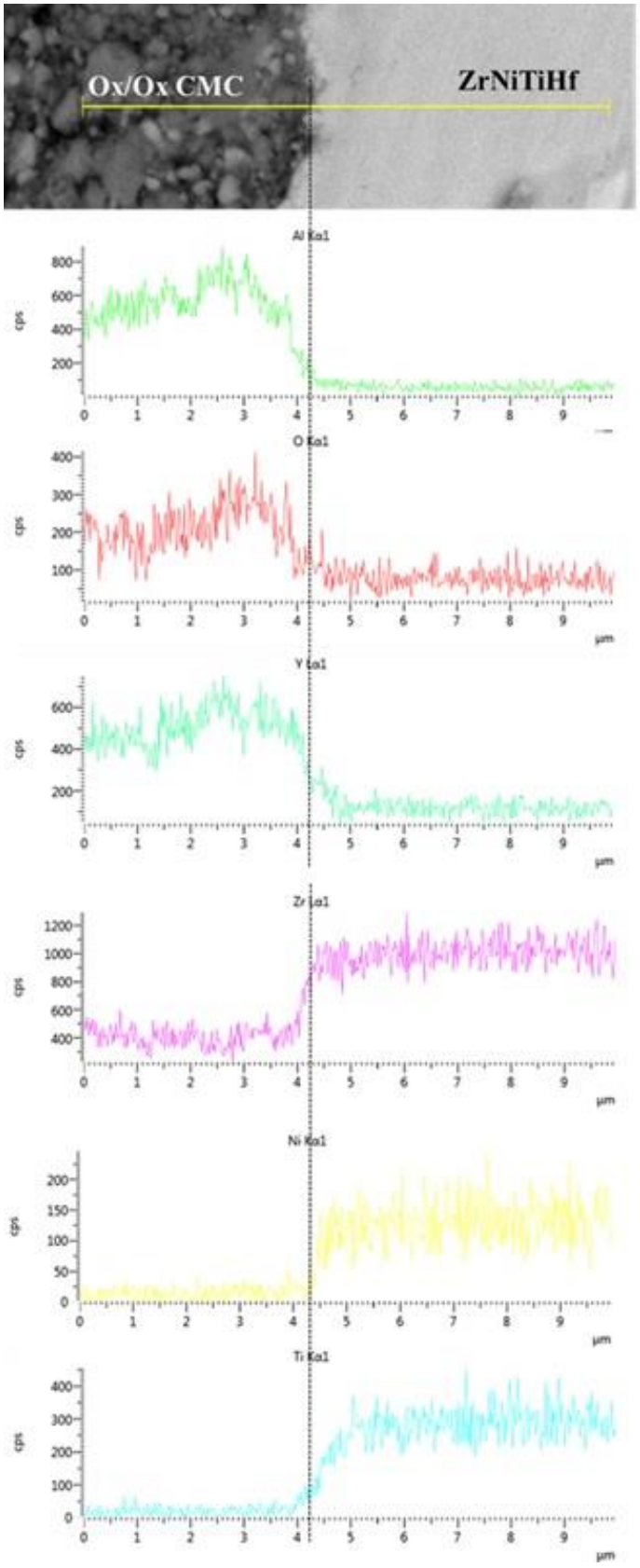

Figure 22: EDS mapping of Nextel^{TM} 610/YAG-ZrO_2 and ZrNiTiHf interface.

Furthermore oxygen has high solubility in zirconium and titanium as shown in Ti-O and Zr-O phase diagrams reported in figure 23 [137][138], so the release of oxygen due to above reaction and oxygen present in furnace atmosphere could further react with titanium and or zirconium to produce the different oxides. High amount of oxygen is also detected in zone 2 and zone 4 as shown in EDS analysis (figure 21) which may also indicate the formation of oxides in these zones. In comparison to as-received composition of brazing alloy, the zone 3 has quite lower amount of nickel, while zone 4 has lower amount of zirconium. Since these zones are small and without any evidence of diffusion of composite constitutes (Y, Al, Zr) so it might be possible that these areas are formed due to some variation within the composition of brazing alloy.

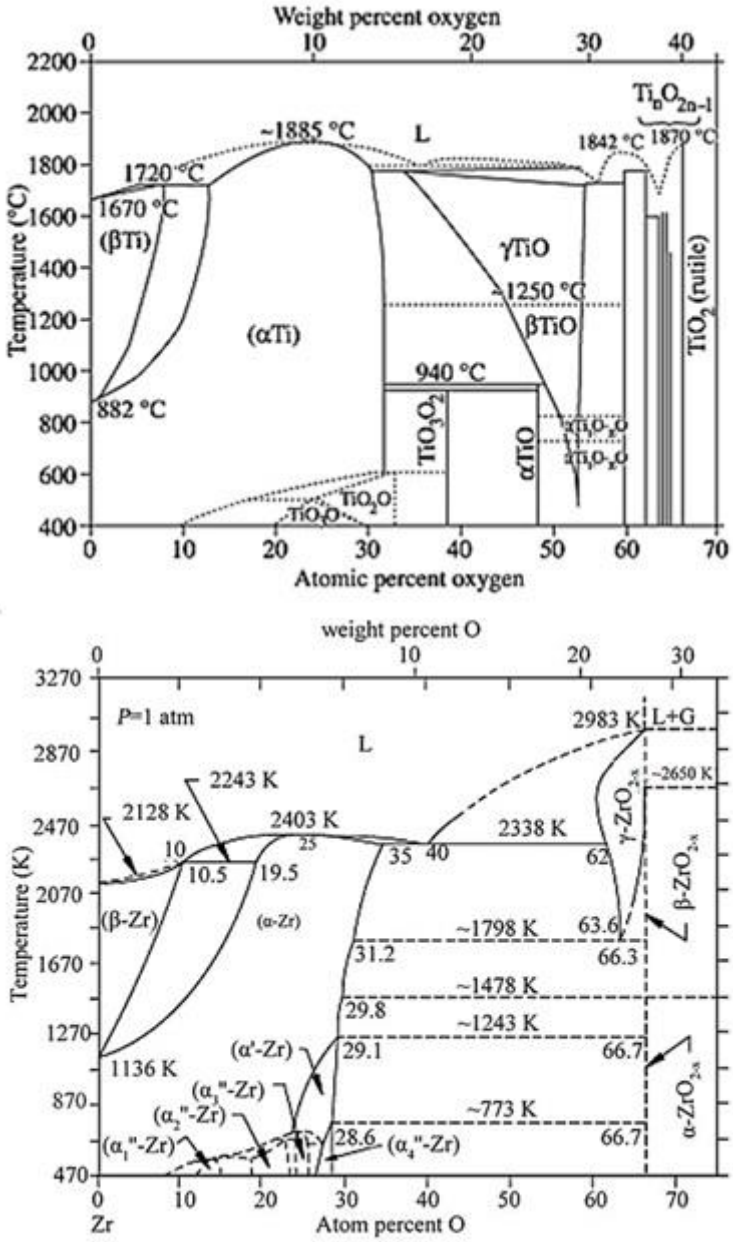

Figure 23: Phase diagrams of Ti-O and Zr-O [137][138]

3.4.4 Joining with TiCuAl brazing system

The SEM micrograph of the Nextel 610^{TM}/YAG-ZrO_2 joined with TiCuAl brazing system is shown in figure 24 a. The joint is well bonded and free from cracks and discontinuities. During the brazing process some of the molten alloy flow out of the sides of composite thus reduces the overall thickness of joining seam.

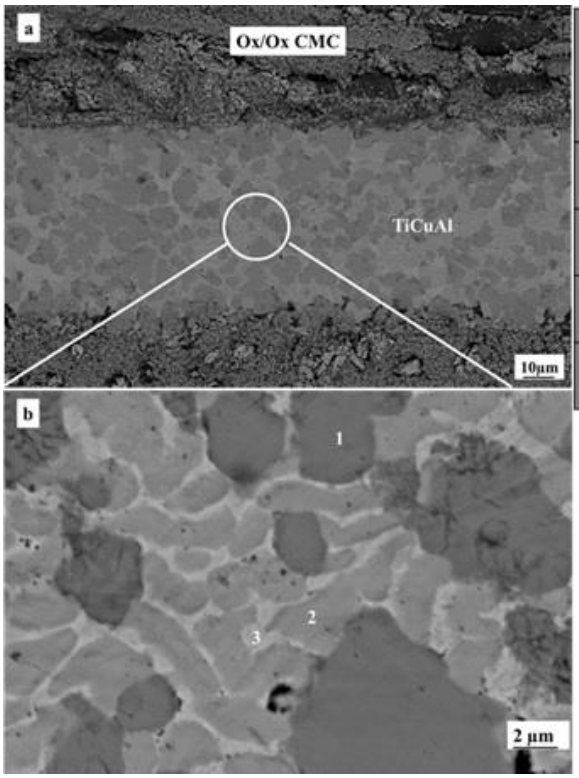

Element	Weight %			Atomic %		
	1	2	3	1	2	3
Cu	37.31	60.06	82.21	22.08	40.53	65.14
Al	6.82	8.77	6.99	9.50	13.94	10.63
Ti	40.18	21.29	3.51	31.54	19.06	1.75
O	15.69	9.88	7.29	36.88	26.47	22.42

Figure 24: EDS analysis of different zones in TiCuAl brazing system

The EDS analysis (figure 24) shows the presence of three distinct zones uniformly distributed in the brazing seam. Zone 1 is a titanium rich zone and is also present exclusively at the composite/ TiCuAl interface. In this zone, along with Cu and Al, a high amount of oxygen is also present. As discussed in section 3.4.2 the oxygen source may be due to presence of residual air in the furnace and/or air trapped inside the pores of composite. Due to presence of oxygen, the possibility of formation of Ti_3Cu_3O and oxides of titanium could not be neglected [133][139]. The ΔG° value for Ti_3Cu_3O formation is -440 kJ/mol at 880 °C [133]. Kelkar et al. [140] proposed that up to 15% of Al is soluble in Ti_3Cu_3O and subsequently form Ti_3Cu_2AlO. The composition of the zone 1 could be related to the composition of Ti_3Cu_2AlO phase reported by Yang et al. [141] as shown in table 10. Therefore, it is concluded that zone 1 could be Ti_3Cu_2AlO and possibility of formation of oxides of titanium and Ti_3Cu_2AlO could be possible which contribute to wetting of Nextel^{TM} 610/YAG-ZrO_2. From the stoichiometry

of elements in zone 2 it is difficult to predict the exact phase; however the possible phases could be Cu (s.s)+ Ti_2Al or $TiCu_2Al$. The zone 3 is a copper rich zone, possibly Cu (s.s) [142].

Table 10: Comparison of composition of zone 1 with studies of Yang et al.[141]

Elements	Atomic % (Yang et al.)	Atomic % (This study)
Cu	27.02	22.08
Ti	43.02	31.54
Al	15.38	9.50
O	14.57	36.88

3.4.5 Oxidation tests

Even though the joining of ox/ox with the brazing alloys was intended for oxygen free applications, some oxidation tests were conducted in air furnace at 550 °C for one hour, for completeness with the following glass-ceramic based joining materials which will be discussed in the following chapterS.

The tests revealed that the samples brazed with AgCuSnTi alloy were completed debonded. At the AgCuSnTi/composite interface, copper rich zone was detected in the EDS and reported in figure 17. During oxidation test it might be possible that copper reacts with oxygen to form Cu_2O and CuO according to following reactions[143]

$$4Cu + O_2 = 2Cu_2O$$
$$2Cu_2O + O_2 = 4CuO$$

The formation of these oxides were also reported by J.Wang et al. [144] when investigating the oxidation of copper in temperature range from 500 °C to 700 °C at 1 atm with Cu_2O as predominating phase and CuO is present in small quantity. X.Jiang et al. [145] also reported the formation of Cu_2O as main phase when oxidation of copper was performed at 500 °C in air. The Cu_2O have a volume expansion 60% greater than that of pure copper and due to this expansion cracking could be possible which may lead to debonding of joining surfaces [120]. Furthermore, the CTE of Cu and Cu_2O are approximately 17 x 10^{-6} K^{-1} and 4x10^{-6} K^{-1} respectively and this difference may cause physical separation of Cu_2O layer from Cu which may contribute towards debonding [120]. R.R.Kapoor et al. [146] investigated the Ag-Cu based alloy oxidation at 600 ^{0}C and also found the formation of copper oxide scale which spalled off due to oxidation.

In case of ZrNiTiHf braze joint the complete oxidation of brazing material occurred and brazing material turns to black ash-like product. G.Balat et al.[147] investigated the thermal oxidation of ZrTi alloys at 500 °C for 2h and found that a very thick TiO_2/ZrO_2 layer of approximately 80µm was formed on Zr25Ti in just 2h. Furthermore, this TiO_2/ZrO_2 oxide layer have defects in the form of cracks and voids. Since the ZrNiTiHf foil used in brazing has very low thickness i.e. 50

μm so it could be possible that due to fast oxidation the whole brazing alloy is oxidized to TiO_2/ZrO_2 and due to cracks and defects it decomposed to black ash-like product.

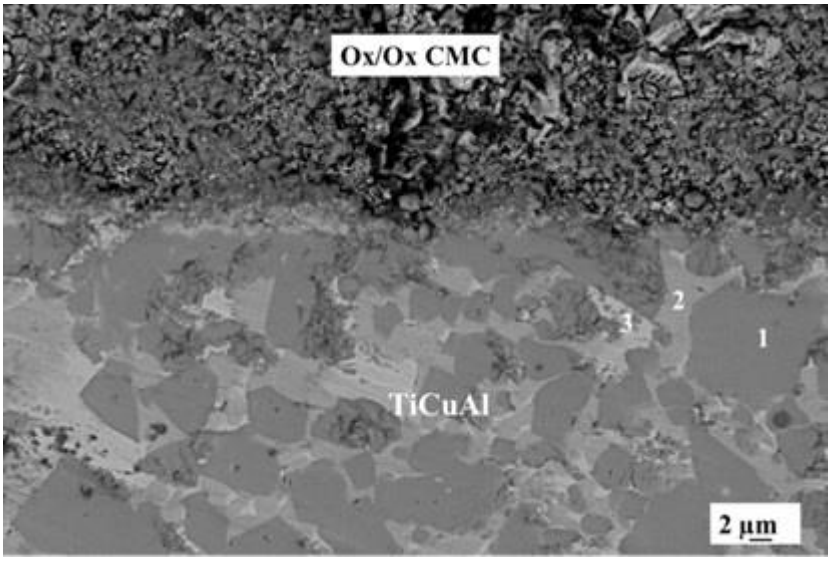

Figure 25: Nextel^{TM} 610/YAG- ZrO_2/ TiCuAl interface after oxidation test

Though the nickel is also present in the brazing alloy, however Zr and Ti have high oxygen affinity as compared to nickel because Zr and Ti have lower electronegativity values than Ni. Hence, predominance of faster growth of TiO_2/ZrO_2 oxide layer as compared to NiO might be possible.

However, in case of newly developed brazing TiCuAl system the joining area and the braze seems unaffected and the joint interface remain well bonded (figure 25). The oxidation resistance of TiCuAl system may be attributed to the presence of uniformly distribution of Al in all the three brazing zones as detected in EDS, shown in figure 24. Aluminum is a protective element in presence of oxygen. Upon increasing temperature a protective thin passivating layer of Al_2O_3 could be formed by preferential oxidation of Al, which further stops the diffusion of oxygen and protects TiCuAl system from oxidation. This is in consistence with studies of G. Plascencia et al. [148], S.Hong [117] and A.G.Akimov et al. [122] who found that the addition of small amount of Al (0-12% at) in Cu-Al alloys increase the oxidation resistance of alloys, as compared to pure Cu, through development of stable Al_2O_3 thin layer.

3.4.6 Mechanical testing

Results of single lap-off set (SLO) shear strength are shown in figure 26. These values are very low as compare to interlaminar shear strength of Nextel^{TM} 610/YAG – ZrO_2 (11.7 ± 1 MPa) composite [11].

In case of AgCuSnTi the SLO was 5.32 ± 1.8 MPa and adhesive failure was observed. The joint shear strength is strongly related to thermally induced residual stresses at the joint interface which arise due to mismatch in coefficient of thermal expansion of substrate and brazing alloy during the cooling process [45].

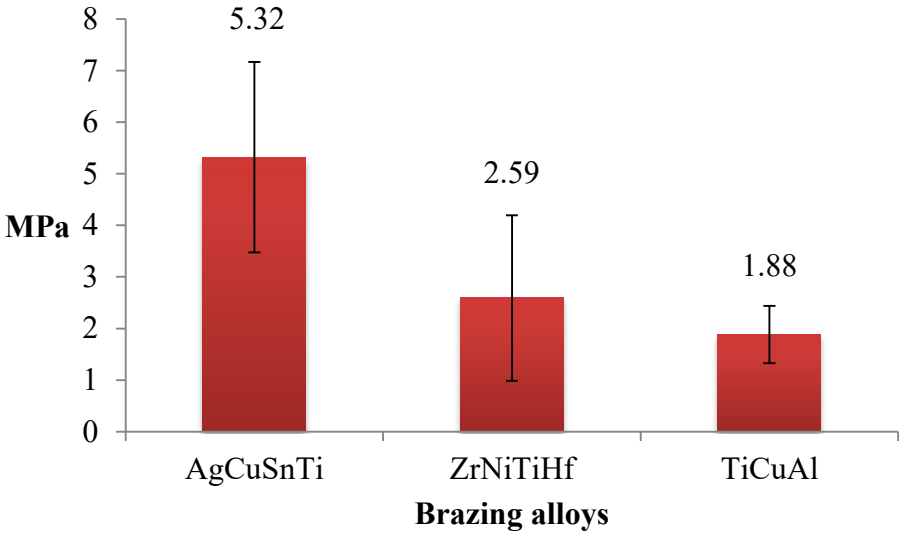

Figure 26: SLO shear strength of AgCuSnTi, ZrNiTiHf and TiCuAl joined Nextel^{TM} 610/YAG- ZrO_2 composite

The difference in CTE of AgCuSnTi and Nextel^{TM} 610/YAG- ZrO_2 (ΔCTE) is approximately 11 x10^{-6} x K^{-1} which is likely to cause residual stresses in the joining area. Several authors reported the possibility of reducing the thermal stresses by using Ag-Cu brazing system which have potential of plastic deformation due to presence of Ag (s.s) in brazing seam [149]. As reported in figure 16 the zone 3 could be Ag (s.s) [149][150] and expected to relieve the thermal stresses which arise due to high ΔCTE [149]. However, the lower strength value might be attributed to the presence of brittle titanium oxide phases at the interface [151][152]. D.Sciti et al. [151], H.Q.Hao et al. [48] and Chuang et al. [53] proposed the formation of TiO_X and TiO phases when brazing ZrO_2 with AgCuTi based brazing fillers at 900 °C, using argon and vacuum. It is likely that these oxides also developed at Nextel^{TM} 610/YAG- ZrO_2 /AgCuSnTi interface and fail to dissipate the residual stresses and cause an adhesive failure [151].

In case of ZrNiTiHf a cohesive failure in brazing material was predominant with a very low SLO of 2.59 ± 1.6 MPa. The ΔCTE of Nextel^{TM} 610/YAG- ZrO_2 composite was < 0.2 x10^{-6} x K^{-1} there were very little or no residual stresses at the interface and this could be the reason that the failure was cohesive. In order to explain the cohesive failure it is necessary to see the EDS of the brazing filler as shown in the figure 21 .The zone 3 and the zone 4 have different composition as compared to the bulk brazing filler. Due to presence of this heterogeneity the thermal expansion during cooling may not be uniform which give rise to residual stresses within the ZrNiTiHf brazing filler. Furthermore, high amount of oxygen

is present in all zones of brazing filler except zone 3.The small atomic radius of oxygen allows it to move in Ti and Zr to occupy interstitial position in crystal lattice[153][154]. The inclusion of oxygen in zirconium and titanium induces embrittlement, which deteriorate the ductility and material became susceptible to cracks [154][155][156][157]. Therefore, it can be concluded that possibility of oxygen induced embrittlement and presence of local residual stresses within the brazing filler may badly affect the SLO of joint and as a result a cohesive failure with very low SLO value was observed.

In case of TiCuAl adhesive failure was observed with average SLO values of 1.88 ± 0.5 MPa. The CTE of TiCuAl system is not known however with such a low shear strength the possible reason could be very high residual thermal stresses, presence of brittle oxides of titanium at the interface and low adhesion of the interfacial compounds (Ti_3Cu_2AlO and/or oxides of titanium) for this brazing system, which, differently from the other brazing alloys selected to join these ox/ox CMC, exhibited a very good oxidation behavior.

3.5 Conclusion

The NiCr based brazing filler failed to wet the surface of the Nextel^{TM} 610/YAG- ZrO_2 composite. However, the composite was successfully joined using AgCuSnTi, ZrTiNiHf and newly developed TiCuAl brazing alloys. The joint interfaces were continuous and free from defects and cracks. The joining temperature for these brazing alloys is in the range of 900 °C-1100 °C which is well below the sintering temperature of this composite.

In order to evaluate the oxidation resistance of the joint samples a preliminary oxidation test was performed in air furnace at 550 °C with1 atm for 1 h. The debonding of interface occurred in case of AgCuSnTi while complete oxidation of brazing material was observed for ZrTiNiHf brazing alloy. The joints made with TiCuAl system remained well bonded after the oxidation test. The oxidation resistance of TiCuAl braze joint could be attributed to presence of Al in TiCuAl brazing system. The uniform distribution of Al in the TiCuAl alloy may develop Al_2O_3 passive protective layer on top of TiCuAl alloy. This oxide layer could be formed due to preferential oxidation of Al which further stopped the diffusion of oxygen in the TiCuAl system.

SLO shear strength of values of joint samples braze with AgCuSnTi, ZrTiNiHf and TiCuAl are 5.32 ± 1.8 MPa, 2.59 ± 1.6 MPa and 1.88 ± 0.5 MPa respectively. The possibility of high residual stress at AgCuSnTi/Composite interface due to ΔCTE and possible of presence of brittle oxides of titanium could resulted to lower values and adhesive failure of joint samples. The samples joined with ZrTiNiHf show cohesive failure which might be due to oxygen embrittlement and residual stresses due to composition variation within the brazing alloy. The TiCuAl brazed samples undergo adhesive failure and low SLO shear values might be due to residual thermal stresses, brittle oxides at interface

and low adhesion of phases formed at TiCuAl/composite interface. Though the newly developed TiCuAl system shows good oxidation resistance as compared to commercial AgCuSnTi, ZrTiNiHf brazing alloys, more research work is required to optimized its shear strength values when used to join Nextel^{TM} 610/YAG- ZrO_2 .

Chapter 4

Joining of oxide/oxide CMCs using glass-ceramics

This chapter discusses the joining of Nextel^{TM} 610/YAG- ZrO_2 and Nextel^{TM} 610/Al_2O_3-ZrO_2 using silica based glass-ceramics. Dilatometry measurements were carried out to tailor the coefficient of thermal expansion, while sintering and crystallization behaviours were investigated by hot stage microscopy and differential thermal analysis, respectively. Field emission scanning electron microscope was used to investigate the joint interfaces while X-ray diffraction (XRD) was performed on glass-ceramic samples to identify the formation of different phases. Single Lap Off-set shear tests (SLO) and four-point bending tests were performed at room temperature to check the mechanical strength of the joints. To know the mechanical strength at high temperature, four-point bending tests were performed at 850 °C. The thermal stability of the glass-ceramics joined samples was evaluated by thermal ageing of samples up to 850 °C and 930 °C for 100 h and 50 h in air, respectively. Matusita, Sakka and Ozawa equations were used to study the crystallization kinetic behavior of developed glasses.

Part of the work described in this chapter is already published by author (M. Y. Akram *et al.*, "Journal of the European Ceramic Society, Joining and testing of alumina fibre reinforced YAG-ZrO_2 matrix composites," vol. 38, no. November 2017, pp. 1802–1811, 2018 and M. Y. Akram *et al.,* "Journal of the European Ceramic Society, Joining and mechanical testing of oxide / oxide (Nextel ^{TM} 610 / alumina- zirconia) ceramic composites," *J. Eur. Ceram. Soc.*, vol. 39, no. 7, pp. 2510–2517, 2019).

4.1 Experimental

4.1.1 Synthesis of glasses

Two new glass systems based on SiO_2-Al_2O_3-CaO-MgO and SiO_2-CaO-Y_2O_3-Al_2O_3-MgO-ZrO_2 were designed, synthesis, characterized and used for joining of Nextel^{TM} 610/YAG-ZrO_2 and Nextel^{TM} 610/Al_2O_3-ZrO_2 respectively. The composition of these two glass systems were developed using SciGlass 6.6 database with CTE as main criteria. The compositions of SiO_2-Al_2O_3-CaO-MgO, labelled as SACM, and SiO_2-CaO-Y_2O_3-Al_2O_3-MgO-ZrO_2 , labelled as GOX, are given in table 11.

Table 11: Composition of SACM and GOX glasses

Glass system	**Composition (wt%)**					
	SiO_2	**CaO**	**Y_2O_3**	**Al_2O_3**	**MgO**	**ZrO_2**
Purity/ Supplier	99%pure/ Sigma Aldrich	99% pure $CaCO_3$/ Sigma Aldrich	99.9% pure/ Sigma Aldrich	99.9% pure/ Alfa Aesar	99.9% pure $MgCO_3$/ Sigma Aldrich	99% pure/ Sigma Aldrich
SACM	42	20	--	32	6	--
GOX	39.5	21.5	12.5	12.5	12.5	1.5

To ensure the homogenization, the oxides of relevant glass are mixed together for 24 hours. The oxide mixture was then put in Platinum-Rhodium crucible and transferred to Nabertherm furnace. The temperature of furnace was raised to 1600 °C with 10 °C min^{-1} in air and holds it for 1 h to ensure the homogeneity. In case of GOX glass, the temperature of furnace was raised to 1650 °C due to inadequate melting observed at 1600 °C. After that the glass was air quenched on brass plate and afterward the SACM glass and GOX glass were grounded by using zirconia ball milling. The ball milling was performed in vibratory Analysette 3 Spartan pulverisette 0 (FRITSCH) micro mill equipped with 50 mm diameter zirconia ball by using amplitude of 2 mm and 10 minutes for the first cycle and 1 mm amplitude and 5 minutes for the subsequent two cycles. Glass powders were then sieved to get final particle size < 38µm by using stainless steel sieve.

4.1.2 Characterization of glasses and glass-ceramics

4.1.2.1 Hot-stage microscopy (HSM)

The sintering behavior of SACM and GOX glasses were evaluated using HSM (MISURA HSML 1600-3002, Expert system solution, Italy) and HSM (EM 301, Hesse instruments, Germany). The HSM experiments were performed with 5 °C min^{-1} in air from room temperature to 1500 °C. The samples of SACM and GOX glasses were prepared by pressing the glass powders, using a stainless steel punch, in a cylindrical mould with base diameter of 2 mm and height 3 mm. An alumina sample holder of 12 mm x 10 mm x 1 mm was placed under the cylinder mould and the samples were demould on alumina sample holder using stainless steel punch.

Three samples were tested for each of SACM and GOX glasses. The HSM characteristic temperatures were acquired with an error of ± 8 °C for SACM and ± 5 °C for GOX glass. Sample sintering percent at different temperature can be estimated as

$$S_T = (1 - A_{RT}/A_T) \times 100 \qquad \text{Equation 4.1}$$

Where,

A_{RT} = Area at room temperature

A_T = Area at selected temperature.

The key information obtained from HSM characterization were sintering start temperature, sintering end temperature, softening temperature, half ball temperature and melt temperature. According to Scholze [158] these points can be defined as

Sintering start/ first shrinkage temperature: It is the temperature at which the glass powder sample starts to shrink.

Sintering end/ Maximum shrinkage temperature: It is the temperature at which the maximum shrinkage of the glass powder sample takes place before its start to soften.

Softening/ Deformation temperature: It is the temperature at which the glass powder sample starts to soften. At this temperature rounding of small protrusions at the edges of the glass powder sample is observed.

Half ball/ Hemisphere temperature: It is temperature at the glass powder sample form a semi-circle shape.

4.1.2.2 Differential thermal analysis (DTA)

The differential thermal analysis (DTA) involves heating of a sample and a reference inert material simultaneously under the same conditions. The difference in temperature of sample and reference material is measured and differential temperature is plotted against the time or temperature. Any thermally induce physical or chemical change lead to either heat evolved (exothermic) or absorbed (endothermic).

To investigate the crystallization behavior, the DTA of SACM glass and GOX glass were performed using DTA 404 PC, Netzsch, Germany) with 100 mg glass powders from room temperature to 1300 °C in air with heating rate of 5 °C min^{-1} using alumina crucible. For the baseline measurement and reference, alumina powder (99.9% pure, Sigma Aldrich) was used. The characteristics temperatures of SACM and GOX glasses such as glass transition temperature (Tg), crystallization onset temperature (T_{OC}), crystallization peak temperature (T_P), melt temperature (T_M) were observed. These characteristic temperatures were acquired with an error of ± 5 °C for SACM and ± 3 °C for GOX glass. It is imperative to mention that T_M is not the melting of glass but instead melting of glass-ceramic as during the course of heating the crystals of respective phase/phases evolve in crystallization regime. To study the crystallization kinetics (activation energy (E_a) and Avrami exponent (n)) the DTA was also performed with heating rates of 10 °C min^{-1} and 20 °C min^{-1}.

4.1.2.3 Dilatometry

Every time a material undergoes heat changes, it demonstrates some variation in its dimensions. The joined components are often passing through some sort of thermal cycling during their operations life. It is important to know the CTE of the joining material as well as the joined components in the operational temperature range. A good match of CTE between joining material and substrate results to less residual stresses and more robust joining.

The push-road dilatometry technique was utilized for measuring the linear CTE of samples using the following expression

$$\alpha = 1/L_O \times \Delta L/\Delta T \times 10^{-6}\ °C^{-1} \qquad \text{Equation 4.2}$$

Where,
α = Coefficient of thermal expansion
L_O = Original length of sample
ΔL = Change in length of sample at selected temperature
ΔT = Change in temperature

The CTE of the SACM and GOX glass-ceramics was measured using Dilatometry (DIL 402 PC Netzsch, Germany) in temperature range from 100 °C up to 900 °C in air with heating rate of 5 °C min^{-1}. The dilatometry measurement was performed on glass-ceramic pellets (figure 27) with 10 mm diameter and 5 mm height. These pellets were sintered under same joining conditions that used in joining of composites. Three samples were tested for each of SACM and GOX glass-ceramics. The CTE values were obtained with an error of ± 0.2 x 10^{-6} $°C^{-1}$ and ± 0.1 x 10^{-6} $°C^{-1}$ for SACM and GOX glass-ceramics, respectively. Thermographs of respective glass-ceramics were taken between temperature vs percent change in length.

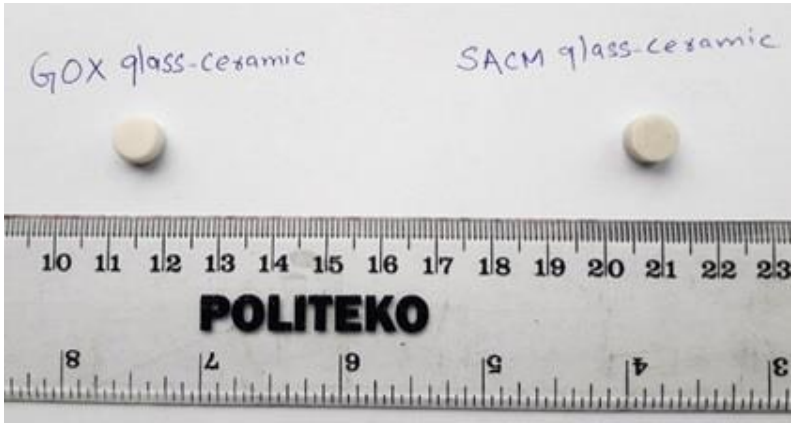

Figure 27: GOX and SACM glass-ceramic pellets ready for Dilatometry analysis

4.1.2.4 Sample joining

The joining was performed on 10 mm x 10 mm x 2 mm samples for both Nextel^{TM} 610/YAG- ZrO_2 and Nextel^{TM} 610/Al_2O_3-ZrO_2 composites as shown in figure 28.

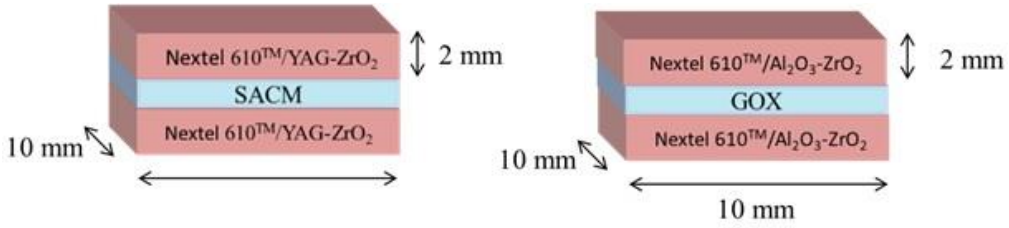

Figure 28: Joining configuration of ox/ox CMCs with respective glass systems

SACM and GOX respective glass slurries were made with ethyl alcohol and then applied manually to the respective ox/ox CMC samples. The second ox/ox CMC sample was placed on the top so that a sandwich like configuration CMC /glass/CMC was obtained as shown in figure 28. The samples were then transformed to furnace (Carbolite 1300,UK) and program the furnace according to selected joining conditions (temperature, dwell, heating and cooling rates). All the ox/ox CMCs samples were joined in air atmosphere without applying any pressure with heating and cooling rates of 5 °C min^{-1}.For SACM, the dwell time was 1 h while for GOX; the dwell time was 2 h.

4.1.2.5 Field emission scanning electron microscopy (FE-SEM) and Energy dispersive X-ray spectroscopy (EDS)

Scanning electron microscopy is a non-destructive technique that utilizes high energy electron to observe the surfaces of materials through images analysis. The accelerated electrons dissipated kinetic energy after electron-samples interaction and as result variety of signals are produced. These signals include backscattered electrons for demonstrating the contrast in multiphase materials, secondary electrons responsible for SEM micrographs, characteristic X-rays for elemental analysis.

For FESEM sample preparation, after the completion of thermal cycle of furnace the SACM glass-ceramic joined Ox/Ox samples and GOX glass-ceramic joined Ox/Ox samples were removed from the furnace and polished (without embedding in epoxy resin) with SiC paper (grit size;120-2500). The samples were then silver sputtered and afterwards FESEM and EDS was performed to observe the joint interface and glass-ceramics microstructure in the joining seam. The EDS analysis was performed only to distinguish phase morphology and elemental composition in glass-ceramics. The correct identification of crystalline phases of glass-ceramics is not possible with EDS analysis. Hence, it is important to perform precise method such as XRD to identify the phases in glass-ceramics

4.1.2.6 X-ray Diffraction (XRD)

X-Ray diffraction is also a non-destructive method to determine the chemical composition, physical properties and crystal structure of materials. During XRD analysis the sample and monochromator are rotated to different relative positions. The X-rays interact with atoms in the crystal structure of sample and diffracted according to its structure and orientation. This diffracted pattern from the crystal structure contains reflections of different intensities which are then utilized to identify the crystal structure using Bragg's law ($n\lambda=2d \sin \theta$).

The XRD was performed on SACM and GOX glass-ceramics powders at room temperature to determine the crystalline phases of glass-ceramics. For the sample preparation, the cold press glass powder pellets of SACM and GOX are prepared and giving the same heat treatment as of joining in each case. Afterwards the respective glass-ceramics pellets were ball milled to obtained fine powders for XRD analysis. A Philips X'Pert diffractometer with Cu anode (X-ray source) and monochromatic $K\alpha$ radiation with characteristic wavelength λ= 15.405 Å using step size of 0.02° with 1 s per step in the range of $10° \leq 2\theta \leq 70°$ was used. The crystalline phases in SACM and GOX glass-ceramic powders were identified using X'Pert High score software 2.2b (PANalytical B.V. Almelo, Netherland).For obtaining the glass-ceramic powders for XRD, the glass-ceramic pellets with 10 mm diameter and 3 mm height were prepared and then crushed to

obtained powder, using ball milling. These pellets were sintered under same joining conditions that used in joining of composites.

4.1.2.7 Mechanical testing

The joint components undergo variety of stresses during the operational life hence it is important to assess their mechanical performance and integrity. The stresses during the operational life are the combined effect of residual stresses and operation stresses. Residual stresses arise due to difference in CTE of joining material and substrate during cooling process. Therefore, it is important to select the joining material which has matching CTE with substrate in the operation temperature range. However, one of the main concerns of mechanical testing of joined CMC components is the lack of standardization in testing standards which may restrict the efficient use of CMC components in high performance structures [3]. Several mechanical testing methods such as asymmetrical four-point bending test (ASTM C1469-00), symmetrical four-point bending test (ASTM C1341), single lap shear, single lap off-set shear (ASTM D905-03), double lap off-set shear, Torsion (square, cylindrical, tube, hour-glass), double notched (ASTM C1292-00 and ASTM C1495-99) and Brazilian tests are used in research community [13]. Since the strength of joint is a function of joint geometry and test method so the comparison of test results are not possible [159].

For this study, we selected single lap off-set shear test in compression, adopted as of ASTM D905-03, at room temperature and symmetrical four-point bending tests at room temperature and at selected high temperature on triplicate samples in air was used. The four-point bending tests were performed according to standards ASTM C1341-13 (RT), ASTM C1161 (RT) and DIN EN 843-1 (High temperature, HT). These four-point bending tests were not actually designed for joined components but instead they are used for ceramic matrix composites and monolithic ceramics. For comparison purpose the four-point bending tests were also performed on as-received samples, thermally treated samples (treated with same conditions of joining) and on joined samples at RT and at HT. The HT four-point bending test was performed on GOX glass-ceramic joined samples only.

For SLO shear test in compression, the sample preparation and testing configuration is shown in the figure 29.

The sample size for SLO shear test in compression was 13-16 mm x 4 mm x 2 mm. The apparent shear strength can be obtained by dividing breaking force by joined area.

For four-point bending strength for Nextel^{TM} 610/YAG-ZrO_2 a the test was performed according to ASTM C1341-13 with sample size of 50 mm x 6 mm x 2 mm at RT.

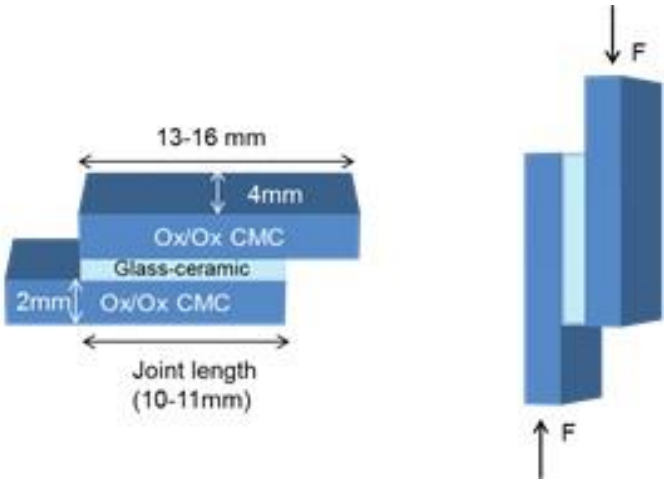

Figure 29: SLO shear test configuration

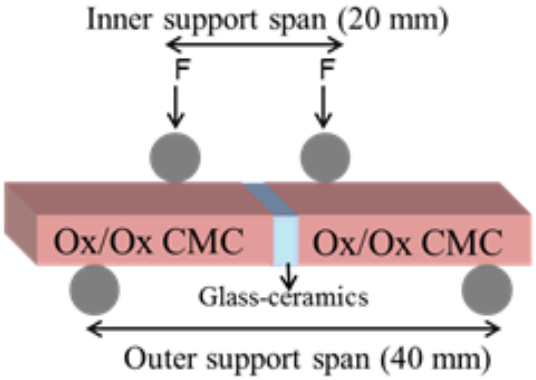

Figure 30: Four-point bending configuration for glass-ceramics joined ox/ox CMCs

For Nextel ^{TM} 610/Al_2O_3-Zirconia composite the four-point bending strength was performed according to standard ASTM C1161 (RT) and DIN EN 843-1 (HT) with sample size of 45 mm x 4 mm x 2 mm in each case. For high temperature testing the temperature was raised to 850 °C and hold it for 10 min for thermal equilibrium before proceed for four-point bending test. Four-point bending test configuration is shown in figure 30. The samples for the four-point bending tests were prepared using special sample holder as shown in figure 31.

The four-point bending strength was then calculated using standard formula given below as

$$S = 3PL/4bd^2 \qquad \text{Equation 4.3}$$

Where:
P= Breaking force
L= outer support span
b = specimen width
d = specimen thickness

The four-point bending tests were performed on universal testing machine (MTS criterion, model 43) using cross head speed of 0.5 mm/min. The outer and inner spans for four-point bending tests were 40 mm and 20 mm respectively. The *post-mortem* analysis of fracture surfaces was performed by SEM on as fractured surfaces.

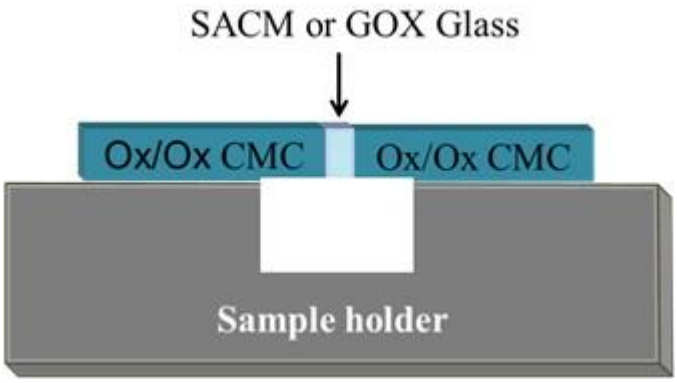

Figure 31: Sample holder for preparation of joined samples for four-point bending test

4.1.2.8 Thermal ageing

In order to evaluate the thermal stability of SACM and GOX glass-ceramics, joined samples were tested at high temperature in triplicate. SACM glass-ceramic joined samples were aged for 930 °C for 50 h and 850 °C for 100 h in air while for GOX glass-ceramic joined samples were aged for 850 °C for 100 h in static air in a Carbolite furnace. The heating and cooling rate were 5 °C min^{-1}. The *post-mortem* of joint interface and joining seam was done using FESEM analysis.

4.2 Results and discussion

4.2.1 Joining of Nextel™ 610/YAG-zirconia with glass-ceramics

4.2.1.1 Glasses and glass-ceramics characterization

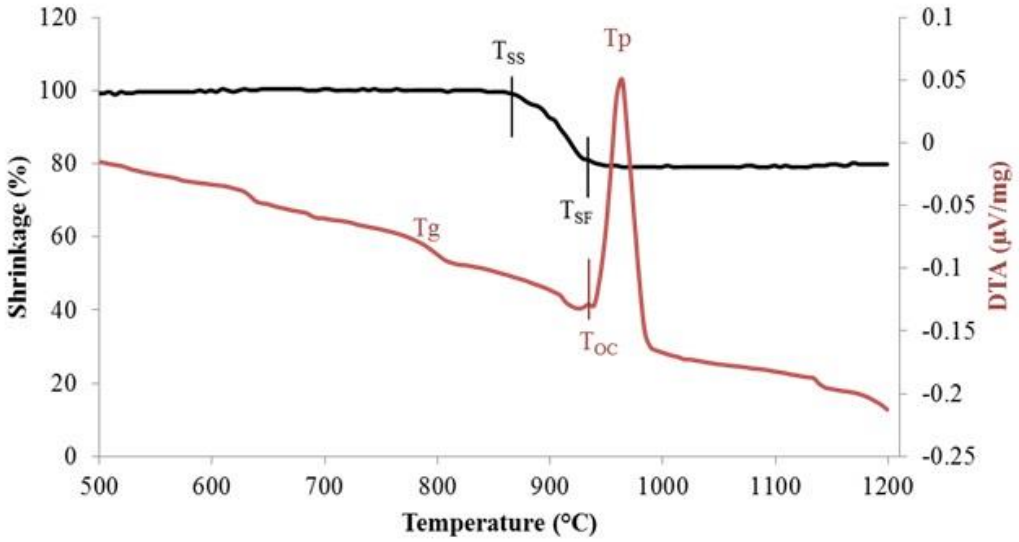

Figure 32: HSM and DTA of SACM glass with 5 °C min^{-1} in air

The figure 4.6 shows the HSM and DTA of SACM glass with 5 °C min^{-1} in air. The sintering started (T_{SS}) at 850 °C and sintering finished (T_{SF}) at 940 °C while the on-set of crystallization temperature (T_{OC}) and crystallization peak temperature (T_P) are 945 °C and 962 °C, respectively. In order to obtain a fully dense glass-ceramic it is important to understand the sequence of sintering and crystallization. If the crystallization started before the end of sintering that is $T_{SF} > T_{OC}$ a complete densification may not be occurred. This could be due to the fact that as the temperature increases the viscosity of glass decrease, hence promoting the sintering/densification, however due to start of early crystallization, the crystal formation causes the viscosity to increase which hinder further densification [160] [161]. In contrast, if the crystallization started at/after the end of sintering a denser glass-ceramic could be obtained. From the figure 32, it is clear that $T_{OC} > T_{SF}$, hence densification precede the crystallization process.

From industrial point of view, it is important to assess the thermal stability of glasses. For this, the criteria proposed by Saad and Poulain [162] (Equation 4.4) and Dietzel [163] (Equation 4.5) can be used

$$S= (T_p - T_{oc})\,(T_{oc} - T_g) / T_g \qquad \text{Equation 4.4}$$

$$\Delta T= T_{oc} - T_g \qquad \text{Equation 4.5}$$

Where, T_{OC}, T_P, and T_g are temperatures corresponding to the onset of crystallization, the crystallization peak, and the glass transition, respectively. Larger the values of these parameters (ΔT and S), greater is the resistance to nucleation/crystallization and the glass is thermally stable. For SACM the values of ΔT and S are 155 °C and 3.3, respectively. Therefore it can be concluded that SACM glass is thermally stable and, thus, a potential candidate for joining of Nextel^{TM} 610/YAG-Zirconia. Moreover, these values of ΔT and S are in agreement with a different SiO_2-CaO-Al_2O_3-MgO based glass-ceramic material used for joining for solid oxide fuel cell applications [164]. The thermal parameters of the SACM glass obtained from DTA and HSM with 5 °C min^{-1} are shown in table 12.

Table 12: Thermal parameters of the SACM glass obtained from DTA and HSM with 5 °C min^{-1}

Parameters (from DTA and HSM)	**Characteristic temperature (°C)**
Sintering start Temperature (T_{SS})	850
Maximum shrinkage Temperature (T_{SF})	940
Glass transition temperature (T_g)	790
Softening temperature (T_S)	837
Onset crystallization temperature (T_{OC})	945
Peak crystallization temperature (T_P)	962
Temperature for half ball (T_{HB})	1448

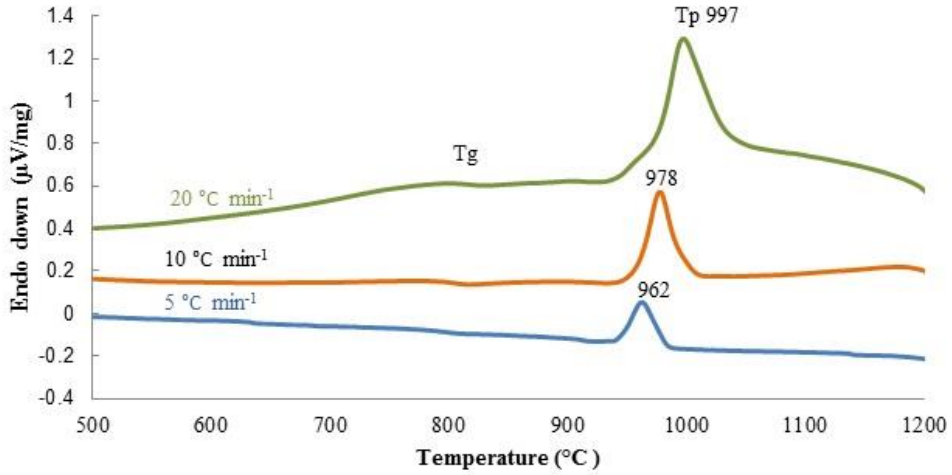

Figure 33: DTA thermographs of SACM with heating rates of 5 °C min^{-1}, 10 °C min^{-1} and 20 °C min^{-1}

Figure 33 shows the DTA thermographs of SACM with heating rates of 5 °C min^{-1}, 10 °C min^{-1} and 20 °C min^{-1}.The dependency of T_P on heating rate (α) is evident. With increasing heating rate, the T_P is shifted to higher temperature as shown in figure 33. This phenomenon can be explained by Bansal et al. [165] as follows: T_P is the temperature at which the transformation rate of viscous glass liquid into crystals of crystalline phase/phases is maximum. When the evolved crystalline phase/phases has the same composition to that of glass liquid then this transformation rate depend on density of crystallization sites. Conversely, when the evolved crystalline phase/phases has different composition, then the transformation rate is controlled by diffusion rate through the viscous glass liquid and the no. of crystallization sites for which diffusion can occur. By selecting the lower heating rates, the nucleation sites are increased and T_P will come off at a temperature at which the viscous glass liquid viscosity is higher, that is at a lower temperature in comparison to T_P with higher heating rates. This kind of behavior was also reported with several other glass systems, reported in [166] [167] [168].

The CTE of SACM glass-ceramic was measured in the range of 125 – 900 °C and found to be 7.37 $x10^{-6}$ C^{-1} as shown in figure 34 a. The CTE of composite was 8.89 $x10^{-6}$ C^{-1} (125 °C – 900 °C). Hence during cooling the composite will contract more than the SACM glass-ceramic and the joint is in compression. Therefore, it is less likely that crack was formed during the cooling [169]. At RT the glass-ceramic are brittle materials and joints could be under great stress due to mismatch of CTE, however the residual stresses in operation conditions are less severe due to viscoelastic behavior of glassy phase near and above Tg.

The DTA curve of SACM glass-ceramic (performed with 5 °C min^{-1}) is shown in figure 434 b. No further crystallization peak was identified which indicates almost complete crystallization of SACM glass-ceramic. Furthermore, the Dilatometry measurement was stopped at 950 °C due to safety reason (on-set melting 1144 °C).No softening was detected up to 950 °C which indicates the thermal stability of SACM glass-ceramic up to this temperature.

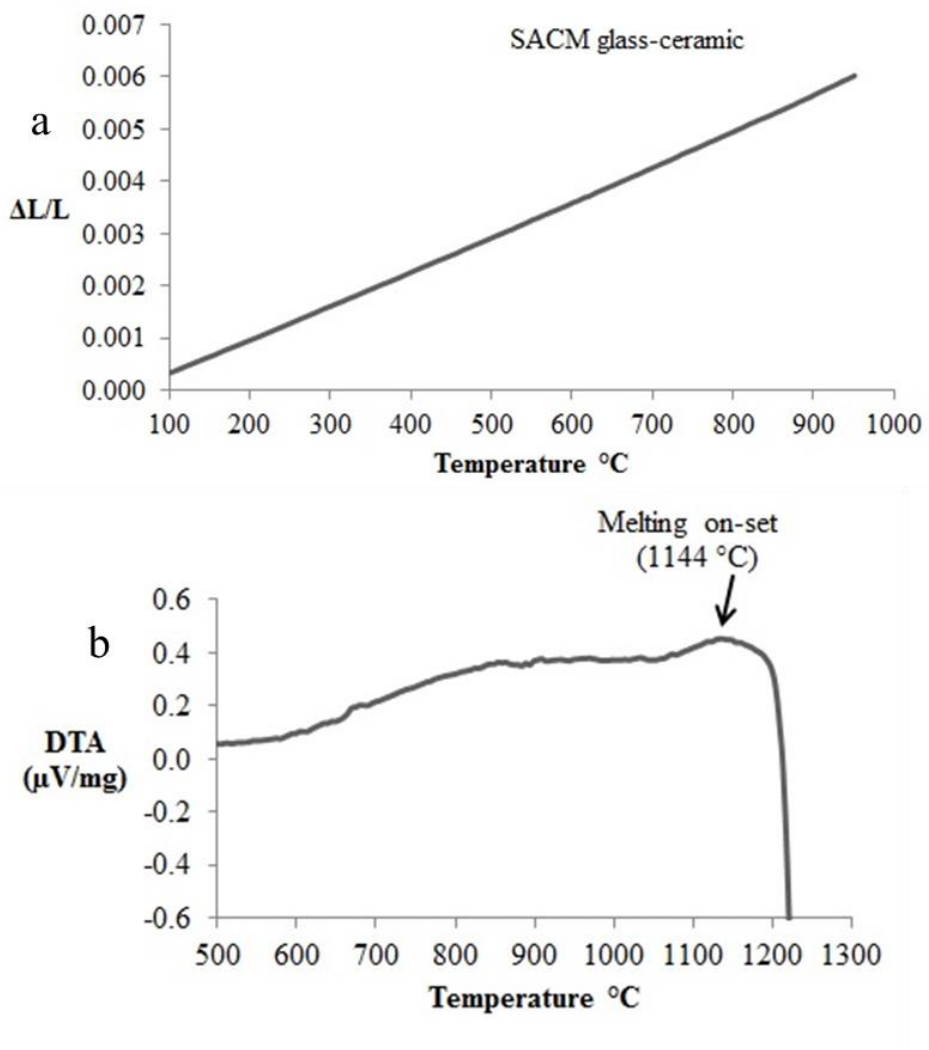

Figure 34 : a) CTE of SACM glass-ceramic b) DTA curve of SACM glass-ceramic.

In order to study the kinetics of the glass-ceramic system, it is important to know the activation energy (Ea) of crystal growth and crystal growth mechanism. Activation energy can be defined as the amount of energy a glass system required to overcome the barrier of phase and structure rearrangement and transform into crystals of evolved crystalline phase/phases during the crystallization process [170]. To study the crystallization kinetic process of glasses, researchers employed isothermal and non-isothermal methods. In isothermal method the glass sample is heated rapidly and held at a temperature above T_g and crystallization take place at a constant temperature [171].While in case of non-isothermal method, the glass sample is heated at a constant heating rate and sample is crystallized during the analysis [172].Non-isothermal method is quicker [172] and adopted in this study using DTA results.

Using DTA results, the kinetic parameters, that is, activation energy of crystallization (E_{ac}) and Avrami parameter can be determined using equations proposed by H.E Kissinger [173], T.Ozawa [174] and K.Matusita and S.Sakka [175]. However, according to K.Matusita and S.Sakka the Kissinger equation can be functional only if the surface crystallization is dominant, in other cases

K.Matusita and S.Sakka equation (modified form of Kissinger equation) could be used.

$\ln (\alpha / T^2_p) = - E_{ac} / R\ T_p + \text{Constant}$ (Kissingerequation) Equation 4.6

$\ln(\alpha^n / T^2_p) = -mE_{ac} / RTp + \text{Constant}$ (K.Matusita and S.Sakka) Equation 4.7

Where α is the heating rate used in DTA analysis, T_p is the crystallization peak temperature, E_{ac} is the activation energy of crystallization, R is the universal gas constant, n is the Avrami kinetic coefficient which is related to the crystal growth mechanism and m gives the dimensionality of crystal growth. The value of m ranges from 1 to 3 as shown in table 13 [175]. For surface crystallization, m=n=1 for all heating rates and hence equation of Matusita and Sakka reduce to Kissinger equation.

Table 13: Values of m and n for different crystallization mechanism [175]

Crystallization mechanism	**n**	**m**
Bulk nucleation with varying number of nuclei (The number of nuclei is inversely proportion to the heating rate)		
Three dimensional growth	4	3
Two dimensional growth	3	2
One dimensional growth	2	1
Bulk nucleation with varying number of nuclei (The number of nuclei constant with heating rate)		
Three dimensional growth	3	3
Two dimensional growth	2	2
One dimensional growth	1	1
Surface nucleation	1	1

If the no. of nuclei is not constant with the heating rate m = n-1.The value of n in equation 4.7 can be determined using Ozawa equation

$$\left[\frac{d \ln(-\ln(1-X))}{d \ln\alpha}\right]_{T_S} = -n \quad \text{(Ozawa)} \quad \text{Equation 4.7}$$

Where X is the Volume Fraction of Precipitated Crystals (VFPC) at selected temperature T_S with heating rate α.VFPC is given as $X=A_{Ts}/A$ where A is total area under the peak between on-set of crystallization temperature (T_{OC}) and crystallization end temperature (T_{CE}), whereas A_{Ts} is partial area under the peak between T_{OC} and selected temperature T_S. For this study, the value of X is calculated using three different heating rates 5 °C min^{-1}, 10 °C min^{-1}, 20 °C min^{-1} and temperatures 965 °C, 970 °C, 975 °C. The T_S is any temperature located between T_{OC} and T_{CE} and situated inside all the three crystallization peaks which are obtained with these three different heating rates.

The value of n can be calculated from the slopes of plots ln(-ln(1-X)) vs 1/ lnα figure 35. The average value of n obtained from the plots was 2.36.

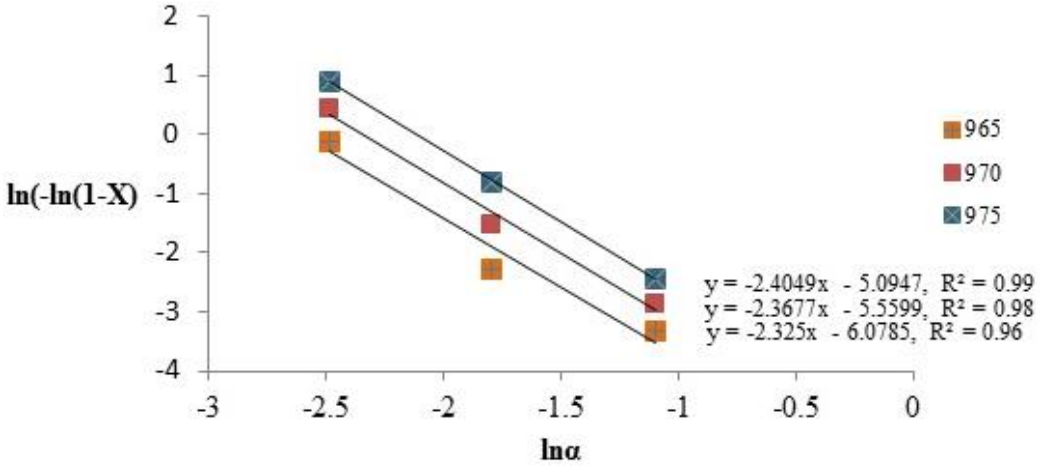

Figure 35: Plots of ln(-ln(1-X)) vs 1/ lnα

Based on the assumption that no. of nuclei is not constant with the heating rate, the value of m was 1.36 (m = n-1).This value of m implies the one dimensional and two dimensional growth of crystals during the crystallization process [175]. The value of E_{ac} was obtained from the slope of plot $\ln(\alpha^n/T_p^2)$ vs $1/T_p$ was 882 KJ/mol. The plot is shown in figure 36.

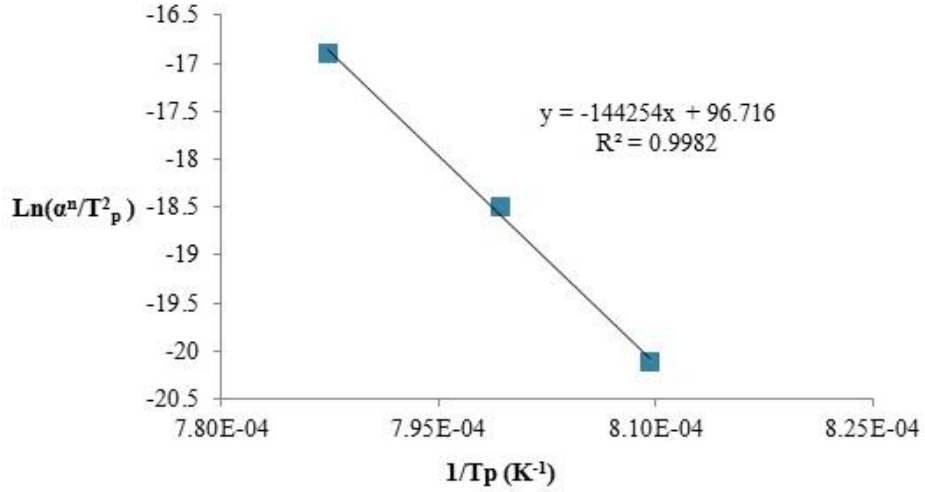

Figure 36: Matusita and Sakka plot for calculating the activation energy of crystallization

4.2.1.2 Joining, mechanical testing and ageing

Generally, for joining of substrates it is better to select a temperature which should be

(i) As low as possible to minimize the thermal stress, energy and cost efficient.
(ii) Guarantee maximum crystallization to give optimum mechanically properties.
(iii) It must not modify the microstructure of ox/ox CMC and/or considerably decrease the mechanically properties of the ox/ox CMC.

From DTA data, the joining temperature was selected as 980 °C. This temperature is located inside the crystallization regime of SACM glass (figure 32) and could assure mechanical properties of joined samples. Furthermore, this joining temperature is well above the softening temperature of the SACM glass (837 °C) and considerably below the sintering temperature (1225 °C) of Nextel ^{TM} 610 /YAG-ZrO_2.Above the sintering temperature the coarsening of Nextel ^{TM} 610 grain could be started and started affecting the mechanical properties of Nextel ^{TM} 610 /YAG-ZrO_2 [3].

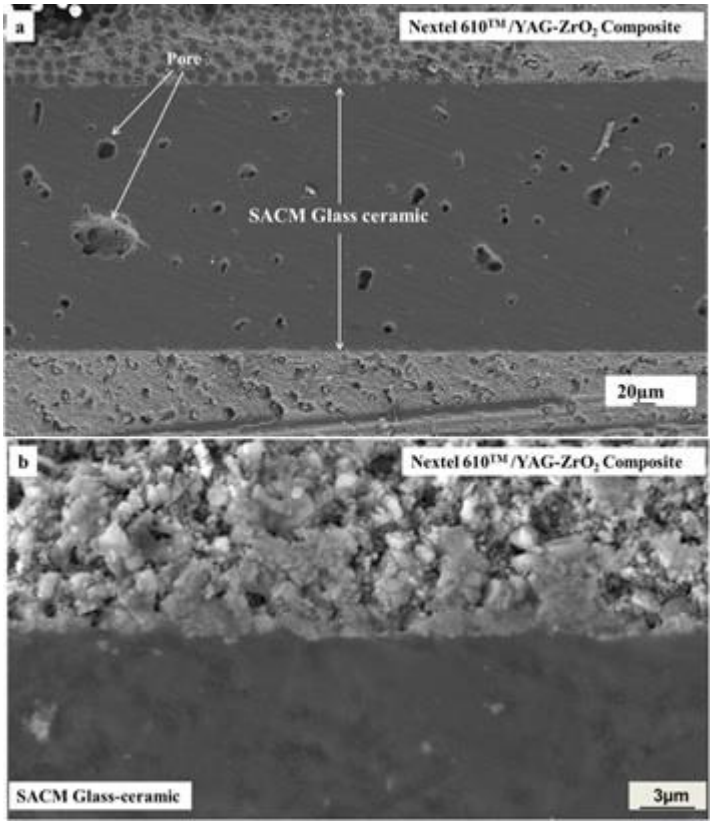

Figure 37: SEM micrograph of SACM glass-ceramic joined Nextel^{TM} 610/YAG-ZrO_2 composite

The micrograph (figure 37) shows the cross section of SACM glass-ceramic joined Nextel^{TM} 610/YAG-ZrO_2. The SACM glass-ceramic/ Nextel^{TM} 610/YAG-ZrO_2 interface is free from defects and discontinuities as shown in figure 37 b. Furthermore, no cracks in parallel or perpendicular directions were observed in glass-ceramic and composite, which might be attributed to matching CTE between SACM glass-ceramic and Nextel^{TM} 610/YAG-ZrO_2. However, some micro-voids are evident in SACM glass-ceramic which may be due to release of soluble and insoluble entrapped gases [176], and/or difference in CTE of glassy phase and crystalline phases [177][178]. B.Dev et al. [179] suggested that heating and cooling rate significantly effects the micro-voids, however even with very slow heating and cooling rate (2 °C min^{-1}), the micro-void still exists. Several other authors, e.g. [180][181] also reported the presence of micro-voids in glass-ceramic systems.

The EDS scan of SACM glass-ceramic joined Nextel^{TM} 610 /YAG-ZrO_2 is shown in the figure 38. Zone 8 and zone 9 are the crystalline regions while zone 10 represents the residual glassy phase. The EDS at zone 10 and zone 11 indicate that there is no diffusion of elements from the composite to glass-ceramic and vice versa, showing the suitability of SACM glass-ceramic for the joining Nextel^{TM} 610 /YAG-ZrO_2.

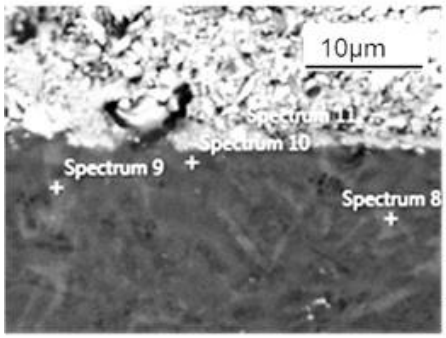

Elements wt %				
Element	Position 8 (Crystallization)	Position 9 (Crystallization)	Position 10 (Glass)	Position 11 (CMC)
Si	16.04	16.64	19.04	0
O	47.81	49	49.05	36.06
Al	9.92	11.01	17.07	14.65
Ca	22.90	18.34	13.74	0
Mg	3.34	4.94	1.10	0
Y	0	0	0	29.93
Zr	0	0	0	19.37
Total	100	100	100	100

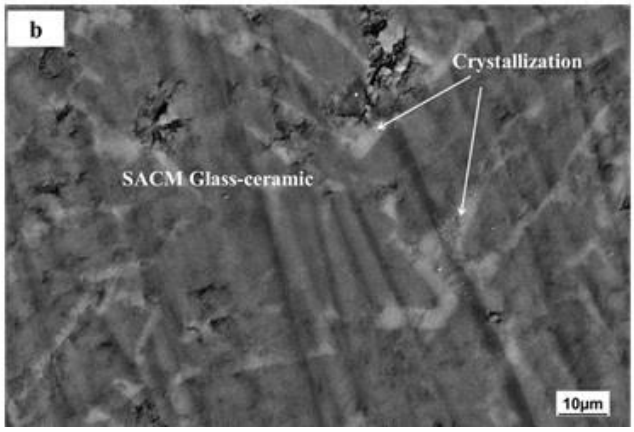

Figure 38: The EDS scan of SACM glass-ceramic joined Nextel^{TM} 610 /YAG-ZrO_2 composite

To identify the phases formed in joined samples, XRD was performed on SACM glass-ceramic powder. The XRD analysis suggests that Gehlenite

magnesia ($Al_{1.5}$ $Ca_2Mg_{0.25}O_7Si_{1.25}$) and Anorthite ($CaAl_2Si_2O_8$) could be the two main crystalline phases. (Fig 40).

Single lap off-set shear (SLO shear) and four point bending tests were performed on SACM joined Nextel^{TM} 610 /YAG-ZrO_2composite. During SLO shear tests the delamination of composite occurred in all three samples as shown in figure 39. The average value of shear strength was 15.4 MPa ± 1.2 MPa which is in agreement with the average interlaminar shear strength (≈12 ± 1.0 MPa) of this composite, as reported in [11].

Figure 39: Delamination of the composite during SLO test

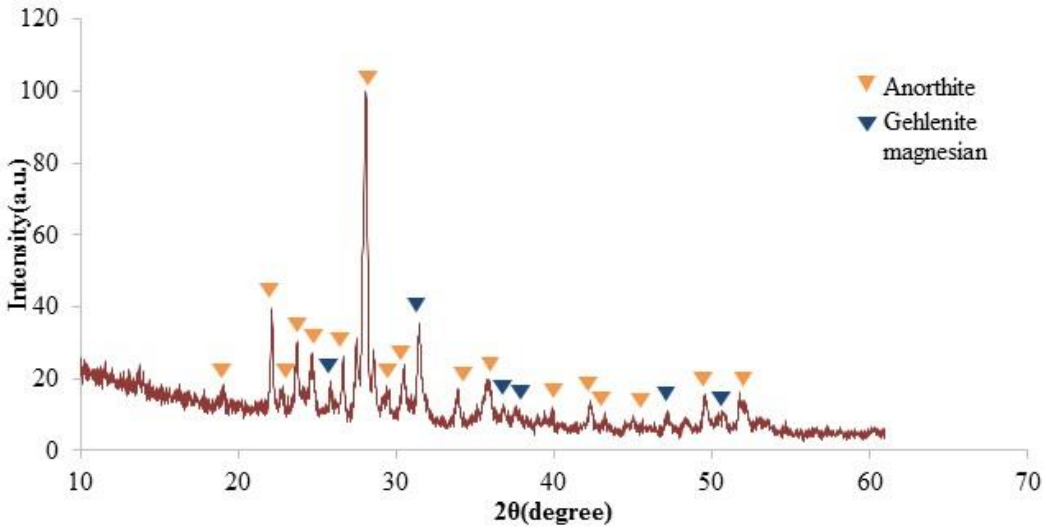

Figure 40: XRD analysis of SACM glass-ceramic

The four-point bending tests for as-received Nextel^{TM} 610/YAG-ZrO_2 composite, thermally treated and SACM glass-ceramic joined Nextel^{TM} 610/YAG-ZrO_2 are shown in the figure 41. The average four-point flexural strength of as-received specimens was 197.3 ± 14.8 MPa. This value is lower than the flexural strength of this composite reported in [11].This discrepancy is may be due to difference in testing method (performed according to EN 658) adopted in [11].The volume of the testing specimens in four-point bending strength is

greater than three-point bending tests, therefore the possibility of finding cracks, fissures and flaws is higher, which may contribute to lower value [182].The four-point bending strength of thermal treated specimen (treated with same conditions of joining i.e. 980 °C in air, 5 °C min^{-1} heating/cooling rate with 1 h dwell) were measured to know the degradation in flexural strength for the selected joining conditions. The mechanical strength degradation of composite/substrate at the joining condition is a concern in research community and ideally the flexural strength of thermal treated specimen should be identical to as-received specimen.

As shown in figure 41, the flexural strength of as-received and thermally treat samples are almost identical, depict that the selected joining conditions are compatible and do not decrease the as-received strength. The average four-point bending strength of SACM glass-ceramic joined specimens was 68.5 ± 12.1 MPa which is approximately 35% of as-received flexural strength. Gadelmeier et al. [107] used commercial SiO_2-BaO-CaO-Al_2O_3 based glass for joining Nextel^{TM} 610/ ZrO_2 based composite and reported flexural strength of 32.5 MPa which is only 12% of flexural strength of as-received Nextel 610^{TM} / ZrO_2 based composite (as-received 263 MPa). Scarce literature is present on four-point bending strength of glass-ceramic as joining materials. Nevertheless, the results of this study are comparable to average four-point bending strength (63 MPa) of glass-ceramic based on SiO_2-BaO-Al_2O_3-B_2O_3 was reported in [183]. An average four-point bending strength of SiO_2-CaO- BaO based glass-ceramic (52 ± 1, 55 ± 7 and for fully crystallized, 91 ± 12 MPa) was reported in [184].

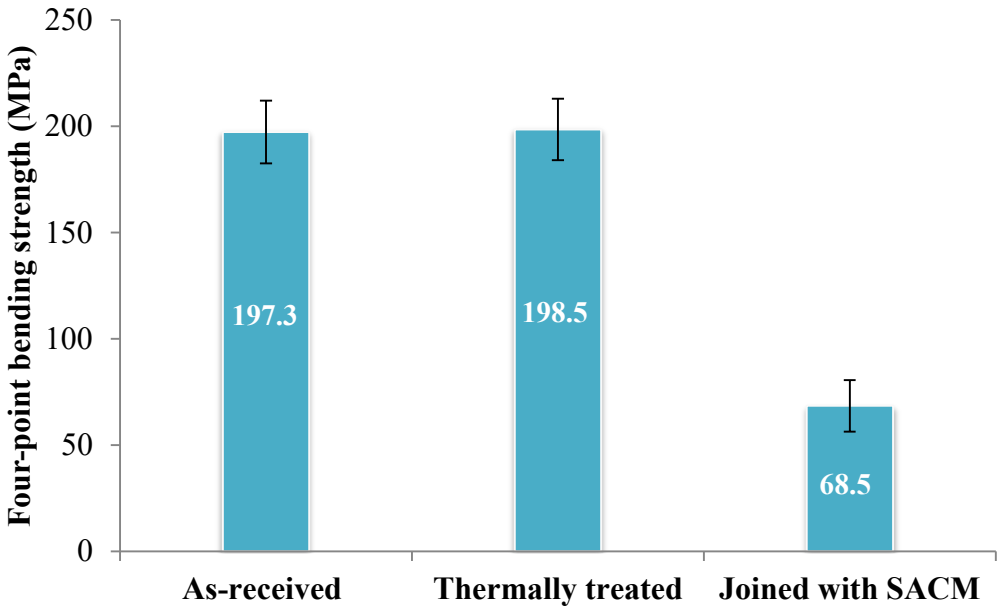

Figure 41: Four-point bending strength of as-received, thermally treated and SACM joined Nextel^{TM} 610 / ZrO_2 samples.

Figure 42 represents the mixed cohesive/adhesive fracture surfaces of joined specimens. Two key features relate to failure of joints: first of all, a part of SACM glass-ceramic was detached from Nextel^{TM} 610 / YAG-ZrO_2 composite,

represented in figure 42 a. During the course of fracture the SACM glass-ceramic pulled out some Nextel^{TM} 610 fibres and YAG-ZrO_2 matrix along with it while leaving behind the broken fibres and matrix, as in figure 42 a. Figure 42 a represents the fracture path, indicated with a green line.

The second feature that could occur simultaneously during the applied force, is the cohesive failure of SACM glass-ceramic which is also represent in figure 42 a and 42 b. The crack path is represented with white line in figure 42 a, and by white arrows in figure 42 c. The cohesive/adhesive fractures indicates strong bonding between SACM glass-ceramic and Nextel^{TM} 610 / YAG-ZrO_2 composite [185] [186]. It is well known in literature that below glass transition the glasses and glass-ceramics are brittle materials and fractures originate from micro-voids and/or defects which are distributed randomly in the glass-ceramics [92].Therefore it may be concluded that, presence of micro-voids in the in SACM glass-ceramic behave as stress concentration factors and cohesive fracture originates from one of these micro-voids which leads to failure. Furthermore, since these CMCs are likely to be utilized for high temperature components in the range of 800-1000 °C, it is possible that above Tg, the presence of a residual glassy phase in the glass-ceramic, could give a non-purely brittle fracture.

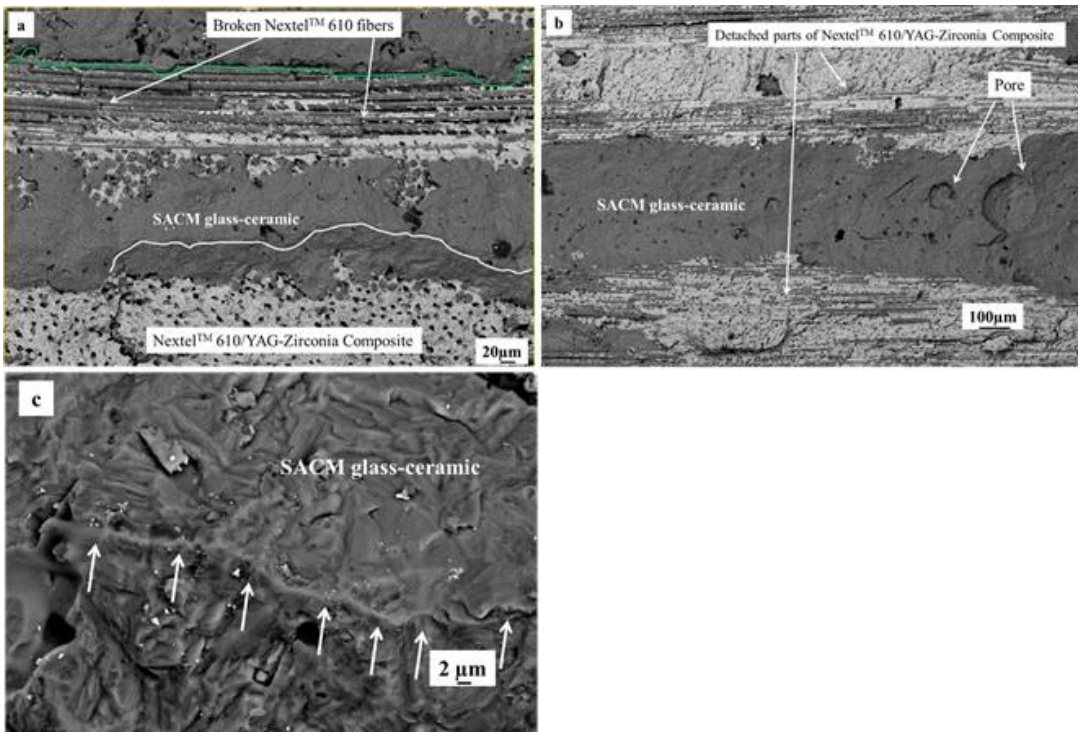

Figure 42: Fracture surfaces after four-point bending test a) represents crack paths with green and white lines b) part of Nextel^{TM} 610 / YAG-ZrO_2 remained attached to SACM glass-ceramic after the failure c) crack path in cohesive failure

The ox/ox CMC joining material must be thermally stable in operational conditions. For ox/ox CMCs, 1000 °C is typically considered as the upper limit because Nextel ^{TM} 610 continuous fibre could be used up to 1000 °C, under load, without considerable decrease in strength [109]. The joining material must also be

chemical stable and preferentially not forming deleterious reaction products at the joining interface.

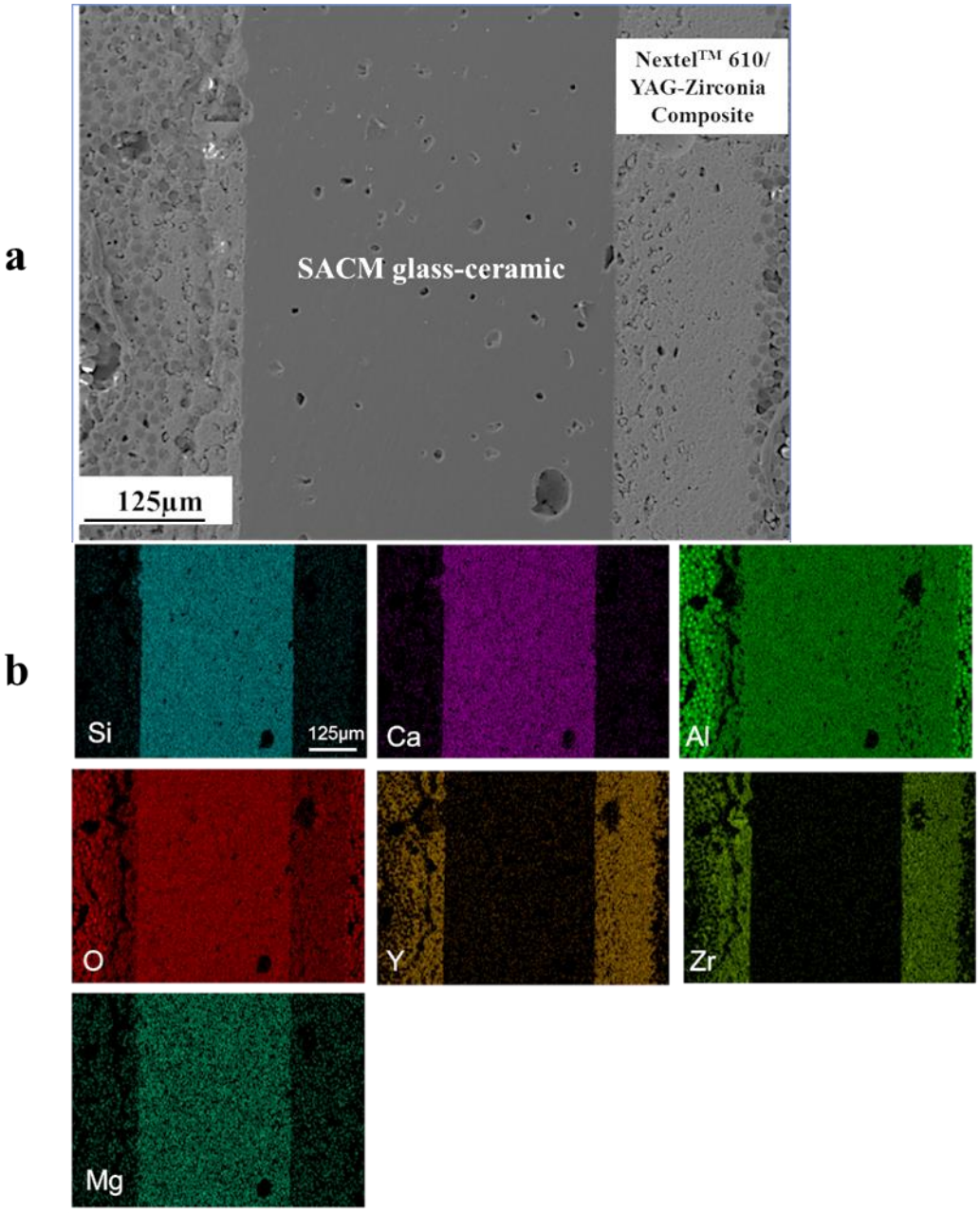

Figure 43: a) Cross section of SACM glass-ceramic joined Nextel™ 610 / YAG-ZrO_2 composite after for 50 h at 930 °C b) EDS maps of SACM joined Nextel™ 610 / YAG-ZrO_2 after ageing for 50 hours at 930 °C in air

For this study 850 °C for 100 h and 930 °C for 50 h in static air was selected as representative working conditions. These temperatures are below the crystallization on-set temperature for SACM glass. In crystallization regime there are chances that further crystallization starts to occurred which may alter the microstructure and properties such as CTE of glass-ceramic [86].

Figures 43 a and 44 a show the interface of SACM glass-ceramic/ Nextel^{TM} 610 / YAG-ZrO_2 composite after 50 h at 930 °C and 100 h 850 °C, respectively. The specimens, after these ageing tests, remained well bonded and interface is continuous and free from defects. Figure 43 b and figure 44 b shows the elemental mapping of SACM glass-ceramic/ Nextel^{TM} 610/YAG-ZrO_2 interface after ageing. There is no clear evidence of diffusion of elements from glass-ceramic to composite and vice-versa which confirm the suitability of SACM glass-ceramic at least for these ageing conditions.

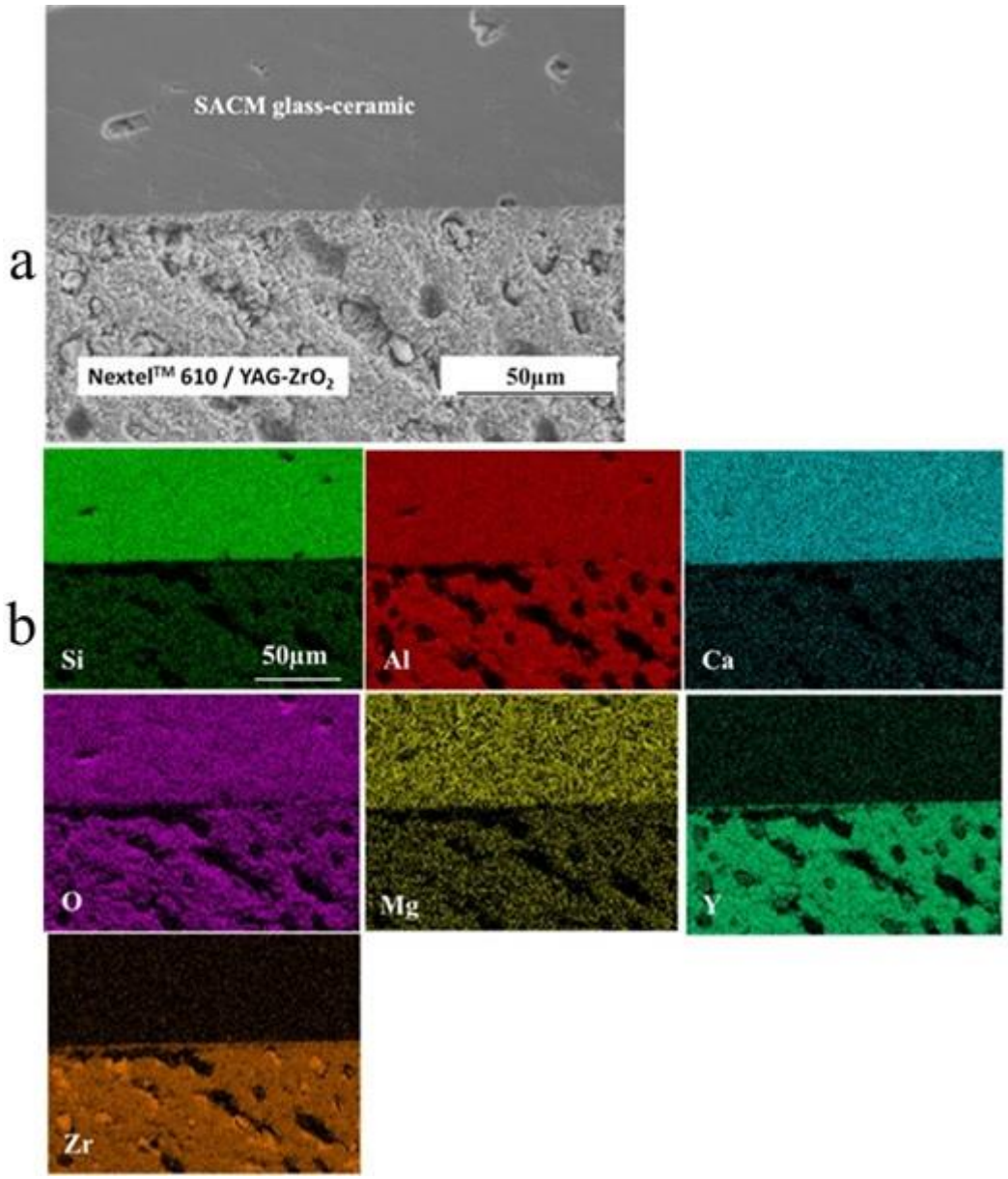

Figure 44: a) Cross section of SACM glass-ceramic joined Nextel^{TM} 610 / YAG-ZrO_2 composite after for 100 h at 850 °C b) EDS maps of SACM joined Nextel^{TM} 610/ YAG-ZrO_2 after ageing 100 hours at 850 °C in air

4.2.2 Joining of Nextel^{TM} 610/alumina-zirconia with Glass-ceramics

4.2.2.1 Glasses and glass-ceramics characterization

The DTA and HSM of GOX glass powder results are represented in figure 45. The sintering process started at 819 °C (T_{SS}) and finished at 891 °C (T_{SF}) while the on-set crystallization temperature (T_{OC}) and peak crystallization temperature (T_P) are 941°C and 1010 °C, respectively. Since $T_{OC} > T_{SF}$ hence the sintering precedes crystallization which could led to dense glass-ceramic with higher mechanical properties.

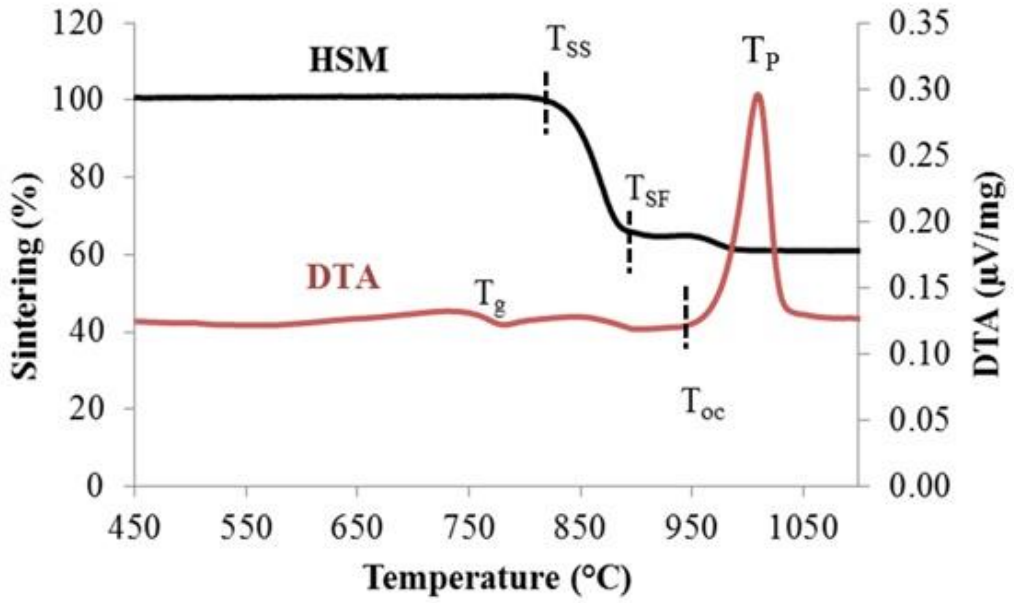

Figure 45: HSM and DTA curve of GOX Glass

During the heating the sintering vs crystallization competition for a glass can be estimated using parameter proposed by by Lara et al. [161] (Equation 4.8)

$$S_C = T_{OC} - T_{SF} \qquad \text{Equation 4.8}$$

The greater the value of S_C, i.e. greater the difference between on-set crystallization temperature (T_{OC}) and sintering end temperature (T_{SF}), the more independent are the kinetics of these two processes. However if the value of $S_C < 0$, that is $T_{SF} > T_{OC,}$ the crystallization process occurs earlier or in competition with the sintering process which could lead to a glass-ceramic with porous

structure. According to Lara et al., a more dense glass-ceramic will obtained for S_C values lie between 40 °C - 60 °C. For GOX glass the value of S_C was 50 °C, hence the resultant GOX glass-ceramic could have large final density with minimum micro-voids which is pre-requisite to obtained higher mechanical properties.

Using the equations 4.4 and 4.5, for evaluating the thermal stability of glass the value of S and ΔT were found to be 17.1 and 187, respectively. Higher values of these parameters show greater resistance to nucleation/crystallization and the resultant glass could be thermally stable during operation. Hence, it could be concluded that GOX glass is potentially a good candidate for joining of Nextel^{TM} 610/alumina-zirconia composite.Table 14 shows the thermal parameters of the GOX glass obtained from DTA and HSM with 5 °C min^{-1}

Table 14: Thermal parameters of GOX glass

Parameters (from DTA and HSM)	**Characteristic temperature (°C)**
Sintering start Temperature (T_{SS})	819
Maximum shrinkage Temperature (T_{SF})	891
Glass transition temperature (T_g)	754
Softening temperature (T_S)	911
Onset crystallization temperature (T_{OC})	941
Peak crystallization temperature (T_P)	1010
Temperature for half ball (T_{HB})	1240

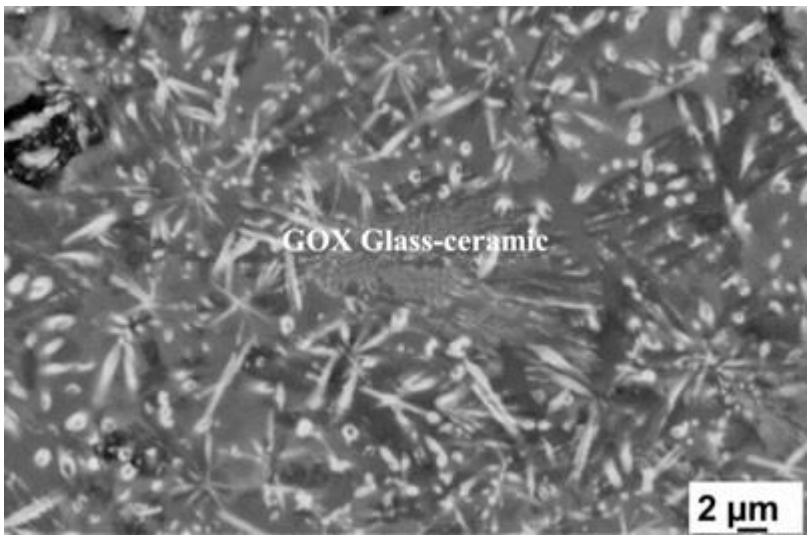

Figure 46: Presence of crystalline phases (bright areas) in GOX glass-ceramic

To investigate the phases formed in the joining seam, the XRD investigation was performed on GOX glass ceramic powder obtained from a GOX glass-ceramic pellet. The GOX glass-ceramic pellet was obtained with same conditions of joining (1010 °C, 2 h dwell and 5 °C min^{-1} heating and cooling rate). The existence of crystalline phases (bright regions) and their microstructure is evident in figure 46.

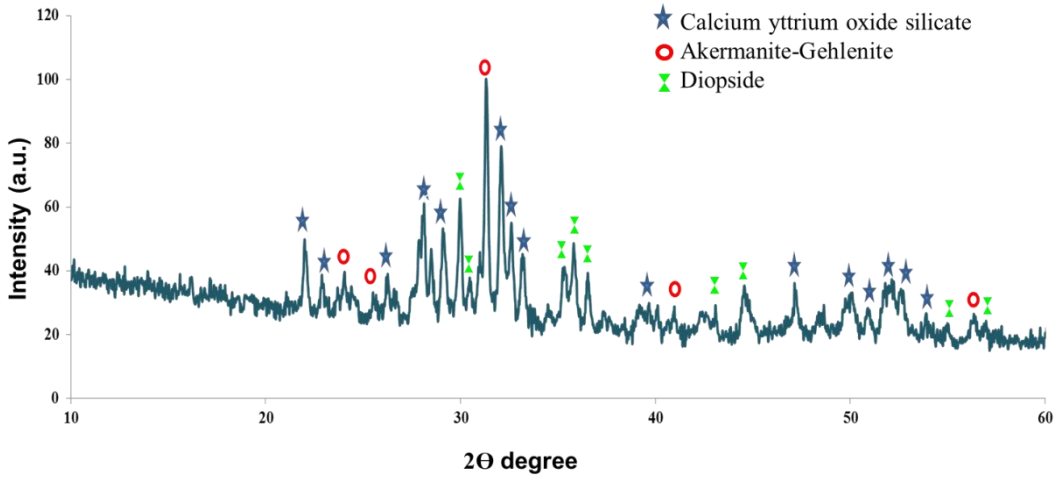

Figure 47: XRD of GOX glass-ceramic

With the help of X'Pert High score software these phase are identified which could be calcium yttrium oxide silicate ($Ca_4Y_6O(SiO_4)_6$, akermanite-gehlenite ($Ca_2Mg_{0.5}Al_{0.5}$)($Si_{1.5}Al_{0.5}O_7$) and diposide ($CaMg(SiO_3)_2$. The XRD pattern is shown in figure 47.

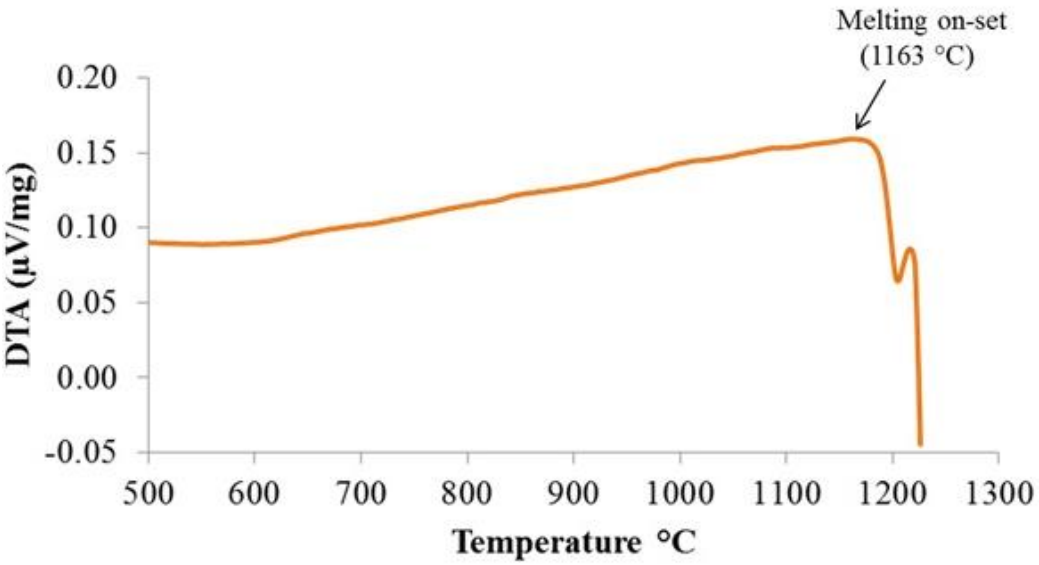

Figure 48: DTA curve of GOX glass-ceramic with heating rate of 5 °C min^{-1}

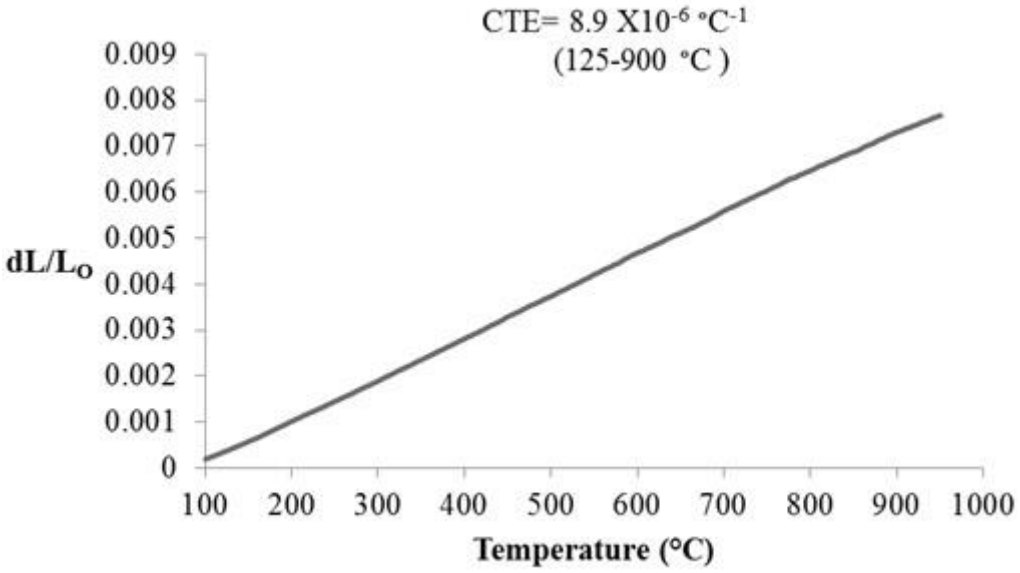

Figure 49: Dilatometry curve of GOX glass-ceramic

In order to investigate the thermal stability and crystallization resistance of GOX glass-ceramic the DTA (heating rate 5 °C min^{-1}) and Dilatometry (heating rate 5 °C min^{-1}) performed on GOX glass-ceramic. The DTA curve of GOX glass-ceramic is shown in the figure 48. No further crystallization peak was identified in DTA thermograph which is an indication of almost complete devitrification/crystallization of GOX glass-ceramic which is for higher mechanical properties of joined component. The Dilatometry curve is shown in the figure 49. The Dilatometry measurement was stopped at 950 °C due to safety reason (on-set melting 1163 °C).No softening was detected up to 950 °C which indicates the thermal stability of GOX glass-ceramic up to this temperature.

To minimize the thermal stresses at the joint zone it is desirable that the difference between the CTEs of joining material and substrate, that is, ΔCTE must be as low as possible. For glass-ceramics, as joining materials, some researchers suggested that the value of ΔCTE should not be greater than $1x10^{-6}$ $°C^{-1}$ [187]. Higher values of ΔCTE may result to interfacial de-bonding, cracks and lower mechanical strength due to high thermal stresses, which arise at the joint area during the cooling process of joining/brazing cycle [188][189]. In case of some metallic brazing systems the thermal stresses could be compensated by the ductile deformation of the brazing alloy [51], however, below T_g glass-ceramic are brittle and thermal stresses could not be relieved so it is important that the glass-ceramic and ox/ox CMC should have a matching CTE. The CTE of the GOX glass-ceramic, reported in figure 49, from 125 °C to 900 °C was 8.93 $x10^{-6}$ $°C^{-1}$ and the CTE of the Nextel™ 610/alumina-zirconia composite was 8.63 $x10^{-6}$ $°C^{-1}$ for the same temperature range. The value of ΔCTE for GOX glass-ceramic and composite was 0.33 $x10^{-6}$ $°C^{-1}$ which suggests lower thermal stresses at the joint area and therefore ensures an excellent thermal compatibility of this system.

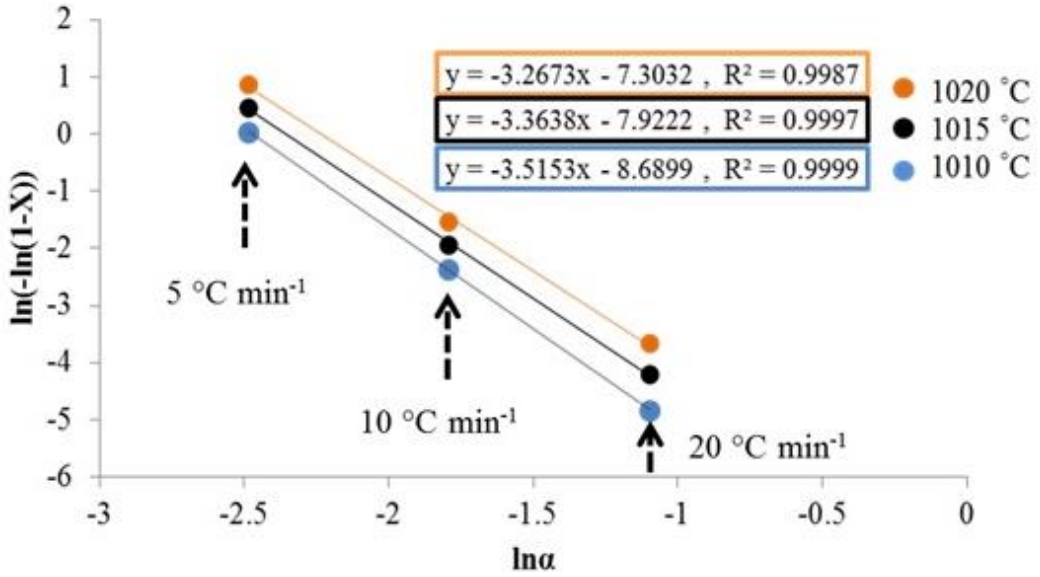

Figure 50: Ozawa plots for calculating the value of n using heating rate of 5 °C min^{-1}, 10 °C min^{-1}, 20 °C min^{-1} and temperature 1010 °C, 1015 °C, 1020 °C

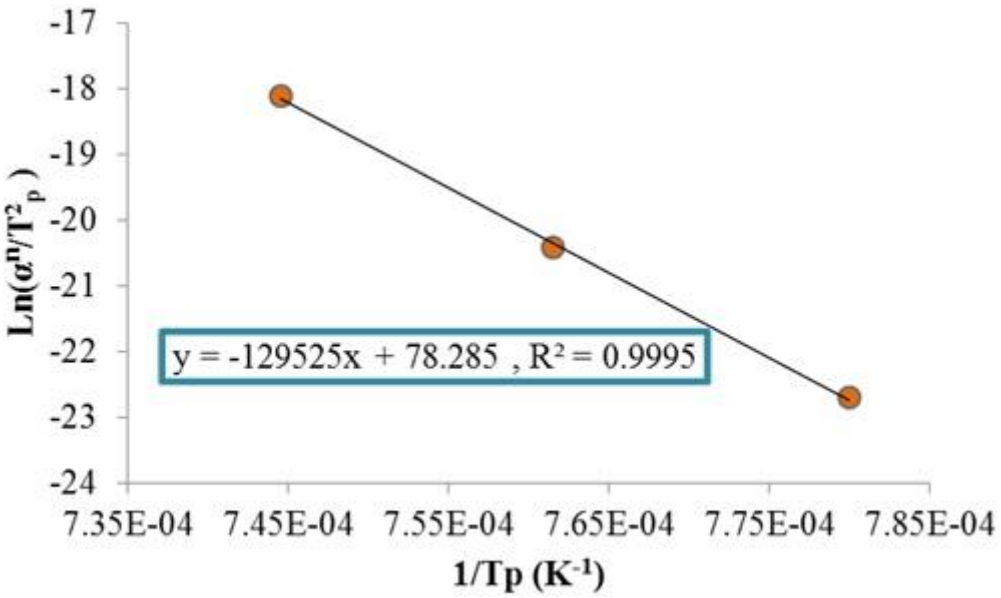

Figure 51: Matusita and Sakka plot for calculating the activation energy of crystallization.

By using the experimental results of DTA, the crystallization kinetic parameters, that is, activation energy of crystallization (E_{ac}) and Avrami parameter (n) can be determined using equations and methods discussed in section 4.2.1.1. For GOX glass-ceramic the T_P values, obtained with heating rates of 5 °C min^{-1}, 10 °C min^{-1}, 20 °C min^{-1}, are 1010 °C,1040 °C,1069 °C respectively Furthermore the values of T_S selected for GOX glass-ceramic are 1010 °C, 1015 °C, 1020 °C for the crystallization peaks obtained with heating rates of 5 °C min^{-1}, 10 °C min^{-1}, 20 °C min^{-1} respectively. The average value of n and m were found to be 3.34 and 2.34 respectively. These values suggested a mix of two dimensional and three dimensional growth of crystals [190]. The plots of ln(-ln(1-X)) vs 1/ lnα and $\ln(\alpha^n/T_p^2)$ vs $1/T_p$ are shown in figures 50 and figure 51, respectively. The value of activation energy of crystallization was found to be 452.85 kJ/ mol.

4.2.2.2 Joining, mechanical testing and ageing

From DTA data, the joining temperature was selected 1010 °C for Nextel^{TM} 610/alumina-zirconia composite. This temperature is located inside the crystallization regime and could assure mechanical properties. This temperature is significantly above the softening temperature (911 °C) of GOX glass and at the same it is well below the sintering temperature (1225 °C) of Nextel^{TM} 610/alumina-zirconia composite. Above sintering temperature of composite, it could be possible that mechanically properties of the composite could be affected due to grain coarsening of Nextel 610^{TM} fibers [3]. Furthermore, as the maximum densification/shrinkage is already completed at 891 °C (sintering end temperature) so this joining temperature could produce dense joints.

The cross-section of GOX glass-ceramic joined Nextel^{TM} 610/alumina-zirconia composite is shown in the figure 52. The joining interface is continuous and free from defects. No cracks were observed either parallel or perpendicular direction of the joining seam. This could be attributed to the perfect matching CTE between GOX glass-ceramic and Nextel^{TM} 610/alumina-zirconia composite. Nevertheless, some micro-voids were observed in GOX glass-ceramic. The possible causes of formation of these micro-voids, due to the pressure-less joining technology based on a slurry, and to the gaseous products trapped in the porous ox/ox CMC, have been are already discussed in section 4.2.1.2.

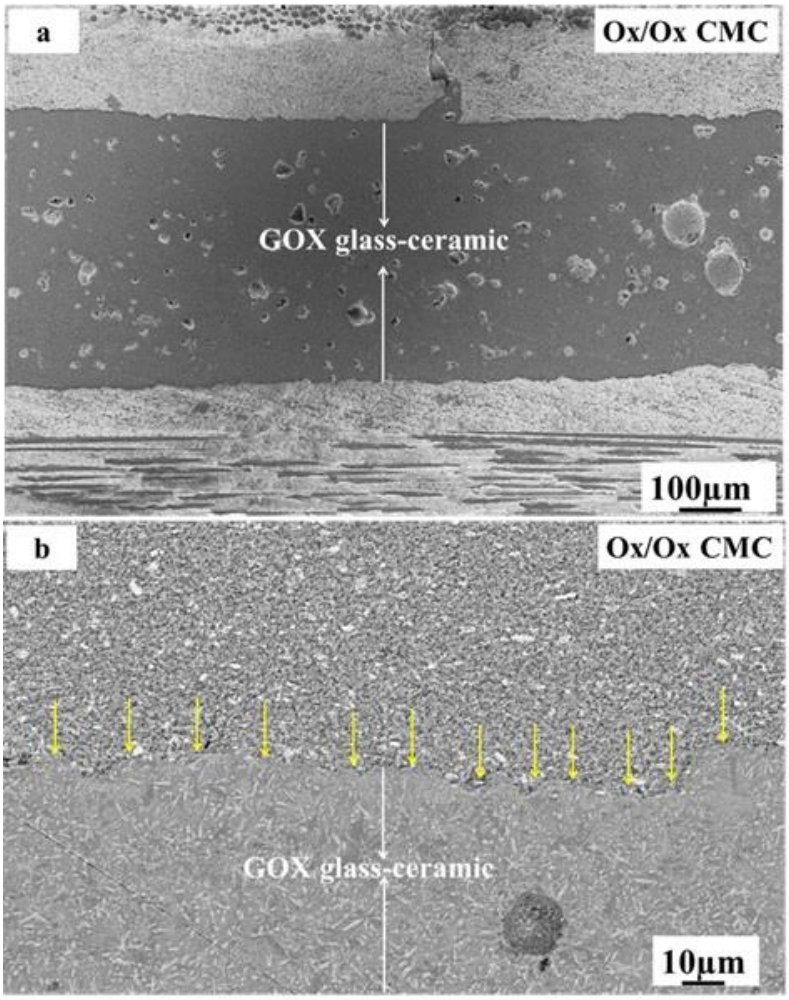

Figure 52: SEM micrograph of a) Joint cross-section b) Joint cross-section in backscattered mode

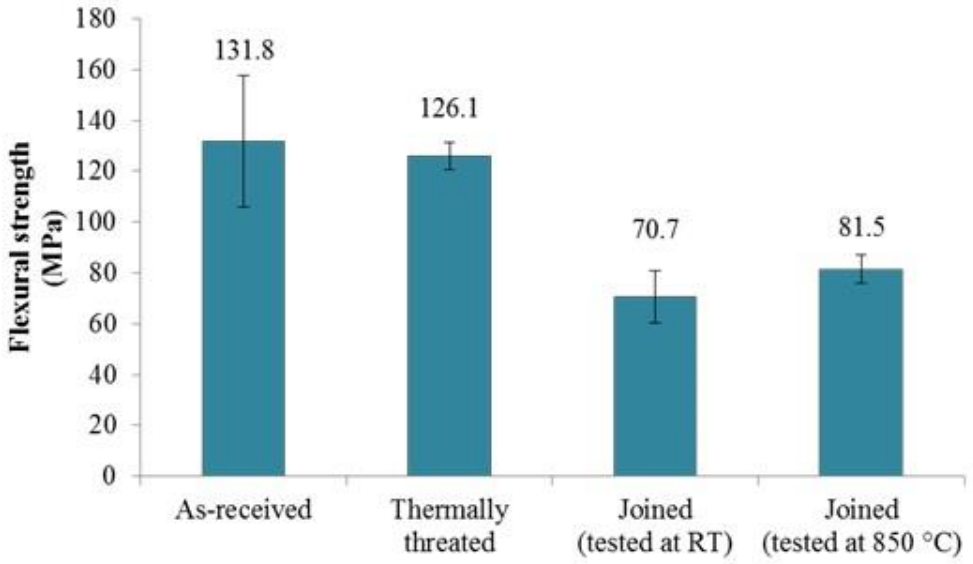

Figure 53: Four-point bending strength of as-received, thermally treated and joined samples tested at RT and at 850 °C in air

For utilization of this composite for high performance structures it is important to know the mechanical strength of GOX joined Nextel ™ 610 /alumina-zirconia composite. The single lap offset (SLO) shear tests again resulted again in delamination of the composite in all the three joined samples without any fracture in the joint zone. The average SLO shear strength at which delamination occurred was 6.8 MPa ± 1.8. From industrial point of view this result is very important, it implies that during the application of a shear force on the GOX joined Nextel™ 610/alumina-zirconia component, during operation, the joint could never fail before the composite actually delaminate.

The average four-point bending strength of as-received, thermally treated, joined samples (tested at RT) and joined samples (tested at 850 °C in air) are reported in the figure 53. The thermally treated samples were given the same heat treatment as of joined samples. The purpose of testing thermally treated samples was to evaluate any degradation in the mechanical strength of Nextel™ 610 /alumina-zirconia composite for the selected joining condition (Temp. 1010 °C, Dwell= 2 h, heating and cooling rates 5 °C min^{-1} in air). Figure 53 shows that decrease in flexural strength of thermally treated sample is negligible (4.3%) and within the experiment error of as-received flexural strength. The GOX glass-ceramic joined samples have average flexural strength of 70.7 MPa ± 10.4, that is, approximately 54 % of as-received samples.

Limited literature is available on joining and mechanical testing of ox/ox composite, however, four-point bending strength of joined samples is considerably higher that reported in literature. For example, Gadelmeier et al. studied joining of CerOx Z-N6-R (Nextel ™ 610 reinforced with pure zirconia matrix) using a commercial SiO_2-CaO-BaO-Al_2O_3 based glass/glass-ceramic and performed joining in furnace in air atmosphere. The flexural strength of as-

received CerOx Z-N6-R composite was 263 MPa, however the flexural strength of SiO_2-CaO-BaO-Al_2O_3 joined CerOx Z-N6-R samples was 32.5 MPa which was only 13 % (approx.) of as-received CerOx Z-N6-R composite [107]. In other study, Gadelmeier et al. studied joining of CerOx Z-N6-R (Nextel ^{TM} 610 reinforced with pure zirconia matrix) was joined using commercial available SiO_2-CaO-Y_2O_3 based glass/glass-ceramic using furnace joining and CO_2 laser joining method. The flexural strength of as-received samples of this composite was 368 MPa. The SiO_2-CaO-Y_2O_3 furnace joined CerOx Z-N6-R composite had a flexural strength of 39 MPa which was 11 % (approx.) of as-received values(368 MPa). For CO_2 laser joined samples (using the SiO_2-CaO-Y_2O_3 based glass/glass-ceramic) the joint strength was 15 MPa which was only 4% of as-received CerOx Z-N6-R composite (368 MPa) [108].

As ox/ox CMCs are potential candidates for high temperature applications, it is imperative to evaluate the mechanical strength of joined samples at high temperature. As reported in figure 53 the four-point bending strength of joined samples tested at 850 °C was 81.5 ± 5.5 MPa. The slightly higher flexural strength values at 850 °C respect to RT could be due to completion of sintering, or to a further crystallization of the residual amorphous phase or to a stress release due to the testing temperature, as will be discussed in the following paragraph.

It must be pointed out that flexural strength at RT and at 850 °C was tested according to different testing standards, namely, ASTM C1161 was used for room temperature and DIN EN 843-1 for high temperature (850 °C). However due to the same sample size, similar cross head speed (0.5 mm/min), equal length for outer and inner spans used for both of these tests/standards, it could be possible to compare the results.

Malzbender et al. [184] reported that glass-ceramic which are almost completely crystallized showed similar flexural strength at RT and at high temperature (above the glass transition). However in case of GOX glass-ceramic joined samples the flexural strength at 850 °C is approximately 15% higher as compared to flexural strength at RT. This behavior of GOX glass-ceramic could be explained by taking into consideration the viscoelastic behavior of the residual glassy phase and crack growth behavior at high temperature. At RT glasses and glass-ceramics behave as brittle materials and GOX glass-ceramic joined Nextel 610^{TM} /alumina-zirconia composite sample might be under a limited but not negligible stress due to the small CTE mismatch between GOX glass-ceramic and the composite. Cheeseman et al.[191] reported that residual glassy phase containing ceramics showed an increase in flexural strength at high temperature as compared to flexural strength at RT. This effect at high temperature is caused by energy dissipated in viscous stretching of glassy phase which bridge the opposite crack surface. In other words, as the crack grows it require increase energy due to bridging effect between opposite crack surfaces which in turn require more load until crack propagation become finally unstable. Wang et al.[192] also reported that at high temperature, the residual silica glassy phase containing ceramics showed a similar behavior due to plastic deformation of residual glassy phase. Recently, Hasanabadi et al. [93] observed an increase in flexural strength of a

SiO_2-BaO-CaO-Al_2O_3-B_2O_3 based glass-ceramic at high temperature (800 °C) as compare to flexural strength at RT.

The fracture surfaces of four-point bending tests at RT and at 850 °C are reported in the figure 54. In both cases the cohesive failure was observed. The cohesive failure of GOX glass-ceramic showed strong adhesion and wetting of GOX glass-ceramic with Nextel™ 610/alumina-zirconia.

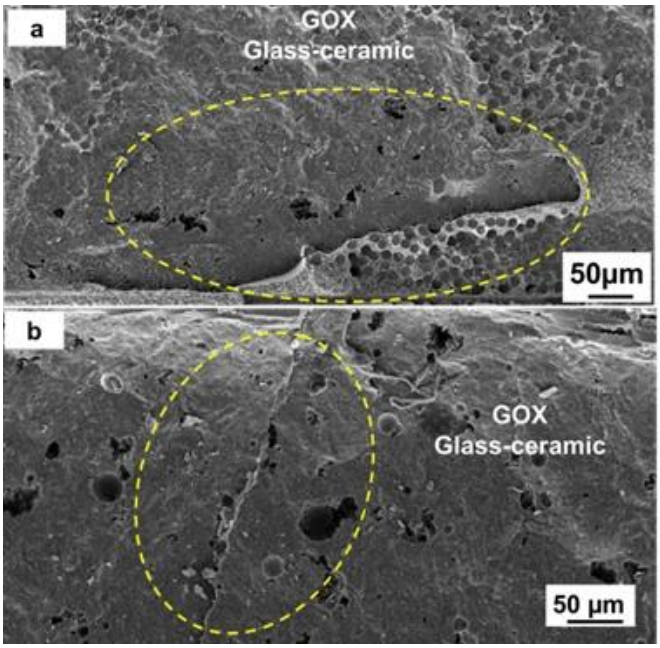

Figure 54: SEM micrographs of fracture surfaces of GOX glass-ceramic joined Nextel™ 610/alumina-zirconia a) tested at RT b) tested at 850 °C

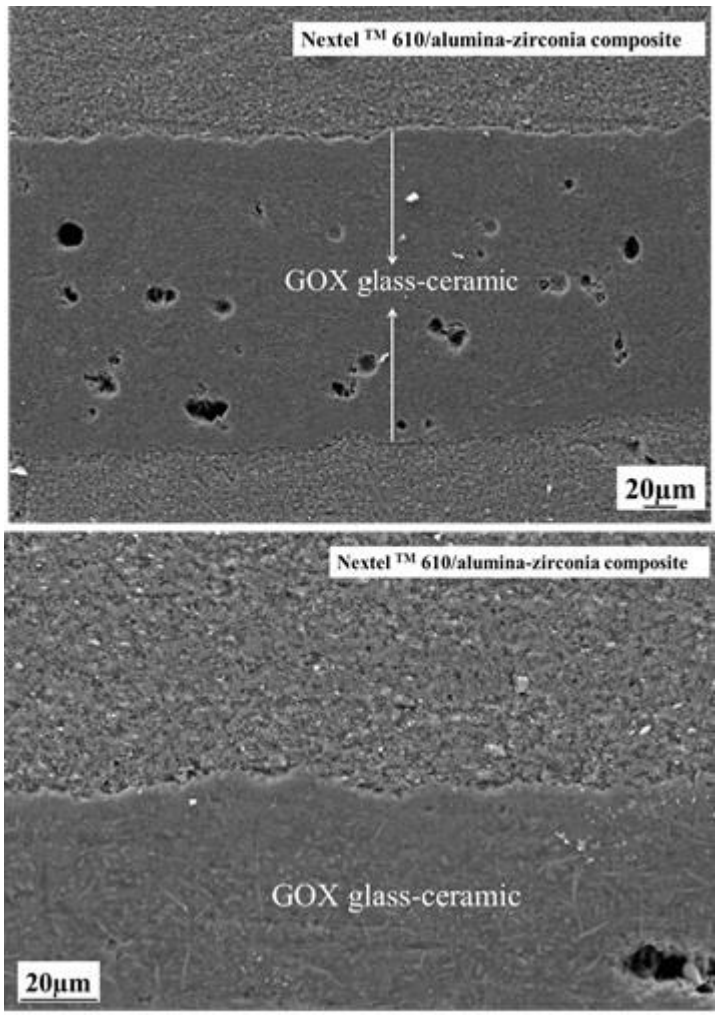

Figure 55 : Joint cross-section after thermal ageing for 100 h at 850°C in air

The thermal stability of joined structural parts at operation temperature for longer hours is crucial. The joining material must with stand the working temperature without forming deleterious reaction products at the joining interface. For GOX glass-ceramic joined Nextel^{TM} 610/alumina-zirconia composite a preliminary ageing at a temperature of 850 °C for 100 h in air was selected as working conditions. The selected temperature (850 °C) was well below the on-set crystallization temperature (941 °C) of GOX glass-ceramic. If the working/ageing temperature lies in the crystallization regime of glass-there is chance that further crystallization starts to occur rapidly this could alter the microstructure (crystalline phases) and properties of the glass-ceramics such as CTE [86]. Once the CTE of joining material is altered it could cause crack in the joining materials and/or composite which eventually lead to failure of the system.

Furthermore, even though the selected working temperature (850 °C) is somehow below the upper limit of ox/ox CMC (under load at 1000 °C), still this temperature is of high interest as it is above the service temperature of titanium-based alloys [193], nickel-based super alloys, such as, Inconel 706 [194], Inconel 718 [195] and comparable to operational temperature of AISI 304L/304/316/321/347 stainless steels [196]–[198] all of them having three times

the density of these ox/ox CMC. Figure 55 show the cross-section of GOX joined Nextel^{TM} 610/alumina-zirconia composite after thermal ageing of 100 h at 850 °C in air. The joint interface is continues and free from any defects. Figure 56 illustrates the elemental mapping at the joint area after thermal ageing of 100 h at 850 °C in air. There was no clear evidence of diffusion of elements from GOX glass-ceramic to Nextel^{TM} 610/alumina-zirconia composite and vice versa. This confirms the suitability and stability of GOX glass-ceramic to join Nextel 610^{TM} /alumina-zirconia composite [199].

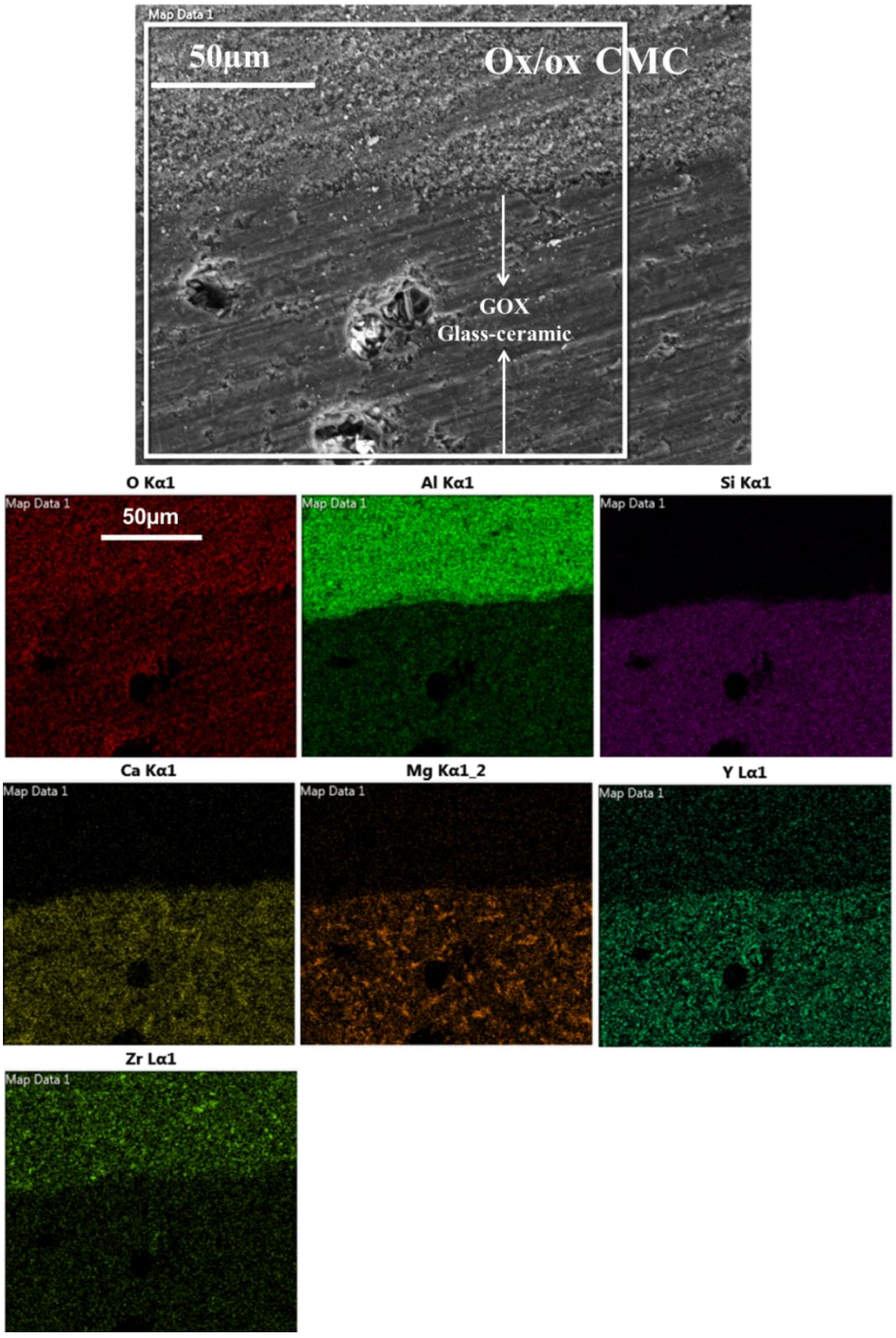

Figure 56: Elemental mapping of joint interface after 100 h at 850 °C in air

4.3 Conclusion

Nextel^{TM} 610/YAG-zirconia and Nextel^{TM} 610/alumina-zirconia composite were successfully joined using novel SiO_2-Al_2O_3-CaO-MgO (SACM) and SiO_2-Al_2O_3-CaO-MgO-Y_2O_3-ZrO_2 (GOX) based glass-ceramics, respectively. HSM and DTA analysis showed that for both GOX and SACM glasses the sintering is completed well before the start of crystallization process. As a result, dense glass-ceramics were produced which are vital for higher mechanical properties. From the DTA analysis, the joining temperatures for SACM and GOX glasses were chosen within the crystallization zone of respective glasses. The selected joining temperatures were significantly above the softening temperatures of respective glasses and well below the sintering temperature of Nextel^{TM} 610/YAG-zirconia and Nextel^{TM} 610/alumina-zirconia composites. Above sintering temperature of composite, it could be possible that mechanically properties of the composite could be affective due to grain coarsening of Nextel ^{TM} 610 fibers. The SACM and GOX glass-ceramics have matching coefficient of thermal expansion with Nextel^{TM} 610/YAG-zirconia and Nextel^{TM} 610/alumina-zirconia composites, respectively, which resulted to lower residual thermal stresses and higher mechanical properties of joint components.

Ox/ox CMCs are potential candidates for high temperature application therefore thermal ageing of joints must be investigated. For this study, 850 °C for 100 h and 930 °C for 50 h in static air was selected as representative working conditions.Though this working temperature is somewhat below the upper limit of ox/ox CMC (1000 °C under load), it is still of great interest, as it is above the service temperature of titanium-based alloys, nickel-based super alloys and comparable with the operation temperatures of AISI 304/304L/321/316L/347 stainless steel.The joint interfaces were continuous and free from cracks and defects after ageing tests, showing that joints are oxidation resistant at least for these ageing conditions. Furthermore, after the ageing test, elemental mapping shows that there is no considerable diffusion of elements from glass-ceramic to composites and vice versa.

SLO shear and four-point bending tests were performed at RT and at 850 °C on joined samples. SLO shear test resulted to delamination of composites. This result suggested that during the application of a lap shear force on the SACM joined Nextel^{TM} 610/YAG-zirconia or GOX joined Nextel^{TM} 610 /alumina-zirconia composites, the composite delaminate and break before the joining material itself, due to stress concentration distribution typical of lap shear tests for brittle joining materials. Four-point bending strength for the SACM joined Nextel^{TM} 610/YAG-zirconia samples were 68.5 MPa (RT) while for GOX joined samples it was 70.7 MPa (RT) and 81.5 MPa (at 850 °C). Four-point bending strength of thermally treated samples was found similar to as-received composited which showed that the joining condition did not degrade the mechanically properties of composites. The reported four-point bending strengths are considerably higher than those reported in literature for glass-ceramics joined ox/ox CMCs. For SACM joined Nextel^{TM} 610/YAG-zirconia composites both

cohesive and adhesive failures were observed, while for GOX joined composites , cohesive failure was observed for both RT and high temperature (at 850 °C) with four-point bending tests.

Chapter 5

Conclusion

Joining of two types of ox/ox CMCs (Nextel^{TM} 610/YAG-zirconia and Nextel^{TM} 610/alumina-zirconia) were performed using brazing alloys and glass-ceramics. At first nickel-chromium (NiCrB and NiCrSiB) brazing alloys were selected due to their demonstrated oxidation resistance and brazing temperature below 1200°C: however these alloys failed to wet the Nextel^{TM} 610/YAG-zirconia composite. Further studies would be necessary to overcome this problem, due to the interesting properties of these brazing allows. However, for the purpose of this Thesis, it was decided to focus on other joining materials, such as active brazing alloys.

Active metal based commercial brazing alloys, such as AgCuSnTi and ZrNiTiHf were selected for Nextel^{TM} 610/YAG-zirconia composite. The motivation of using the Ag-Cu system is due to its reactivity with oxide ceramics, low eutectic temperature and ductile properties which can possibly accommodate the thermal stresses due to difference in CTE of Nextel^{TM} 610/YAG-zirconia composite and brazing alloy. The ZrNiTihf system was selected due to a closer match of CTE between Zr NiTiHf and Nextel^{TM} 610/YAG-zirconia composite and also because of its heat resistance up till 550 °C for long term and 650 °C for short term applications. The joining was performed in inert atmosphere and above the liquidus temperature of the brazing alloys. The joints samples were free from cracks and discontinuities. A preliminary oxidation test for the joined samples was then performed in air furnace at 550 °C for 1 h. The AgCuSnTi joint samples debonded during oxidation test. The formation of Cu_2O as main phase during oxidation was considered the most likely reason. The Cu_2O has CTE 4 X 10^{-6} K^{-1}, while CTE of Cu is 17x 10^{-6} K^{-1}. The difference in CTE of Cu_2O and Cu could have caused cracking and physical separation of Cu_2O from Cu, which may results to debonding. In case of ZrTiNiHf complete oxidation of brazing material to ZrO_2/TiO_2 was observed.

Together with the oxidation behaviour, also the mechanical strength of these brazing alloys was far from being satisfactory. The average Single Lap

Offset (SLO) shear strength of AgCuSnTi and ZrNiTiHf joint samples were measured to be 5.3 ±1.8 MPa and 2.59 ± 1.6 MPa, respectively. For AgCuSnTi brazing system, the formation of brittle TiO_X phases at the composite/brazing interface could be responsible for low SLO values. For ZrNiTiHf brazing alloy, there were some zones (detected during EDS post brazing analysis) which have different compositions as compared to the bulk brazing alloy; furthermore, a considerable amount of oxygen was also detected within the brazing alloy during EDS analysis. The small atomic radius of oxygen allows may occupy interstitial positions in Ti and Zr crystalline lattices which deteriorate their ductility. Therefore, the heterogeneity within the brazing alloy and oxygen induced embrittlement might be responsible for low SLO value. Due to poor oxidation resistance and low mechanical strength these alloys are not recommended for joining of ox/ox CMCs.

In order to find a suitable brazing alloy for these composites, a new system based on Ti, Cu, and Al was developed within this Thesis, by using the metallic interlayer approach. The system was designed because of good wetting properties of Ti with oxides and ductility of copper, which could accommodate the residual stresses, while aluminium was included due to its oxidation resistance behavior. The configuration of the brazing assembly was CMC/Ti/Cu/Al/Cu/Ti/CMC and it was called TiCuAl. The joints interfaces were continues and free of cracks even after the oxidation test (at 550 °C for 1 h in air). The better oxidation resistance might be due to the formation of a protective thin passivating layer of α-Al_2O_3 formed by preferential oxidation of Al which further stop the diffusion of oxygen and protect TiCuAl system from oxidation, upon increasing temperature. However, the average SLO shear strength value was 1.88 ± 0.5 MPa only. The CTE of TiCuAl system is not known, however with such a low shear strength the possible reason could be very high residual thermal stresses and/or presence of brittle titanium oxides phases at the interface. Further research is required to optimize the mechanical strength of this promising brazing system, especially designed for oxide-based composites.

In parallel with metal-based brazing materials, and by considering as main requirements for the joining material oxidation resistance, stability at high temperature, wetting with oxide ceramics and tailorable properties, glass-ceramics were selected. The composition of glass-ceramics were developed using SciGlass 6.6 database with CTE of ox/ox CMCs as the main criteria. Several glass-ceramics with matching CTE to ox/ox CMCs were developed to minimized the residual stresses.

For Nextel^{TM} 610/YAG-zirconia a glass-ceramic based on SiO_2 -Al_2O_3-CaO-MgO (labelled as SACM) was developed. For Nextel^{TM} 610/alumina-zirconia CMC, a glass-ceramic based on SiO_2 -Al_2O_3-CaO-MgO-Y_2O_3-ZrO_2 (labelled as GOX) was developed. Hot stage microscopy, DTA and dilatometry measurement were performed to investigate their sintering and CTE properties. The joining temperatures were selected at 980 °C and 1010 °C for of SACM and GOX, respectively. The XRD analysis showed that Gehlenite magnesia ($Al_{1.5}Ca_2Mg_{0.25}O_7Si_{1.25}$) and Anorthite ($CaAl_2Si_2O_8$) are the dominant phases in

SACM. For GOX the identified phases are calcium yttrium oxide silicate ($Ca_4Y_6O(SiO_4)_6$, akermanite-gehlenite $(Ca_2Mg_{0.5}Al_{0.5})(Si_{1.5}\ Al_{0.5}O_7)$ and diopside $(CaMg(SiO_3)_2$. SACM and GOX slurries were made with ethyl alcohol and applied manually to the ox/ox CMC samples. The joining was performed in air without applying any pressure. The joining interfaces were sound and free from defects. During SLO shear test, the composite delaminates both for SACM and GOX joined samples. From an industrial point of view, this result is very important: it means that during the application of a lap shear force on SACM and GOX joined ox/ox CMC component, the joint does not fail during operation, but it is the composite which actually delaminates.

To further investigate the mechanical properties without the uncertainties related to lap tests, four-point bending strength was used for joined samples at RT and HT. The four-point bending strength was also performed for as-received and thermally treated not joined composites. Thermally treated ox/ox CMC composites were heat treated at the same conditions of joining to investigate if the selected joining conditions affected their mechanical properties. Nextel^{TM} 610/YAG-zirconia as-received and thermally treated samples have similar bending strength. A similar behaviour was also observed for Nextel^{TM} 610/alumina-zirconia. This showed that the selected joining conditions do not affect the mechanical strength of Nextel^{TM} 610/YAG-zirconia and Nextel^{TM} 610/alumina-zirconia composites. For SACM joined Nextel^{TM} 610/YAG-zirconia the average four-point bending strength at RT was 68.5 ± 12.1 MPa and for GOX joined Nextel^{TM} 610/alumina-zirconia, 70.7 ± 10.4 MPa. These values are considerably higher than the values reported in literature for joining ox/xo CMCs using glass-ceramics. The matching CTE of SACM and GOX with Nextel^{TM} 610/YAG-zirconia and Nextel^{TM} 610/alumina-zirconia, respectively, led to lower residual stresses and contribute to higher mechanical properties in both cases. The mixed adhesive/cohesive failure was observed in SACM joined Nextel^{TM} 610/YAG-zirconia composite while cohesive failure was detected in GOX joined Nextel^{TM} 610/alumina-zirconia composite. Micro-voids were observed in both SACM and GOX glass-ceramics joined composites. These micro-voids, due to the slurry based joining method, can act as stress concentrating factors and the fracture was observed originating from these micro-voids, leading to failure during four-point bending test. A different, or improved, slurry based joining technology should further improve the mechanical strength of these joints.

In order to evaluate mechanical properties of these joint at high temperature, the four-point bending strength of GOX glass-ceramic joined Nextel^{TM} 610/alumina-zirconia was also performed at 850 °C, giving an average value of 81.5 ± 5.5 MPa which is about 15 % higher than the RT value, which can be due to the presence of a small (not detectable by XRD) residual glassy phase in the GOX glass-ceramic: the energy dissipated in the viscous regime may bridge cracks and increase the overall mechanical strength. Both at RT and at 850 °C, the cohesive failure was dominant.

The thermal stability of joined structural parts at working temperature very important: thermal ageing at 850 °C for 100 h in air for SACM joined Nextel^{TM}

610/YAG-zirconia and GOX joined Nextel^{TM} 610/alumina-zirconia composite showed that the joint interfaces remained well bonded, without any cracks and defects. Furthermore, the elemental mapping after ageing showed no evidence of diffusion of elements from glass-ceramics (SACM and GOX) to Nextel^{TM} 610/YAG-zirconia or Nextel^{TM} 610/alumina-zirconia. This justifies the suitability and compatibility of both SACM and GOX glass-ceramics for Nextel^{TM} 610/YAG-zirconia and Nextel^{TM} 610/alumina-zirconia composites, respectively.

Finally, the two glass-ceramics designed, prepared and tested within this thesis have been proven to be promising joining material for ox/ox CMCs. The joining process was performed in air without applying any pressure so it can be commercially feasible for joining all ox/ox CMC shapes and sizes without degradation in mechanical properties during joining process.

References

[1] C. J. Armani, M. B. Ruggles-Wrenn, G. E. Fair, and R. S. Hay, "Creep of Nextel 610 fiber at 1100C in air and in steam," *Int. J. Appl. Ceram. Technol.*, vol. 10, no. 2, pp. 276–284, 2013.

[2] F. W. Zok, "Developments in oxide fiber composites," *J. Am. Ceram. Soc.*, vol. 89, no. 11, pp. 3309–3324, 2006.

[3] N. P.Bansal and J. Lamon, Eds., *Ceramic Matrix Composites Materials,Modeling and Technology*. Wiley, 2015.

[4] N. Al Nasiri, N. Patra, N. Ni, D. D. Jayaseelan, and W. E. Lee, "Oxidation behaviour of SiC/SiC ceramic matrix composites in air," *J. Eur. Ceram. Soc.*, vol. 36, no. 14, pp. 3293–3302, 2016.

[5] P. D. Sarkisov, N. V. Popovich, L. A. Orlova, and Y. E. Anan'Eva, "Barrier coatings for type C/SiC ceramic-matrix composites (Review)," *Glas. Ceram. (English Transl. Steklo i Keramika)*, vol. 65, no. 9–10, pp. 366–371, 2008.

[6] Q. Ma and L. Cai, "Fabrication and oxidation resistance of mullite/yttrium silicate multilayer coatings on C/SiC composites," *J. Adv. Ceram.*, vol. 6, no. 4, pp. 360–367, 2017.

[7] B. Kanka and H. Schneider, "Aluminosilicate ® ber / mullite matrix composites with favorable high-temperature properties," vol. 20, pp. 619–623, 2000.

[8] J. J. Haslam, K. E. Berroth, and F. F. Lange, "Processing and properties of an all-oxide composite with a porous matrix," vol. 20, pp. 607–618, 2000.

[9] C. Kaya, F. Kaya, E. G. Butler, A. R. Boccaccini, and K. K. Chawla, "Development and characterisation of high-density oxide fibre-reinforced oxide ceramic matrix composites with improved mechanical properties," vol. 29, pp. 1631–1639, 2009.

[10] M. Gerendás *et al.*, "IMPROVEMENT OF OXIDE/OXIDE CMC AND DEVELOPMENT OF COMBUSTOR AND TURBINE COMPONENTS IN THE HIPOC PROGRAM," in *Proceedings of ASME Turbo Expo*, 2011, pp. 477–490.

[11] T. Wamser, S. Scheler, B. Martin, and W. Krenkel, "Novel oxide fiber composites by freeze casting," *J. Eur. Ceram. Soc.*, vol. 34, no. 15, pp. 3827–3833, 2014.

[12] R. W. Messler, "Joining advanced materials," *Adv. Mater. Process.*, vol. 147, no. 2, pp. 47–49, 1995.

[13] N. Bansal and J. Lamon, Eds., *CERAMIC MATRIX COMPOSITES*. WILEY, 2015.

[14] T. W. Eagar, "Challenges in Joining Emerging Materials," in *International Conference on Advances in Joining Newer Structural Materials*, 1990.

[15] M. Gerendás *et al.*, "DEVELOPMENT AND VALIDATION OF OXIDE/OXIDE CMC COMBUSTORS WITHIN THE HIPOC PROGRAM," in *Proceedings of ASME Turbo Expo 2013: Turbine Technical Conference and Exposition GT2013*, 2013.
[16] E. Volkmann, K. Tushtev, D. Koch, C. Wilhelmi, J. Göring, and K. Rezwan, "Assessment of three oxide/oxide ceramic matrix composites: Mechanical performance and effects of heat treatments," *Compos. Part A Appl. Sci. Manuf.*, vol. 68, pp. 19–28, 2015.
[17] M. C. Halbig, M. H. Jaskowiak, J. D. Kiser, D. Zhu, and N. Glenn, "Evaluation of Ceramic Matrix Composite Technology for Aircraft Turbine Engine Applications," 2013.
[18] J. D. Kiser *et al.*, "Oxide/Oxide Ceramic Matrix Composite (CMC) Exhaust Mixer Development in the NASA Environmentally Responsible Aviation (ERA) Project," in *ASME Turbo Expo 2015: Turbine Technical Conference and Exposition*, 2015.
[19] R. Riedel, I. Chen, and R. Chen, *Ceramics Science and Technology Volume 4:Applications*. Wiley-VCH are, 2013.
[20] C. Wilsey, "Continuous Lower Energy , Emissions and Noise (CLEEN) Technologies Development Boeing Program Update Boeing CLEEN Program Overview," 2012.
[21] S. T. Gonczy, "Federal Aviation Administration (FAA) airworthiness certification for ceramic matrix composite components in civil aircraft systems," in *MATEC Web of Conferences*, 2015, vol. 29.
[22] T. Ullmann, Y. Shi, N. Rahner, and M. Schmücker, "Quality Assurance for the Manufacturing of Oxide Fiber Reinforced Ceramic Composites for Aerospace Applications," in *4th International Symposium on NDT in Aerospace 2012 - We.2.B.1*, 2012.
[23] A. Stamminger and H.-E. Marcus, "The Sharp Edge Flight Experiment SHEFEX 1 - A Mission Overview," in *Proceedings 5th European Workshop on Thermal Protection Systems and Hot Structures Noordwijk, The Netherlands, 17 - 19 May 2006*.
[24] A. Rüdinger, "Oxide Ceramic Matrix Composites – Manufacturing , Machining , Properties and Industrial Applications," *CERAMICAPPLICATIONS*, no. 3, 2015.
[25] A. Harris and J. A. Yeomans, "Surface Preparation of Alumina for Improved Adhesive Bond Strength in Armor Applications," *Ceram. Eng. Sci. Proc.*, 2013.
[26] A. Bellosi, T. Kosmac, and A. P. Tomsia, Eds., *Interfacial Science in Ceramic Joining*. Kluwer Academic Publishers.
[27] B. Tang, M. Wang, R. Liu, J. Liu, H. Du, and A. Guo, "Journal of the European Ceramic Society Feature article A heat-resistant preceramic polymer with broad working temperature range for silicon carbide joining," *J. Eur. Ceram. Soc.*, no. July, pp. 0–1, 2017.
[28] C. A. Lewinsohn and I. Reimanis, "Using Preceramic Polymers," vol. 44, pp. 2240–2244, 2001.
[29] X. Luan, J. Wang, Y. Zou, and L. Cheng, "Materials Science & Engineering A A novel high temperature adhesive for bonding Al 2 O 3 ceramic," *Mater. Sci. Eng. A*, vol. 651, pp. 517–523, 2016.
[30] X. Wang, J. Wang, and H. Wang, "International Journal of Adhesion & Adhesives Performance and structural evolution of high-temperature organic adhesive for joining Al 2 O 3 ceramics," *Int. J. Adhes. Adhes.*, vol.

45, pp. 1–6, 2013.
[31] Y. Qin, Z. Rao, Z. Huang, H. Zhang, J. Jia, and F. Wang, “International Journal of Adhesion & Adhesives Preparation and performance of ceramizable heat-resistant organic adhesive for joining Al 2 O 3 ceramics,” *Int. J. Adhes. Adhes.*, vol. 55, pp. 132–138, 2014.
[32] K. Kita, N. Kondo, Y. Izutsu, and H. Kita, “Joining of alumina by using organometallic polymer,” pp. 658–662, 2011.
[33] W. D. Mucdonald and T. W. Eagar, “TRANSIENT LIQUID PHASE BONDING,” vol. 1, no. 1, pp. 23–46, 1992.
[34] G. O. Cook and I. I. I. Carl, “Overview of transient liquid phase and partial transient liquid phase bonding,” pp. 5305–5323, 2011.
[35] T. B. Reynolds, “UC Berkeley UC Berkeley Electronic Theses and Dissertations,” 2012.
[36] L. Chang and C. Huang, “Transient liquid phase bonding of alumina to alumina via boron oxide interlayer,” vol. 30, pp. 2121–2127, 2004.
[37] O. B. Dehkordi and A. M. Hadian, “Transient liquid phase bonding of alumina to alumina via Bismuth oxide interlayer,” vol. 829, pp. 136–140, 2014.
[38] H. Kato and K. Kageyama, “Chemical reaction assisted transient liquid phase bonding of alumina in combination with cold isostatic pressing,” vol. 0836, no. March, 2016.
[39] P. Lo, L. Chang, and Y. Lu, “High strength alumina joints via transient liquid phase bonding,” vol. 35, pp. 3091–3095, 2009.
[40] M. Engineering, “Ceramic joining Part I Partial transient liquid-phase bonding of alumina via Cu / Pt interlayers,” vol. 28, 1993.
[41] M. Engineering, “Ceramic joining II Partial transient liquid-phase bonding of alumina via Cu / Ni / Cu multilayer interlayers ~ ~ rRefractory Homogeni i ~ rlay zed melting point,” vol. 29, pp. 3200–3208, 1994.
[42] M. Engineering, “Ceramic joining III bonding of alumina via Cu / Nb / Cu interlayers,” vol. 29, pp. 3678–3690, 1994.
[43] T. Akashi, T. Nukui, and H. Kiyono, “Liquid-phase oxidation joining of oxide ion conducting ceramics via Al / heat resistant alloy / Al multilayer interlayers,” pp. 983–986, 2009.
[44] D. M. Jacobson and G. Humpston, *Pinciple of brazing Brazing*. ASM International.
[45] Dušan P. Sekulić, Ed., *Advances in brazing*. Woodhead Publishing Limited, 2013.
[46] M. G. Nicholas and S. D. Peteves, “Scripta Metallurgica,” vol. 31, no. 8, pp. 1091–1096, 1994.
[47] R. Voytovych, L. Y. Ljungberg, and N. Eustathopoulos, “The role of adsorption and reaction in wetting in the CuAg – Ti / alumina system,” vol. 51, pp. 431–435, 2004.
[48] H. Q. Hao, Y. L. Wang, Z. H. Jin, and X. T. Wang, “Joining of zirconia to zirconia using Ag-Cu-Ti filler metal,” vol. 52, pp. 238–247, 1995.
[49] M. L. Santella, J. A. Horton, and J. J. Pak, “Microstructure of Alumina Brazed with a Silver-Copper-Titanium Alloy,” vol. 87, no. 6, pp. 1785–1787, 1990.
[50] S. Gambaro, M. L. Muolo, F. Valenza, G. Cacciamani, L. Esposito, and A. Passerone, “Wettability of transparent YAG (Y 3 Al 5 O 12) by molten Ag – Cu – Ti alloys,” *J. Eur. Ceram. Soc.*, vol. 35, no. 10, pp. 2895–2906, 2015.

[51] R. Asthana and M. Singh, “Joining of partially sintered alumina to alumina, titanium, Hastealloy and C-SiC composite using Ag-Cu brazes,” *J. Eur. Ceram. Soc.*, vol. 28, no. 3, pp. 617–631, 2008.
[52] M. Science, “The influence of brazing conditions on joint strength in Al203 / Al203 bonding,” vol. 29, pp. 5041–5046, 1994.
[53] T. H. Chuang, M. S. Yeh, and Y. H. Chai, “Brazing of Zirconia with AgCuTi and SnAgTi Active Filler Metals,” *Metall. Mater. Trans. A*, vol. 31, no. 6, pp. 1591–1597, 2000.
[54] W. B. Hanson, K. I. Ironside, and J. A. Fernie, “ACTIVE METAL BRAZING OF ZIRCONIA,” vol. 48, pp. 4673–4676, 2000.
[55] T. A. Kassam, N. H. Babu, N. Ludford, S. Yan, and A. Howkins, “Secondary Phase Interaction at Interfaces of High-Strength Brazed Joints made using Liquid Phase Sintered Alumina Ceramics and Ag-Cu-Ti Braze Alloys,” *Sci. Rep.*, no. June 2017, pp. 1–11, 2018.
[56] M. Shukla and S. Ghosh, “Microwave Joining of Ceramics : An Overview,” vol. 4, no. 6, pp. 452–457, 2016.
[57] H. Fukusshima, T. Yamanaka, and M. Matsui, “Measurement of Dielectric properties of Ceramics at Microwave Frequency,” *J. Japan Soc. Precis. Eng.*, vol. 53, pp. 743–748, 1987.
[58] H. Fukushima, T. Yamanaka, and M. Matsui, “Microwave heating of ceramics and its application to joining,” *J. Mater. Res. Soc.*, vol. 5, no. 2, pp. 397–405, 1989.
[59] P. David and E. L. Libelo, “Method and apparatus for the microwave joining of ceramic items,” US patent no. 4767902, 1988.
[60] T. Meek, L. Alamos, and B. Rodger, “CERAMIC-GLASS-CERAMIC SEAL BY MICROWAVE HEATING,” US Patent no.4529857, 1985.
[61] T. Meek, L. Alamos, and B. Rodger, “CERAMIC-GLASS-METAL SEAL BY MICROWAVE HEATING,” US Patent no. 4529856, 1985.
[62] J. G. P. BINNER, J.A.FERNIE, P.A.WHITAKER, and T. E. CROSS, “The effect of composition on the microwave bonding of alumina ceramics,” *J. Mater. Sci.*, vol. 3, pp. 3017–3029, 1998.
[63] T. SATO, N. TAKAHASHI, and K. SHIMAKAGE, “Microwave joining of Alumina to Magnesia,” *J. Ceram. Soc. Japan*, vol. 104, no. 10, pp. 905–907, 1996.
[64] N. Kondo, M. Hotta, H. Hyuga, K. Hirao, and H. Kita, “Microwave joining of alumina with alumina / zirconia insert under low pressure and high temperature,” *J. Ceram. Soc. Japan*, vol. 120, no. 9, 2012.
[65] J. G. P. BINNER, J.A.FERNIE, and P.A.WHITAKER, “An investigation into microwave bonding mechanisms via a study of silicon carbide and zirconia,” *J. Mater. Sci.*, vol. 3, pp. 3009–3015, 1998.
[66] P. K. D. V Yarlagadda, R. Chong, and T. Soon, “Characterisation of materials behaviour in microwave joining of ceramics,” vol. 84, pp. 162–174, 1998.
[67] Y. Zhao, X. Zeng, S. Gao, and W. Zhang, “Microwave Joining Alumina Ceramics Using Al-Si Alloy Powders at Low Temperature,” vol. 755, pp. 383–387, 2013.
[68] C. Hille, M. Herrmann, and A. Hurtado, “Laser Joining of Ceramics: A Contribution to High Temperature Range Application of Ceramic Components,” 2008.
[69] F. Börner, W. Lippmann, A. Hurtado, and B. Schön, “Glasses for laser joining of zirconia ceramics,” *J. Eur. Ceram. Soc.*, vol. 34, no. 3, pp. 765–

772, 2014.
[70] F. Börner, W. Lippmann, and A. Hurtado, “Laser-joined Al 2 O 3 and ZrO 2 ceramics for high-temperature applications,” vol. 405, pp. 1–8, 2010.
[71] O. M. Akselsen, “Review of Diffusion bonding of ceramics,” *J. Mater. Sci.*, pp. 569–579, 1992.
[72] N. F. Kazakov, Ed., *Diffusion bonding of materials*, Ist. Pergamon press, 1985.
[73] R. W.Messler, “CERAMIC AND GLASS ATTACHMENT SCHEMES,” in *Integral Mechanical Attachment*, 2006.
[74] T. H. Cross and M. Mayo, “Ceramic-Ceramic difussion bonding using Nanocrystalline interlayers,” *Nano Struct. Mater.*, vol. 3, pp. 163–168, 1993.
[75] N. Hosseinabadi, R. Sarraf-mamoory, and A. Mohammad, “Diffusion bonding of alumina using interlayer of mixed hydride nano powders,” *Ceram. Int.*, vol. 40, no. 2, pp. 3011–3021, 2014.
[76] E. Scott and J. A. Brewer, “Bend Strengths for Diffusion-Bonded Al2O3,” *J. Am. Ceram. Soc.*, vol. 69, no. 8, p. C-178-C-179, 1986.
[77] T. Nagano, H. Kato, and F. Wakai, “Diffusion Bonding of Zirconia/Alumina Composites,” *J. Am. Ceram. Soc.*, vol. 73, no. 11, pp. 3476–80, 1990.
[78] K. Ozturk, R. N. Basu, C. A. Randall, and M. J. Mayo, “DIFFUSION BONDING OF RIGID ZIRCONIA PIECES USING ELECTROPHORETICALLY DEPOSITED PARTICULATE INTERLAYERS,” *Scr. Mater.*, vol. 41, no. 11, pp. 1191–1195, 1999.
[79] H. Miyazaki, M. Hotta, H. Kita, and Y. Izutsu, “Joining of alumina with a porous alumina interlayer,” *Ceram. Int.*, vol. 38, no. 2, pp. 1149–1155, 2012.
[80] J. E. Shelby, *Introduction to glass science and technology*, Second edi. The Royal Society of Chemistry, 2005.
[81] B. S. Mitchell, *An introduction to material engineering and science*. Wiley-Interscience, 2004.
[82] W. Vogel, *Structure and crytsllization of glasses*, Leipzig. Pergamon press.
[83] A. Varshneya, *Fundamentals of inorganic glasses*. Academic press Inc., 1994.
[84] A. G. Sabato *et al.*, “Glass-ceramic sealant for solid oxide fuel cells application: Characterization and performance in dual atmosphere,” *J. Power Sources*, vol. 328, pp. 262–270, 2016.
[85] F. Smeacetto, A. Chrysanthou, T. Moskalewicz, and M. Salvo, “Thermal cycling of Crofer22APU-sealant-anode supported electrolyte joined structures for planar SOFCs up to 3000 h,” *Mater. Lett.*, vol. 111, pp. 143–146, 2013.
[86] A. A. Reddy *et al.*, “Diopside-Ba disilicate glass-ceramic sealants for SOFCs: Enhanced adhesion and thermal stability by Sr for Ca substitution,” *Int. J. Hydrogen Energy*, vol. 38, no. 7, pp. 3073–3086, 2013.
[87] L. Luo *et al.*, “Application of BaO-CaO-Al2O3–B2O3–SiO2 glass–ceramic seals in large size planar IT-SOFC,” *Ceram. Int.*, vol. 41, no. 8, pp. 9239–9243, 2015.
[88] V. Kumar, G. Kaur, O. P. Pandey, K. Singh, and K. Lu, “Effect of Thermal Treatment on Chemical Interaction Between Yttrium Borosilicate Glass Sealants and YSZ for Planar Solid Oxide Fuel Cells,” *Int. J. Appl. Glas. Sci.*, vol. 5, no. 4, pp. 410–420, 2014.

[89] A. Bakal and M. D. Mat, “A novel two-layered glass-ceramic sealant design for solid oxide fuel cells,” *Int. J. Energy Res.*, vol. 41, no. 5, pp. 628–636, 2017.
[90] A. R. Allu *et al.*, “Understanding the formation of CaAl2Si2O8 in melilite-based glass-ceramics: Combined diffraction and spectroscopic studies,” *ACS Omega*, vol. 2, no. 9, pp. 6233–6243, 2017.
[91] E. V. Stephens, J. S. Vetrano, B. J. Koeppel, Y. Chou, X. Sun, and M. A. Khaleel, “Experimental characterization of glass-ceramic seal properties and their constitutive implementation in solid oxide fuel cell stack models,” *J. Power Sources*, vol. 193, no. 2, pp. 625–631, 2009.
[92] C. Hsiu-Tao, C.-K. Lin, and C.-K. Liu, “HIGH TEMPERATURE MECHANICAL PROPERTIES OF A CRYSTALLIZED BaO-B2O3-Al2O3-SiO2 GLASS CERAMIC FOR SOFC,” in *Proceedings of ASME 2009 Seventh International Fuel Cell Science, Engineering and Technology Conference*, 2009, pp. 745–750.
[93] M.Fakouri Hasanabadi, M.A.Faghihi-Sani, A.H.Kokabi, S.M.Groß-Barsnick, and J.Malzbender, “Room- and high-temperature flexural strength of a stable solid oxide fuel/electrolysis cell sealing material,” *Ceram. Int.*, vol. 45, no. 1, 2018.
[94] P. J. Howard and I. Szkoda, “Corrosion Resistance of SOFC and SOEC Glass-Ceramic Seal Materials in High Temperature Steam/Hydrogen,” *J. Fuel Cell Sci. Technol.*, vol. 9, no. 4, p. 041009, 2012.
[95] G. Kaur, *Solid Oxide Fuel Cell Components: Interfacial Compatibility of SOFC Glass Seals*. Springer International Publishing, 2016.
[96] A. Kamonlert, A. Niyompan, and R. Tipakontitikul, “Effect of ZrO2 addition on crystallization and properties of the glass-ceramics contained NaNbO3 crystals,” *Curr. Appl. Phys.*, vol. 11, no. 3 SUPPL., pp. 100–105, 2011.
[97] H. C. Li, D. G. Wang, X. G. Meng, and C. Z. Chen, “Effect of ZrO2additions on the crystallization, mechanical and biological properties of MgO-CaO-SiO2-P2O5-CaF2bioactive glass-ceramics,” *Colloids Surfaces B Biointerfaces*, vol. 118, pp. 226–233, 2014.
[98] T. Schwickert, R. Sievering, P. Geasee, and R. Conradt, “Glass-ceramic materials as sealants for SOFC applications,” *Mater. Sci. Eng. Technol.*, vol. 33, no. 6, pp. 363–366, 2002.
[99] S. F. Wang, Y. R. Wang, Y. F. Hsu, and C. C. Chuang, “Effect of additives on the thermal properties and sealing characteristic of BaO-Al2O3-B2O3-SiO2glass-ceramic for solid oxide fuel cell application,” *Int. J. Hydrogen Energy*, vol. 34, no. 19, pp. 8235–8244, 2009.
[100] A. P. Tomsia, a. M. Glaeser, and J. S. Moya, “Interfaces between Alumina and Refractory Glasses for High Temperature Applications,” *Key Eng. Mater.*, vol. 111–112, pp. 191–208, 1995.
[101] W. Zhu, J. Chen, C. Hao, and J. Zhang, “Microstructure and strength of Al2O3/Al2O3 Joints Bonded with ZnO-Al2O3-B2O3-SiO2 Glass-Ceramic,” *J. Mater. Sci. Technol.*, vol. 30, no. 9, pp. 944–948, 2014.
[102] L. Esposito and A. Bellosi, “Ceramic oxide bonds using calcium aluminosilicate glasses,” *J. Mater. Sci.*, vol. 40, no. 9–10, pp. 2493–2498, 2005.
[103] Y. J. Lin and S. H. Tu, “Joining of mullite ceramics with yttrium aluminosilicate glass interlayers,” *Ceram. Int.*, vol. 35, no. 3, pp. 1311–1315, 2009.

[104] B. Chiou, “Liquid phase bonding of yttria stabilized zirconia with CaO-Ti02-SiO 2 glass,” vol. 30, pp. 1295–1301, 1995.
[105] S. L. SWARTZ, B.S.MAJUMDAR, A.SKIDMORE, and B. C. MUTSUDDY, “Joining of zirconia ceramics with CaO-TiO2-SiO2 interlayer,” *Mater. Lett.*, vol. 7, no. 11, pp. 407–410, 1989.
[106] M. ASHIZUKA and E. ISHIDA, “Joining of Zirconia-to-Zirconia using CaO-MgO-SiO2-Al2O3,” *J. Ceram. Soc. Japan*, vol. 104, no. 4, pp. 345–347, 1996.
[107] C. Gadelmeier, J. Schmidt, M. Göthe, and D. Jovanovic, “Characterization of Furnace Sintered Mullite and Oxide Ceramic Matrix Composites (O-CMC) by Using Glass Solders,” in *Advances in Science and Technology*, 2014, vol. 88, pp. 162–171.
[108] C. Gadelmeier, J. Schmidt, D. Jovanovic, M. Zietkowski, C. Eckardt, and M. Gorywoda, “Adhesive bonding of oxide ceramics for complex ceramic parts in high temperature furnaces,” *Mater. Sci. Forum*, vol. 825–826, pp. 279–286, 2015.
[109] “3M™ Nextel™ Ceramic Fibers and Textiles Technical Reference Guide,” 2016.
[110] B. S. Rangaswamy and D. Fortuna, “Novel , high chromium containing braze filler metals for heat exchanger applications White Paper – New Braze Filler Metals 2007.03,” 2014.
[111] M. Singh, R. Asthana, and T. P. Shpargel, “Brazing of ceramic-matrix composites to Ti and Hastealloy using Ni-base metallic glass interlayers,” vol. 498, pp. 19–30, 2008.
[112] “Metglas-Brazing-Overview.pdf.” p. 15, 2016.
[113] M. L. Muolo, E. Ferrera, L. Morbelli, and A. Passerone, “Wetting , spreading and joining in the alumina – zirconia – Inconel 738 system,” vol. 50, pp. 325–330, 2004.
[114] K. M. Jasim, F. A. Hashim, R. H. Yousif, R. D. Rawlings, and A. R. Boccaccini, “Actively brazed alumina to alumina joints using CuTi , CuZr and eutectic AgCuTi filler alloys,” *Ceram. Int.*, vol. 36, no. 8, pp. 2287–2295, 2010.
[115] P. Siegmund, C. Guhl, E. Schmidt, A. Roßberg, and M. Rettenmayr, “Reactive wetting of alumina by Ti-rich Ni–Ti–Zr alloys,” *J. Mater. Sci.*, vol. 51, no. 8, pp. 3693–3700, 2016.
[116] A. E. Shapiro and Y. Flom, “Brazing of titanium, ceramics, and graphite using new low-temperature Ti- and Zr-based amorphous foils,” 2015.
[117] S. Hong, K. Mimura, Y. Zhu, and M. Isshiki, “Improvement in Oxidation Resistance of Cu-Al Dilute Alloys by Pre-annealing in H 2 and Ar Atmospheres,” *Mater. Trans.*, vol. 46, no. 2, pp. 167–170, 2005.
[118] M. Sundberg, G. Malmqvist, A. Magnusson, and T. El-raghy, “Alumina forming high temperature silicides and carbides,” vol. 30, pp. 1899–1904, 2004.
[119] P. J. Ding, W. A. Lanford, S. Hymes, and S. P. Murarka, “Effects of the addition of small amounts of Al to copper : Corrosion , resistivity , adhesion , morphology , and diffusion Effects of the addition of small amounts of Al to copper : Corrosion , resistivity , adhesion , morphology , and diffusion,” vol. 3627, pp. 1–6, 1994.
[120] N. J. Tannyan, G. Plascencia, T. A. Utigard, N. J. Tannyan, G. Plascencia, and T. A. Utigard, “High Temperature Oxidation of Copper and Copper Aluminum Alloys,” *Can. J. Metall. Mater. Sci. ISSN*, vol. 41, no. 2, 2002.

[121] N. J. Tannyan, G. Plascencia, T. A. Utigard, N. J. Tannyan, G. Plascencia, and T. A. Utigard, "High Temperature Oxidation of Copper and Copper Aluminum Alloys," *Can. Metall. Q.*, vol. 41, no. 2, pp. 213–218, 2002.
[122] T. H. E. Regularities, O. F. Selective, and O. Of, "ITHE REGULARITIES OF SELECTIVE OXIDATION OF COPPER-ALUMINIUM SOLID SOLUTIONS.," in *Material Research Symp.Proc.*, 1993, vol. 280, pp. 565–570.
[123] K. M. Jasim, F. A. Hashim, R. H. Yousif, R. D. Rawlings, and A. R. Boccaccini, "Actively brazed alumina to alumina joints using CuTi, CuZr and eutectic AgCuTi filler alloys," *Ceram. Int.*, vol. 36, no. 8, pp. 2287–2295, 2010.
[124] M. Y. Akram *et al.*, "Journal of the European Ceramic Society Joining and testing of alumina fi bre reinforced YAG-ZrO 2 matrix composites," vol. 38, no. November 2017, pp. 1802–1811, 2018.
[125] C. S. Kanetkar, A. S. Kacar, and D. M. Stefanescu, "The Wetting Characteristics and Surface Tension of Some Ni-Based Alloys on Yttria , Hafnia , Alumina , and Zirconia Substrates," vol. 19, no. July, pp. 1833–1839, 1988.
[126] M. L. Santella, J. A. Horton, and J. J. Pak, "Microstructure of Alumina Brazed with a Silver-Copper-Titanium Alloy," *J. Am. Ceram. Soc.*, vol. 87, pp. 1785–1787, 1990.
[127] M. Ali, K. M. Knowles, P. M. Mallinson, and J. A. Fernie, "Acta Materialia Microstructural evolution and characterisation of interfacial phases in Al 2 O 3 / Ag – Cu – Ti / Al 2 O 3 braze joints," *Acta Mater.*, vol. 96, pp. 143–158, 2015.
[128] T. Zro, C. Ti, and Þ. A. After, "Microstructural evolution and bonding mechanisms of the brazed," no. January, 2014.
[129] M. Singh, "Brazing of Stainless Steel to Yttria-Stabilized Zirconia Using Gold-Based Brazes for Solid Oxide Fuel Cell Applications," vol. 133, pp. 119–133, 2007.
[130] H. L. Chang and M. S. Liang, "Oxygen vacancy estimation of high k metal gate using thermal dynamic model," *Appl. Phys. Lett.*, vol. 97, no. 041912, 2010.
[131] C. Xin, W. Liu, N. Li, J. Yan, and S. Shi, "Metallization of Al 2 O 3 ceramic by magnetron sputtering Ti / Mo bilayer thin fi lms for robust brazing to Kovar alloy," *Ceram. Int.*, vol. 42, no. 8, pp. 9599–9604, 2016.
[132] A. V Durov, Y. V Naidich, and B. D. Kostyuk, "Investigation of interaction of metal melts and zirconia," vol. 0, pp. 2173–2178, 2005.
[133] J. C. PEREIRA, A. E. M. R. M. NASCIMENTO, A. W. ACCHAR, L. A. ROCHA, and ABSTRACT, "Wetting Behavior of Silver Braze Alloys onto Metallized Zirconia Inserts," *Weld. J.*, no. July, pp. 211–218, 2015.
[134] S. Gambaro, F. Valenza, A. Passerone, G. Cacciamani, and M. L. Muolo, "Journal of the European Ceramic Society Brazing transparent YAG to Ti6Al4V : reactivity and characterization," *J. Eur. Ceram. Soc.*, vol. 36, no. 16, pp. 4185–4196, 2016.
[135] Y. Liu, J. Hu, Y. Zhang, and Z. Guo, "Interface Microstructure of the Brazed Zirconia and Ti-6Al-4V Using Ti-based Amorphous Filler," vol. 45, pp. 313–321, 2013.
[136] Yamamoto and Masahiro, "MECHANISM OF OXYGEN ABSORPTION BY ZIRCONIUM," *Kyoto Univ. Res. Inf. Respository*, 1991.
[137] J. L. Murray and H. A. Wreidt:, *Phase diagrams of binary titanium alloys*.

ASTMinternational, 1987.
[138] T. B. Massalski and H.Okamoto, Eds., *Binary alloy phase diagrams, (ASM International, Materials Park)*. 1990.
[139] R. Arroyave, "Thermodynamics and Kinetics of Ceramic / Metal Interfacial Interactions Raymundo Arr ´ oyave," Massachusetts Institute of Technology, 2004.
[140] G. P. Kelkar and A. H. Carim, "Al solubility in M6X compounds in the Ti-Cu-0," vol. 23, no. May, pp. 231–235, 1995.
[141] M. Yang, T. Lin, P. He, and Y. Huang, "In situ synthesis of TiB whisker reinforcements in the joints of Al 2 O 3 / TC4 during brazing," *Mater. Sci. Eng. A*, vol. 528, no. 9, pp. 3520–3525, 2011.
[142] H. B. Liu, L. X. Zhang, L. Z. Wu, D. Liu, and J. C. Feng, "Vacuum brazing of SiO 2 glass ceramic and Ti – 6Al – 4V alloy using AgCuTi filler foil," vol. 498, pp. 321–326, 2008.
[143] C. H. Xu, C. H. Woo, and S. Q. Shi, "The effects of oxidative environments on the synthesis of CuO nanowires on Cu substrates," vol. 36, pp. 31–38, 2004.
[144] J. Wang and W. D. Cho, "Oxidation Behavior of Pure Copper in Oxygen and / or Water Vapor at Intermediate Temperature," vol. 49, no. 12, pp. 1926–1931, 2009.
[145] X. Jiang, T. Herricks, and Y. Xia, "CuO Nanowires Can Be Synthesized by Heating Copper Substrates in Air," 2002.
[146] R. R. Kapoor and T. W. Eagar, "Oxidation Behavior of Silver and Copper Based Brazing Filler Metals for Silicon Nitride/Metal Joints," *J. Am. Ceram. Soc.*, vol. 72, no. 3, pp. 448–454, 1989.
[147] G. Bolat, J. Izquierdo, D. Mareci, D. Sutiman, and R. M. Souto, "Electrochimica Acta Electrochemical characterization of ZrTi alloys for biomedical applications . Part 2 : The effect of thermal oxidation," *Electrochim. Acta*, vol. 106, pp. 432–439, 2013.
[148] G. Plascencia, T. Utigard, and T. Marín, "The Oxidation Resistance of Copper-Aluminum Alloys at Temperatures up to 1000 ° C," *Jom*, vol. 57, no. 1, pp. 80–84, 2005.
[149] G. Feng, Z. Li, Z. Zhou, Y. Yang, D. P. Sekulic, and M. R. Zachariah, "Microstructure and mechanical properties of C f / Al-TiAl laser-assisted brazed joint," *J. Mater. Process. Tech.*, vol. 255, no. October 2017, pp. 195–203, 2018.
[150] P. R. Subramanian, U. E. Systems, and J. H. Perepezko, "The Ag-Cu (Silver-Copper) System," vol. 14, no. 1, pp. 62–75, 1993.
[151] D. Sciti, A. Bellosi, and L. Esposito, "Bonding of zirconia to super alloy with the active brazing technique," vol. 21, pp. 45–52, 2001.
[152] R. Voytovych, F. Robaut, and N. Eustathopoulos, "The relation between wetting and interfacial chemistry in the CuAgTi / alumina system," vol. 54, pp. 2205–2214, 2006.
[153] M. V Glazoff, "Modeling of Some Physical Properties of Zirconium Alloys for Nuclear Applications in Support of UFD Campaign," no. July 2013, 2014.
[154] B. Sefer, "Oxidation and Alpha–Case Phenomena in Titanium Alloys used in Aerospace Industry: Ti–6Al–2Sn–4Zr–2Mo and Ti–6Al–4V," Luleå University of Technology, 2014.
[155] M. V. Glazoff, "Effect of oxygen and hydrogen on mechanical properties of commercial purity titanium," 2013.

[156] M. L. Wasz, F. R. Brotzen, R. B. Mclellan, and A. J. Griffin, “Effect of oxygen and hydrogen on mechanical properties of commercial purity titanium,” vol. 41, no. 1, pp. 1–12, 1996.
[157] R. Kaden and O. E. Zir-, “Oxygen Embrittlement of Zirconium-Copper Alloys at High Temperatures,” 1969.
[158] H. Scholze, “Influence of viscosity and surface tension on hot-stage microscopy measurements on glasses,” *Ver. Dtsch. Keram. Ges.*, vol. 391, pp. 63–68, 1962.
[159] S. M. Mrityunjay Singh, Tatsuki Ohji, Rajiv Asthana, Ed., *Ceramic Integration and Joining Technologies: From Macro to Nanoscale*. 2011.
[160] E. Bernardo, G. Scarinci, E. Edme, U. Michon, and N. Planty, “Fast-sintered gehlenite glass-ceramics from plasma-vitrified municipal solid waste incinerator fly ashes,” *J. Am. Ceram. Soc.*, vol. 92, no. 2, pp. 528–530, 2009.
[161] C. Lara, M. J. Pascual, and A. Durán, “Glass-forming ability, sinterability and thermal properties in the systems RO-BaO-SiO2(R = Mg, Zn),” *J. Non. Cryst. Solids*, vol. 348, pp. 149–155, 2004.
[162] M. Saad and M. Poulain, “Glass Forming Ability Criterion,” *Mater. Sci. Forum*, vol. 19–20, pp. 11–18, 1987.
[163] Dietzel, “Glass structure and glass properties,” *Glas. Ber.*, vol. 22, pp. 41–50, 1968.
[164] A. A. Reddy *et al.*, “Study of calcium-magnesium-aluminum-silicate (CMAS) glass and glass-ceramic sealant for solid oxide fuel cells,” *J. Power Sources*, vol. 231, pp. 203–212, 2013.
[165] N. P. Bansal and E. A. Gamble, “Crystallization kinetics of a solid oxide fuel cell seal glass by differential thermal analysis,” *J. Power Sources*, vol. 147, no. 1–2, pp. 107–115, 2005.
[166] C. . Paßlick, B. . Ahrens, B. . Henke, J. A. . Johnson, and S. Schweizer, “Differential scanning calorimetry investigations on Eu-doped fluorozirconate-based glass ceramics,” *J Non Cryst Solids.*, vol. 356, no. 52–54, pp. 3085–3089, 2011.
[167] A. G. Sabato, M. Salvo, A. De Miranda, and F. Smeacetto, “Crystallization behaviour of glass-ceramic sealant for solid oxide fuel cells,” *Mater. Lett.*, vol. 141, pp. 284–287, 2015.
[168] A. Goel, E. R. Shaaban, D. U. Tulyaganov, and J. M. F. Ferreira, “Study of crystallization kinetics in glasses along the diopside-Ca- Tschermak join,” *J. Am. Ceram. Soc.*, vol. 91, no. 8, pp. 2690–2697, 2008.
[169] F. Smeacetto *et al.*, “Glass-ceramic joining material for sodium-based battery,” *Ceram. Int.*, vol. 43, no. 11, pp. 8329–8333, 2017.
[170] H.-P. Liu, L.-P. Ma, X.-F. Huang, J.-X. Tang, J. Yang, and J. Yang, “Effect of different amounts of slag on the crystallization behavior of glass-ceramics produced by natural cooling yellow phosphorus slag,” *RSC Adv.*, vol. 6, no. 90, pp. 87696–87702, 2016.
[171] K. Cheng, “Determining crystallization kinetic parameters of analysis curves,” *Mater. Sci. Eng. B*, vol. 60, no. 3, pp. 194–199, 1999.
[172] M. Erol and S. Küçükbayrak, “The application of differential thermal analysis to the study of isothermal and non-isothermal crystallization kinetics of coal fly ash based glasses,” *J. Non. Cryst. Solids*, vol. 355, no. 9, pp. 569–576, 2009.
[173] H. E. Kissinger, “Variation of peak temperature with heating rate in differential thermal analysis,” *J. Res. Natl. Bur. Stand. (1934).*, vol. 57, no.

4, p. 217, 1956.
[174] T. Ozawa, “Kinetics of non-isothermal crystallization,” *Polymer (Guildf).*, vol. 12, no. 3, pp. 150–158, 1971.
[175] Matusita and S. Sakka, “Kinetic Study on Non-Isothermal Crystallization of Glass by Thermal Analysis,” *Bull. Inst. Chem. Res. Kyoto Univ. (1981), 59(3) 159-171*.
[176] F. Smeacetto, M. Salvo, M. Ferraris, J. Cho, and A. R. Boccaccini, “Glass-ceramic seal to join Crofer 22 APU alloy to YSZ ceramic in planar SOFCs,” *J. Eur. Ceram. Soc.*, vol. 28, no. 1, pp. 61–68, 2008.
[177] W. Liu, X. Sun, and M. A. Khaleel, “Predicting Young ’ s modulus of glass / ceramic sealant for solid oxide fuel cell considering the combined effects of aging , micro-voids and self-healing,” vol. 185, pp. 1193–1200, 2008.
[178] W. N. Liu, X. Sun, B. Koeppel, and M. Khaleel, “Experimental Study of the Aging and Self-Healing of the Glass / Ceramic Sealant Used in SOFCs,” vol. 29, pp. 22–29, 2010.
[179] B. Dev, M. E. Walter, G. B. Arkenberg, and S. L. Swartz, “Mechanical and thermal characterization of a ceramic/glass composite seal for solid oxide fuel cells,” *J. Power Sources*, vol. 245, pp. 958–966, 2014.
[180] Y.-S. Chou, J.-P. Choi, W. Xu, E. Stephens, B. Koeppel, and and J. Stevenson, “Compliant Glass Seals for SOFC Stacks,” 2014.
[181] Y. Zhao, J. Malzbender, and S. M. Gross, “The effect of room temperature and high temperature exposure on the elastic modulus , hardness and fracture toughness of glass ceramic sealants for solid oxide fuel cells,” *J. Eur. Ceram. Soc.*, vol. 31, no. 4, pp. 541–548, 2011.
[182] S. A. R. Junior, J. L. Ferracane, and Á. Della Bona, “Flexural strength and Weibull analysis of a microhybrid and a nanofill composite evaluated by 3- and 4-point bending tests,” *Dent. Mater.*, vol. 24, no. 3, pp. 426–431, 2008.
[183] H. T. Chang, C. K. Lin, C. K. Liu, and S. H. Wu, “High-temperature mechanical properties of a glass sealant for solid oxide fuel cell,” *J. Power Sources*, vol. 189, pp. 1093–1099, 2009.
[184] J. Malzbender and Y. Zhao, “Flexural strength and viscosity of glass ceramic sealants for solid oxide fuel cell stacks,” *Fuel Cells*, vol. 12, no. 1, pp. 47–53, 2012.
[185] W. Zhu, J. Chen, C. Jiang, C. Hao, and J. Zhang, “Joining of Porous Alumina with a CaO-Al 2 O 3 -SiO 2 Glass-Ceramic,” *J. Am. Ceram. Soc.*, vol. 96, pp. 1738–1744, 2013.
[186] F. Smeacetto *et al.*, “Novel glass-ceramic composition as sealant for SOFCs,” *J. Am. Ceram. Soc.*, vol. 97, no. 12, pp. 3835–3842, 2014.
[187] A. Goel, A. A. Reddy, M. J. Pascual, L. Gremillard, A. Malchere, and J. M. F. Ferreira, “Sintering behavior of lanthanide-containing glass-ceramic sealants for solid oxide fuel cells,” *J. Mater. Chem.*, vol. 22, no. 19, p. 10042, 2012.
[188] J. X. Zhang, R. S. Chandel, Y. Z. Chen, and H. P. Seow, “Effect of residual stress on the strength of an alumina-steel joint by partial transient liquid phase (PTLP) brazing,” *J. Mater. Process. Technol.*, vol. 122, no. 2–3, pp. 220–225, 2002.
[189] R. Asthana and M. Singh, *Active metal brazing of advanced ceramic composites to metallic systems*. Woodhead Publishing Limited, 2013.
[190] K. Matusita and S. Sakka, “Kinetic study on Non-Isothermal crystallization,” *Bull. Inst. Chem. Res. Univ.*, vol. 59, no. 3, 1981.
[191] C. R. Cheeseman and G. W. Groves, “The mechanism of the peak in

strength and toughness at elevated temperatures in alumina containing a glass phase," *J. Mater. Sci.*, vol. 20, no. 7, pp. 2614–2622, 1985.
[192] J. Wang, P. A. Withey, C. B. Ponton, and P. M. Marquis, "The loading rate dependence of fracture strength in a reaction-sintered mullite ceramic," *J. Mater. Sci. Lett.*, vol. 11, no. 17, pp. 1201–1205, 1992.
[193] H. J. Maier, "High-temperature fatigue of titanium alloys," *Mater. High Temp.*, vol. 15, no. 1, pp. 3–14, 1998.
[194] N. Wanderka, V. Kindrachuk, J. Banhart, D. Mukherji, D. D. Genovese, and J. Rösler, "Effect of Re Addition on the Microstructural Stability of Inconel 706 Superalloy at Elevated Temperatures," *Microsc. Microanal.*, vol. 13, no. S02, pp. 1632–1633, 2007.
[195] R. E. Schafrik, D. D. Ward, and J. R. Groh, "Application of Alloy 718 in GE Aircraft Engines: Past, Present and Next Five Years," 2001.
[196] A. Y. Kina, V. M. Souza, S. S. M. Tavares, J. M. Pardal, and J. A. Souza, "Microstructure and intergranular corrosion resistance evaluation of AISI 304 steel for high temperature service," *Mater. Charact.*, vol. 59, no. 5, pp. 651–655, 2008.
[197] A. Y. Kina, V. M. Souza, S. S. M. Tavares, J. A. Souza, and H. F. G. de Abreu, "Influence of heat treatments on the intergranular corrosion resistance of the AISI 347 cast and weld metal for high temperature services," *J. Mater. Process. Technol.*, vol. 199, no. 1, pp. 391–395, 2008.
[198] "Metallic Materials," Teadit N.A., 2008.
[199] M. Yasir, V. Casalegno, M. Ferraris, G. Puchas, W. Krenkel, and S. Roszeitis, "Journal of the European Ceramic Society Joining and mechanical testing of oxide / oxide (Nextel ^{TM} 610 / alumina- zirconia) ceramic composites," *J. Eur. Ceram. Soc.*, vol. 39, no. 7, pp. 2510–2517, 2019.